A New Regenerative Anti-Idling System for Service Vehicles: Load Identification, Optimal Power Management

by

Soheil Mohagheghi Fard

A thesis

presented to the University of Waterloo

in fulfillment of the

thesis requirement for the degree of

Doctor of Philosophy

in

Mechanical Engineering

Waterloo, Ontario, Canada, 2016

AUTHOR'S DECLARATION

I hereby declare that I am the sole author of this thesis. This is a true copy of the thesis, including any required final revisions, as accepted by my examiners.

I understand that my thesis may be made electronically available to the public.

Soheil Mohagheghi Fard

Abstract

Service vehicles, such as refrigerator trucks and tour buses, are equipped with auxiliary devices, including refrigeration systems and cabin air conditioning systems, which consume significant amount of energy. The engine of these vehicles should idle to supply power for auxiliary devices when they stop for a long time, e.g. for loading and unloading goods. This study proposes a new anti-idling system for service vehicles that powers auxiliary devices by a battery pack and an engine-driven generator (or alternator). In addition to idle elimination which is the main objective of all current anti-idling systems, the proposed system called Regenerative Auxiliary Power System (RAPS) attempts to reduce fuel consumption by enabling regenerative braking and utilizing an optimal power management system. The objectives of this study are to identify drive and service loads of a service vehicle for component sizing of the RAPS and to develop an optimal power management system for more fuel saving.

In order to determine the size of required components (a battery pack and a generator) for the RAPS, drive and service loads of a given service vehicle should be identified. The drive load is the amount of power that is required for moving the vehicle, and the service load is the power consumption of the auxiliary devices. To identify drive and service loads, all the parameters in power balance equation of the engine should be either measured or estimated. As two inputs with unknown variations in this equation, vehicle mass and torque of auxiliary devices are required to be estimated. This study proposes a model-based algorithm that utilizes available signals in the CAN bus of the vehicle as well as a signal from a GPS receiver (road grade information) for simultaneous estimation of the vehicle mass and torque of auxiliary devices.

The power management system of the RAPS should determine the split ratio of auxiliary power demand between the generator and battery in order to minimize fuel consumption. It should also guarantee that the battery has enough energy for powering auxiliary devices at all the engine-OFF stops. To meet these objectives, a two-level control system is proposed in this study. In the high-level control system, a fast dynamic programming (DP) technique which utilizes extracted features of the predicted drive and service loads obtains an SOC trajectory. In the low-level control system, a refined Adaptive Equivalent Fuel Consumption Minimization (A-ECMS) technique is employed to track the SOC trajectory obtained by the high-level control scheme.

Many numerical simulations are carried out to test the functionality of the proposed identification algorithm and power management system. Moreover, the numerical simulations are validated by Hardware-In-The-Loop (HIL) simulations. The results show the idling is completely eliminated and a significant amount of fuel is saved by implementing the RAPS on a service vehicle. Therefore, the cost of energy can be noticeably reduced and consequently the cost of RAPS is recouped in a short period of time.

Acknowledgements

I would like to express my gratitude to my supervisor, Professor Amir Khajepour, for his valuable guidance, understanding, and patience during my PhD studies at University of Waterloo.

I would also like to thank my thesis committee, Prof. Roydon Fraser, Prof. Baris Fidan, Prof. Nasser Lashgarian Azad, and Prof. Ali Emadi for their insightful comments and encouragement.

My sincere thanks to all the colleagues (researchers and technicians) at Mechatronics Vehicle System Laboratory, especially Mr. Jeff Graansma for his technical help and support.

Finally, I must express my very profound gratitude to my parents, my sister, and my wife for providing me with support and encouragement during my years of study and through the process of researching and writing this thesis. This accomplishment would not have been possible without them.

To Darya

Table of Contents

List of Figures

List of Tables

Nomenclature

A_f	Frontal area of the vehicle
C	Battery capacity
C_D	Coefficient of aerodynamic resistance
C_{rr}	Coefficient of rolling resistance
D	Distance travelled by the vehicle
D_{tot}	Total distance that the vehicle travels in a segment
$E_{aux-seg}$	Total auxiliary energy demanded in a segment
E_{batt}	Battery energy
$E_{batt-rem}$	Remaining energy in the battery
$E_{gen-seg}$	Total produced electrical energy by the generator in a segment
$E_{regen-seg}$	Total electrical energy generated by regenerative braking in a segment
Eps	Neighborhood radius
e	Estimation error
F_A	Aerodynamics resistance
F_g	Grade resistance
F_{RR}	Tire rolling resistance
g	Gravitational acceleration
I_d	Rotational inertia of the driveshaft
I_e	Rotational inertia of the engine
I_t	Rotational inertia of the transmission
I_w	Rotational inertia of the wheels and axles shafts
J	Cost function
K	Kalman gain
k	Discrete time instant
k_p	Proportional gain
k_{p-high}	Proportional gain with a high value

k_{p-low}	Proportional gain with a low value
k_i	Integral gain
LHV	Lower heating value of the fuel
M	Vehicle mass
M_{est}	Estimated vehicle mass in the first stage of the estimation algorithm
$MinPts$	Minimum number of data points in a cluster
m_f	Fuel consumption of the engine
$\dot{m}_f$	Fuel consumption rate of the engine
$\dot{m}_{f,equ}$	Equivalent fuel rate of the engine and battery
N_s	Number of segments plus one
N_t	Numerical ratio of the transmission
N_{tf}	Combined ratio of the transmission and final drive
n_{pi}	Number of Pi groups
n_{soc}	Number of discritized state
n_u	Number of discretized control input
P	Estimation error covariance
P_{aux}	Demanded auxiliary power
P_{batt}	Battery power
P_{dl}	Drive load
P_{eng}	Engine power
P_{gen}	Generator power
P_{sl}	Service load
P_{t-in}	Input power of transmission
P_{t-out}	Output power of transmission
p	Number of variables
q	Number of dimensions
R	Tire radius

R_{int}	Internal resistance of the battery
R_1	Covariance matrix of process noise
R_2	Covariance matrix of measurement noise
s	Equivalent weight factor
s_0	Initial guess for equivalent weight factor
s_{opt}	Optimal equivalent weight factor
S_M	Ratio of vehicle mass in HIL system to that of a real vehicle
S_T	Ratio of engine torque in HIL system to that of a real vehicle
S_u	Ratio of vehicle speed in HIL system to that of a real vehicle
S_{ω_e}	Ratio of engine speed in HIL system to that of a real vehicle
SOC	State of the charge of the battery
SOC_0	Initial SOC of a segment
SOC_f	Final SOC of a segment
SOC_{opt}	Optimal SOC (SOC that is obtained by utilizing s_{opt})
SOC_{ref}	Reference SOC
T	Torque of dynamometers
T_{aux}	Torque of auxiliary devices
T_e	Engine torque
T_{gen}	Generator torque
T_{t-in}	Input torque of transmission
T_{t-out}	Output torque of transmission
u	Vehicle longitudinal speed
u_d	Control input of DP
u_h	Control input in the high-level of DP-AECMS
u_l	Control input in the low-level of DP-AECMS
$\dot{u}$	Vehicle longitudinal acceleration
V_{OC}	Battery open circuit voltage

v	Measurement noise
w	Parameter variation (noise)
z	Process output
$\hat{z}$	Model output
α	Angle of slope
α_1	Weighting factor for the data collected in the last day
α_2	Weighting factor for the data collected in 4th week
α_3	Weighting factor for the data collected first three weeks
Δt	Step time
δ_i	Value of the parameter based on collected data in i_th day
δ_{pred}	Predicted value of a parameter
η_{dl}	Efficiency of driveline
η_t	Efficiency of transmission
θ	Actual values of parameters
$\hat{\theta}$	Estimated values of parameters
ρ	Mass density of air
ϕ	Regression vector
ω_e	Engine rotational speed
$\dot{\omega}_e$	Engine rotational acceleration
ω_{gen}	Generator rotational speed
ω_{t-in}	Input speed of transmission
ω_{t-out}	Output speed of transmission
A-ECMS	Adaptive equivalent fuel consumption minimization strategy
APU	Auxiliary power unit
BPS	Battery-powered systems
CAN	Control area network
DBSCAN	Density-based Spatial Clustering of Application with Noise

DP	Dynamic programming
ECMS	Equivalent fuel consumption minimization strategy
FCPS	Fuel-cell-powered system
GIS	Geographical information system
GPS	Global Positioning System
HEV	Hybrid electric vehicle
HIL	Hardware in the loop
ITS	Intelligent transportation system
MOSFET	Metal-oxide semiconductor field-effect transistor
MPC	Model predictive control
PHEV	Plug-in hybrid electric vehicle
PTO	Power take-off
RAPS	Regenerative auxiliary power system
RLS	Recursive least squares
RMSE	Root mean square error
TSE	Truck stop electrification

Chapter 1
Introduction

Service vehicles, such as refrigerator trucks and tour buses, are equipped with auxiliary devices, including refrigeration systems and cabin air conditioning systems, which consume significant amount of energy. The engine of these vehicles should idle to supply power for auxiliary devices when they stop for a long time, e.g. for loading and unloading goods. The idling time of trucks is estimated between 1,600 and 1,800 hours in a year [1]. Diesel engines have a high efficiency (up to 40%) at highway speeds while their efficiency drops to 1-11% during idling [2], [3]. The average fuel consumption for each truck during idling is estimated at 6,056 L (1,600 gal) per year [4]. Therefore, service vehicles with their frequent idling contributes to greenhouse gas emissions due to increased fuel consumption. That is why anti-idling provisions have existed in many cities in Canada and other countries for at least three decades.

1.1 Motivation

Auxiliary devices of service vehicles must have either a mechanical or an electrical power source. In the former option, as shown in Figure 1-1, the power generated by the engine is transmitted to an engine-driven auxiliary device by a belt and pulley mechanism or a power take-off (PTO). In some applications, such as in heavy-duty refrigerator trucks, an auxiliary engine is employed to supply the auxiliary power. In the latter option, the electrical power generated by an engine-driven generator is consumed by an electric auxiliary device (see Figure 1-2).

One major issue in relation to these configurations is a significant increase of the idling time. As delivery and service vehicles have frequent stops, the engine should operate all the time to supply the power required by auxiliary devices. To reduce idling of service vehicles, many anti-idling systems have been developed recently. As shown in Figure 1-3, a Battery-Powered System (BPS) is a new technology that uses electrical power generated by an engine-driven generator and a battery pack to run the auxiliary devices.

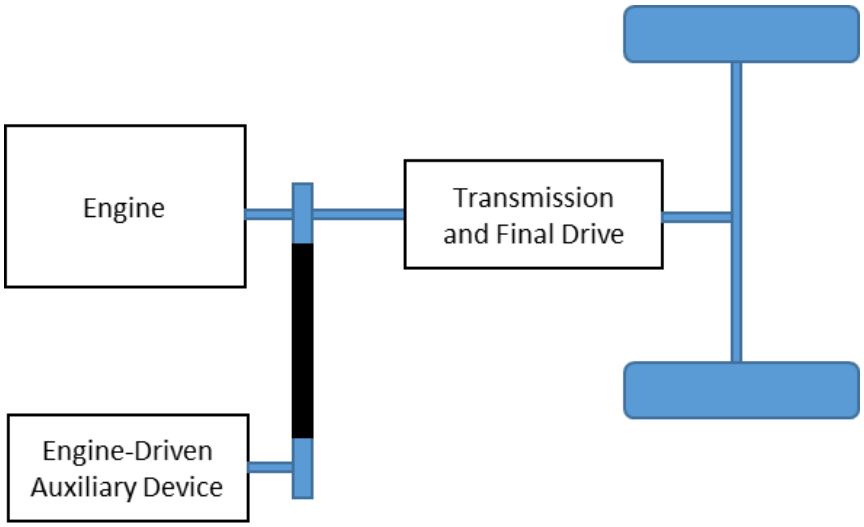

Figure 1-1 Configuration of a vehicle's powertrain system with an engine-driven auxiliary device

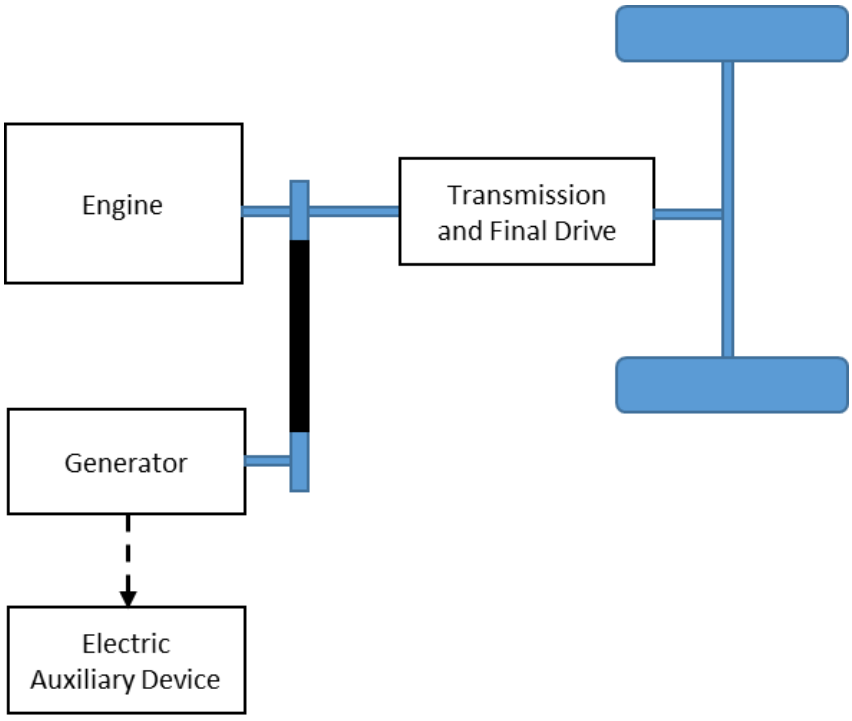

Figure 1-2 Configuration of a vehicle's powertrain system with an electric auxiliary device

A BPS has many advantages over former configurations. In this system, idling can be eliminated as the engine is turned OFF and the battery supplies auxiliary power at engine-OFF stops. In addition, unlike the configuration shown in Figure 1-1, the auxiliary device in BPS can operate at a constant speed (or desired variable speed independent from engine speed), thereby improving its performance and efficiency. This study proposes a new system, called Regenerative Auxiliary Power System (RAPS), which is a great improvement over BPS.

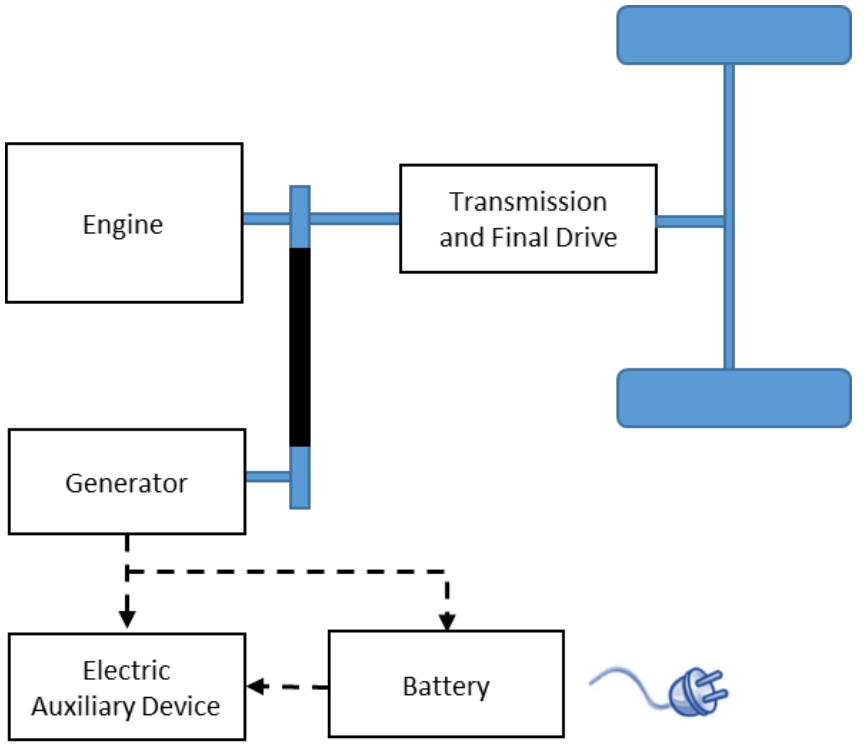

Figure 1-3 Configuration of a vehicle's powertrain system with a BPS

1.2 Regenerative Auxiliary Power System (RAPS)

A regenerative auxiliary power system (RAPS) has components similar to those of BPS (an engine-driven generator, a battery pack, and electric auxiliary devices). However, RAPS enables regenerative braking that lowers fuel consumption and reduces wear on friction braking components. In addition to idle elimination, which is the main objective of all current BPS, the RAPS attempts to reduce fuel

consumption by utilizing an optimal power management system. Therefore, the cost of energy can be noticeably reduced and consequently the cost of replacing components is recouped in a short period of time.

A schematic of a RAPS is illustrated in Figure 1-4. In this system either the main alternator of the vehicle (OEM alternator) or a secondary generator (which can be connected to a power take-off (PTO) unit) is utilized for generating electric power. The battery can be charged by the generator or grid power. Moreover, a control box, which includes a metal–oxide semiconductor field-effect transistor (MOSFET) and a microcontroller, governs the amount of current that should be drawn from the generator for running auxiliary devices and/or charging the battery.

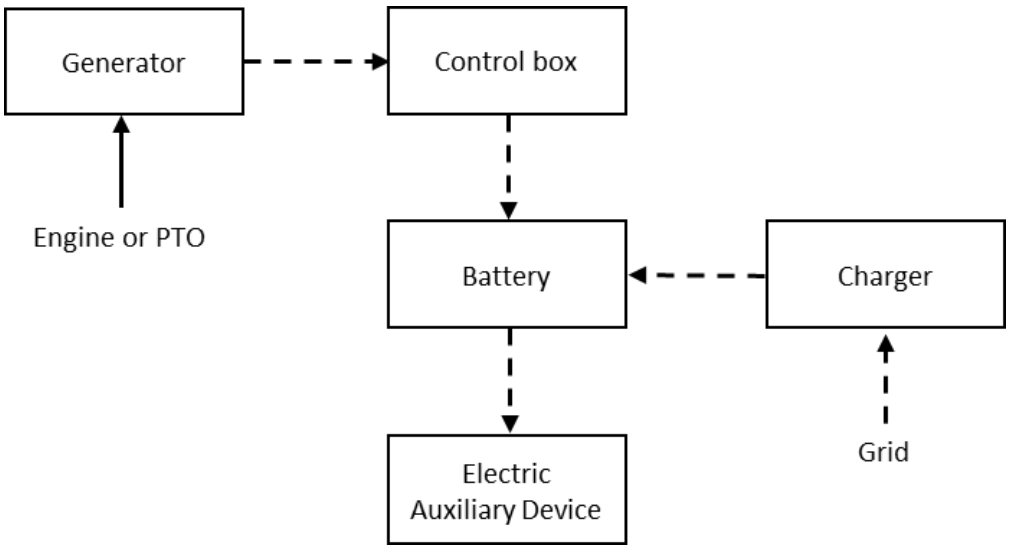

Figure 1-4 A schematic of the RAPS

The RAPS operates in three modes: engine-OFF, traction, and braking. When the engine is OFF all the demanded auxiliary power is supplied by the battery. To ensure the main battery of the vehicle (OEM battery) is not discharged in this mode, a zero signal is sent to the MOSFET to cut off the connection of OEM battery and the battery of the RAPS. Additionally, when the state of the charge (SOC) of the battery reached the minimum allowable value, the RAPS is shut off, and a message is sent to the driver to turn the engine ON for keeping the auxiliary devices ON.

During traction, as shown in Figure 1-5, the generator and the battery either individually or together supply electric power to the auxiliary device. Extra electric power can be also generated by the generator to charge the battery. The optimal split ratio of the auxiliary power between the battery and generator is determined by a power management system.

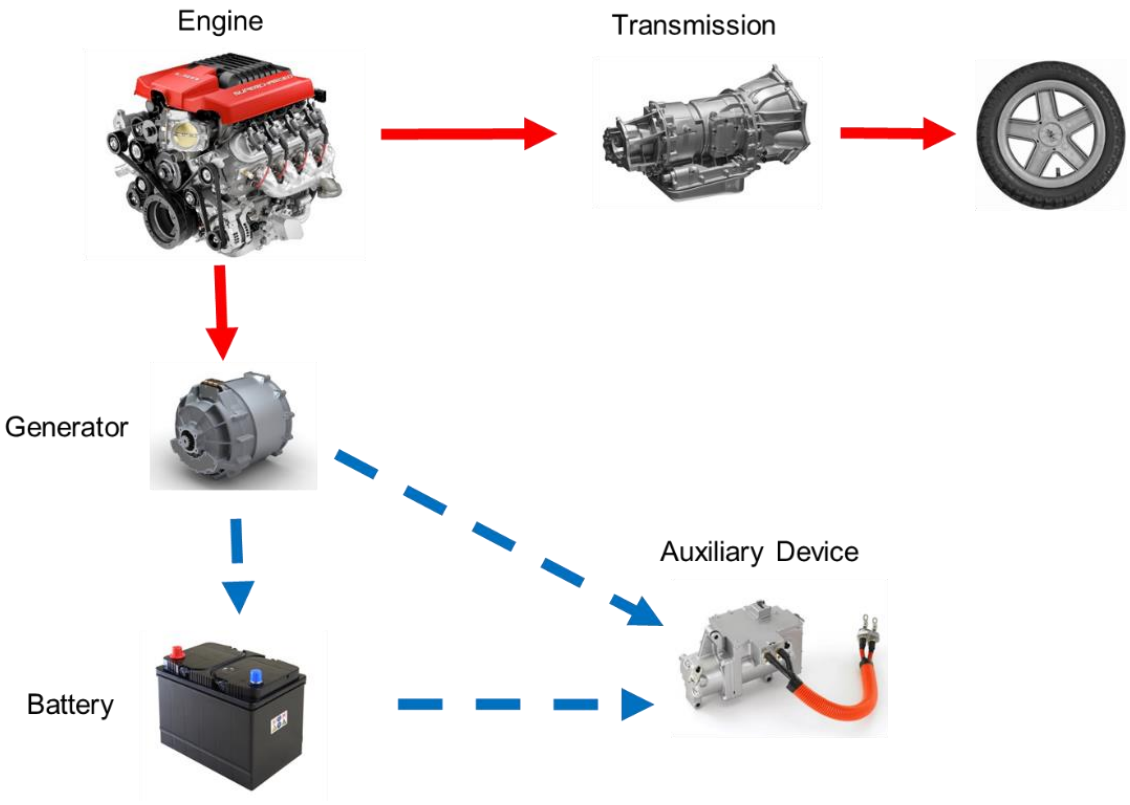

Figure 1-5 Performance of the RAPS during traction

When braking is demanded, as presented in Figure 1-6, a portion of the vehicle kinetic energy can be converted to electrical energy, thereby decelerating the vehicle. This electrical energy can be used to run auxiliary devices and/or stored in the battery. In a case that the regenerated power is less than demand auxiliary power, battery is discharged to provide remaining required power. When generator cannot supply generative braking torque, friction brake is applied as much as required.

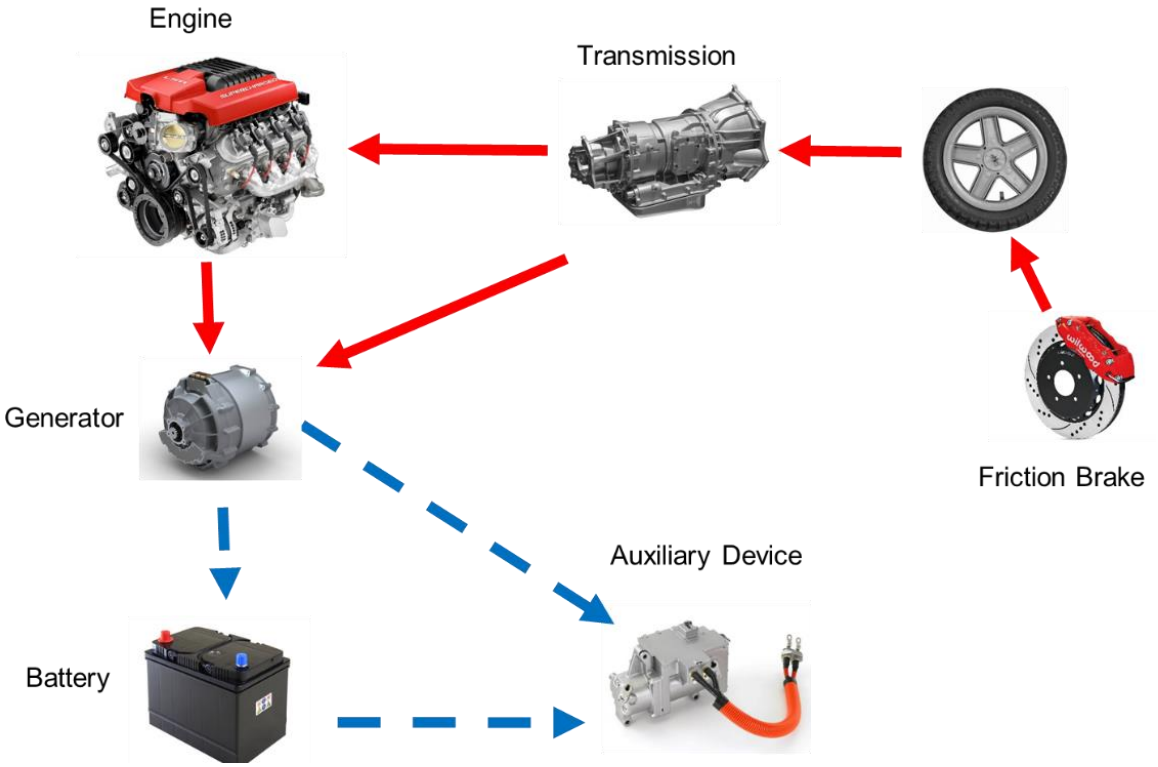

Figure 1-6 Performance of the RAPS during braking

1.3 Problem Statement

Due to the different needs of fleet service vehicles and the power requirements for their auxiliary devices, one RAPS design will not fit all. As a result, necessary tools and methods should be developed and implemented to arrive at an optimum RAPS for a given service fleet. To design an optimum RAPS for a given service fleet, the primary step is to identify drive and service loads. The drive load will indicate the portion of engine power that is required for moving the vehicle. Also, drive load will show the amount of potential power, which can be utilized for charging the battery. On the other hand, the service load will indicate the amount of engine power consumed by engine-driven auxiliary devices. Identification of drive and service loads has two main applications: first, it provides important information for sizing the components of the RAPS, and second, it is essential for an optimum operation of the power management system. Therefore, it is crucial to identify drive and service loads independently. This calls for a new approach, where the power extracted from the engine for the

auxiliary devices can be identified and separated from the power consumed for driving the vehicle. To meet this objective, all the parameters with unknown variation in the vehicle power balance equation should be either measured or estimated.

As stated earlier, in addition to idle elimination, the RAPS attempts to reduce fuel consumption of service vehicles. Since the RAPS has two sources of power, a battery pack and a generator, a power management system is required to determine the split ratio of auxiliary power between them in order to reduce fuel consumption. Moreover, when brake is applied by the driver, the power management system uses the regenerative braking power to run auxiliary devices and the extra power is stored in the battery. The other role of the power management system is to ensure the battery has enough energy for all possible stops that the engine is OFF. This can be achieved using prediction of locations and duration of the stops based on historical data. Therefore, an optimal real-time power management system to meet all these requirements is demanded.

1.4 Objectives

This thesis seeks to develop required tools and methods to achieve following objectives:

- **Drive and Service Loads Identifications**

To determine the size of the RAPS' components, drive and service loads of a given service vehicle should be identified. For this identification, auxiliary power and vehicle mass, as two parameters with unknown variations in the power balance equation of the engine, need to be estimated simultaneously. Vehicle mass individually or together with other parameters, such as road grade, has been estimated by many different methods. Moreover, the auxiliary power is usually obtained by sensor-based methods using extra sensors installed on the vehicle, which is not cost effective or feasible. This research aims to propose a model-based estimation algorithm that utilizes signals available through the vehicle control area network (CAN) to obtain vehicle mass and auxiliary power for identification of drive and service loads. Moreover, to ensure the identification algorithm is reliable in more realistic situations, it should be evaluated by HIL simulations.

- **Real-time Controller for the power management system of the RAPS**

The control scheme of the power management system should discharge and charge the battery so that it has enough energy for all the engine-OFF stops and is ideally fully depleted at the end of a trip, where it can be charged by an external electrical source. Furthermore, the controller needs to determine the optimal split ratio of the auxiliary power between the generator and battery in order to minimize fuel consumption. To achieve these requirements, a two-level control system is required. In the high-level control system, an optimal SOC trajectory for the whole trip is obtained based on the prediction of drive and service loads. The time steps for this level are very large (i.e. from an engine-OFF stop to the next one) to be able to update the SOC trajectory quickly when it is required. In the low-level control system, a real-time controller tracks the SOC trajectory obtained by the high-level control system so that the fuel consumption is minimized.

- **Drive and Service Loads Prediction**

As mentioned earlier, the high-level controller of the power management system takes advantage of the load preview for obtaining the SOC trajectory in order to ensure the battery has enough energy in all engine-OFF stops and it is fully depleted at the end of a trip. Therefore, a method is demanded to predict drive and service loads. Due to the fact that service vehicles have almost the same duty and drive cycles every day, a prediction based on historical data would be reliable. This study attempts to propose a method to predict all the parameters involved in drive and service loads.

1.5 Thesis Outline

The remaining of this thesis is organized as follows:

Chapter 2 reviews the literature on idle-reduction technologies as well as all methods for identification of drive and service loads. Moreover, this Chapter reviews the power management systems of plugin hybrid electric vehicles which have similar configuration to the proposed anti-idling system.

An algorithm for drive and service loads identification is proposed in Chapter 3. The performance of this algorithm is also tested in some numerical simulations.

Chapter 4 presents a test bench that is developed for hardware-in-the-loop (HIL) simulations of service vehicles' powertrain system. The identification algorithm is evaluated by HIL simulations in more realistic situations.

Chapter 5 proposes a power management system for the RAPS. Some simulations are conducted to show the capability of the controller to meet all the defined objectives.

A technique for prediction of drive and service loads, which is required for a better performance of the power management system, is proposed in Chapter 6.

Finally, Chapter 7 discusses the conclusions of this thesis and presents some recommendations for future research in this area.

Chapter 2
Literature Review

In this Chapter, the literature in several areas relevant to the research conducted in this thesis is reviewed.

2.1 Idle Reduction Technologies for Service Vehicles

Engine idling has many drawbacks including emission and noise pollutions, higher fuel consumption, maintenance cost, and driver discomfort [5]. A study by United States Environmental Protection Agency (EPA) in 2008 shows that heavy-duty diesel vehicles can produce up to 34.4 g/hr of CO and 42.3 g/hr of NOx [6]. The idling time and amount of emissions are greater in Canada because of a harsher climate. Many attempts have been made in the last decade to reduce or eliminate idling of service vehicles. Some of these technologies are reviewed in this section and their advantages and disadvantages are discussed.

2.1.1 Truck Stop Electrification

Truck Stop Electrification (TSE) is a stationary terminal that offers a wide range of services including heated and cooled air, internal and external AC power for hotel loads, block heating, chilled or frozen transport refrigeration, satellite television, and high-speed internet access [7]. The available TSE technologies can be categorized into two groups: on-board systems and off-board systems.

In the on-board systems, all the equipment (air conditioning system, heater, inverter, etc.) are installed in the truck. As shown Figure 2-1, external electrical power is transferred to the truck via an extension cord to run on-board equipment. Off-board systems, on the other hand, offer all the services without requiring the operator to have any on-board equipment. As illustrated in Figure 2-2, services including air ducting, 115 VAC power outlets, Ethernet, television, phone connections, and video touch screen are provided via a window interface [7].

The on-board solution costs more for the operator to adapt the vehicle, but this cost is offset by a lower hourly service charge compared to off-board systems. TSE technology can reduce fuel consumption and emissions, and it also increases the quality of life for drivers and increases safety by providing amenities and rest for drivers. The main disadvantage of TSE technology is the limited

number of available electrified parking spots despite the fact that many more trucks on the road need their services. In addition, this solution is more suitable for long-haul trucks, which travel for long distances. As a result, for delivery/service vehicles that have many stops in the cities for loading and unloading, other anti-idling technologies should be considered.

Figure 2-1 Truck stop electrification (TSE), On-board System [8]

Figure 2-2 Truck stop electrification (TSE), Off-board System [8]

2.1.2 Auxiliary Power Unit

An auxiliary power unit (APU) consists of a small internal combustion engine that uses fuel from a truck's fuel tank when the truck's engine is OFF to provide power for auxiliary devices. Fuel consumption of APUs depends greatly on the size of engine and the auxiliary load, but the average fuel consumption is estimated at 0.75-2.0 l/h (0.2-0.5 gal/h) under standard conditions [9]. This value is less than the fuel consumption of the main truck's engine during idling. APUs also address the issue of the TSE technology by allowing the driver the flexibility of stopping the vehicle everywhere a parking spot is available. The main shortcoming of this technology is emissions produced by the auxiliary engine. To resolve this problem, diesel particulate filters (DPF), which are relatively expensive, should be utilized. Moreover, the noise caused by APUs is disturbing for drivers.

2.1.3 Battery-Powered Systems

A Battery-Powered System (BPS) generates required power for auxiliary devices by a battery pack instead of using a small engine. The battery is either recharged by the truck's alternator or an external electrical power supply. This technology offers all the features of APUs without emissions and noise caused by the small auxiliary engine. The number of batteries employed by this system depends on the total demanded auxiliary power. Recharging time is also dependent on the number of batteries, level of depletion, and alternator amperage. The drawbacks of this technology are short battery service life, performance inhibition in extreme ambient temperatures, and limited capacity.

2.1.4 Fuel-Cell-Powered Systems

Fuel-cell-powered systems (FCPS) have received significant scientific attention as a clean and efficient auxiliary power system recently. FCPS based on solid oxide fuel cell (SOFC) and polymer electrolyte membrane fuel cell (PEM FC) have been investigated in the literature extensively [10]–[12]. These systems offer all the benefits of BPS, but many challenges, such as lack of hydrogen fuel supply chain, and use of expensive and exotic materials have prevented FCPS from being commercialized [7]. Another reason that makes FCPS less interesting than BPS is inability of FCPS to capture wasted energy of the vehicle (regenerative braking), which is one of the main goals of this thesis.

2.2 Drive and service Loads Identification

A drive load represents a portion of total power that is required for moving a vehicle. To identify the drive load of a service vehicle, all the associated parameters of resistance forces on the vehicle in longitudinal direction should be either measured or estimated. Vehicle mass, and road grade are two parameters with unknown variations, and there is no measurable signal in the vehicle control area network (CAN) for obtaining these parameters directly. As a result, these two parameters need to be estimated.

A service load represents an amount of power that is consumed by engine-driven auxiliary devices. In most control systems that use longitudinal dynamics, the power consumption of auxiliary devices is neglected. When this amount of power is significant, such as the power consumption of a refrigeration system, the performance of the controller is not reliable. Therefore, an estimation of auxiliary power is required to find accurate delivered power to drive wheels.

2.2.1 Vehicle Parameter Estimation

Vehicle parameter estimation is attainable through two approaches: sensor-based and model-based. In the sensor-based approach, some sensors required for the parameter estimation, which adds manufacturing cost. A model-based approach is a cheaper alternative to the sensor-based estimation. In this method, standard signals available through the vehicle CAN are used for the estimation. Additionally, these two approaches can be used together to provide the needed system redundancy.

In order to implement a parameter estimator in the real vehicle, many qualities should be considered [13]:

- **Simple:** The estimation algorithm should be simple enough to be capable of operating online with fast computational time.
- **Accurate:** Based on the application of the estimator, the error of the parameter estimation should be small enough.
- **Fast:** The rate of convergence should be fast enough for detecting parameter variations.
- **Robust:** The estimation algorithm should be robust to disturbances such as variations of wind speed and road conditions.

- **Inexpensive:** The estimation algorithm should be implementable inexpensively to be viable, especially for economy-priced vehicles.

2.2.2 Vehicle Mass Estimation

A considerable amount of literature has been published on the estimation of the vehicle mass. These studies can be classified based on the dynamics that is used for the estimation. Explicitly, the literature presents mass estimation methods based on suspension, powertrain, lateral, and longitudinal dynamics [13].

Suspension deflection can provide good information for the vehicle mass estimation. This can be measured by installing a sensor on the suspension. Rajamani et al. used this method to design an adaptive observer for estimating suspension states and parameters including the vehicle mass [14]. Moreover, Zarringhalam et al. used suspension dynamics along with longitudinal and pitch dynamics to estimate the vehicle mass, pitch moment of inertia, and height of the center of gravity [15].

Powertrain dynamics can be also used for the estimation of the vehicle mass. Fremd in [16] showed that " The natural oscillation in transmission line of a motor vehicle and the mass of motor vehicle are in a one-to-one relationship if the instantaneous transmission ratio remains unchanged". He estimated the vehicle mass by measuring the natural frequency of the vehicle's cardan shaft.

The relationship between lateral forces and lateral acceleration is affected by the vehicle mass. Therefore, handling dynamics can be used to estimate the vehicle mass. Best et al. in [17] as well as Wenzel et al. in [18] used lateral dynamics to estimate states and parameters (including mass) by applying extended Kalman filter and dual extended Kalman filter, respectively.

The vehicle mass also impacts the relationship between longitudinal forces and longitudinal acceleration. Literature presents many different algorithms using longitudinal dynamics to estimate the vehicle mass along with other vehicle states and parameters. Rhode et al. used longitudinal dynamics to estimate vehicle driving resistance parameters [19]. They used recursive least squares (RLS) algorithm with exponential forgetting factors to estimate the vehicle mass, rolling resistance coefficient, and drag coefficient.

Some studies used sharp longitudinal acceleration and deceleration to estimate the mass. Considering the vehicle mass is excited significantly during these events, the estimation will results in a more accurate result. Breen in [20] proposed a method to estimate the vehicle mass by measuring applied braking force. Similar methods are presented by Klatt and Reiner et al. in [21] and [22], respectively. In addition, Genise determined vehicle mass immediately after upshifts of a transmission by measuring the engine torque and vehicle acceleration [23]. Zhu et al. suggested a similar approach to estimate the vehicle mass and drag coefficient in [24] and [25].

2.2.3 **Road Grade Estimation**

Many sensor-based and model-based approaches for the road grade estimation can be found in the literature. One of the earliest sensors for measuring the road grade was a patent by Gaeke [26]. He used the road grade signal to refine the wheel brake pressure command. Most recent sensor-based approach for estimating the road grade have employed a Global Positioning System (GPS) unit [27], [28]. These methods need accurate GPS devices, and cannot work properly with low cost GPS, which are expected to be standard in the next few years [29]. However, some methods have been proposed to estimate road grade by using commonly available GPS along with sensor fusion algorithm such as extended Kalman filter [30]. Furthermore, the road grade information can be obtained by using other sensors such as accelerometer [31], [32].

Model-based road grade estimation was first proposed by Lingman et al. in [33]. They used Kalman filtering to process measured or estimated propulsion force and measured vehicle speed to estimate the road grade. Many model-based estimation methods for estimating the road grade along with the vehicle mass have been presented in the literature, which will be discussed in the next part.

2.2.4 **Simultaneous Vehicle Mass and Road Grade Estimation**

Considerable research has been done for simultaneous vehicle mass and road grade estimation in the past few years. In the sensor-based approach, the road grade is usually estimated using sensors, and the vehicle mass is estimated using a parameter estimation algorithm [27], [31]. In the model-based approach, typically longitudinal dynamics is utilized to estimate the vehicle mass and road grade. Vahidi et al. proposed Recursive Least Squares (RLS) with multiple forgetting factors for this estimation [34]–[36]. They showed that "if the chosen forgetting factors reflect relative rate of variation

of the parameters, both parameters can be estimated with good accuracy." In another research, a two-stage estimator was proposed by McIntyre et al. for the estimation of a heavy-duty vehicle mass and road grade [37]. In the first stage, a similar RLS method used to determine the vehicle mass and an estimate for a constant road grade. In the second stage, a nonlinear estimator that provides a more-accurate estimate of the road grade was developed. Winstead et al. combined an Extended Kalman Filter (EKF) to generate estimation of the vehicle mass and road grade and a Model Predictive Controller (MPC) to control vehicle speed trajectory [38]. Finally, Mahyuddin et al. designed an adaptive nonlinear observer for the estimation of the mass and road grade by using vehicle speed and driving torque [39].

Many control systems in the vehicle, particularly heavy-duty ones, require simultaneous estimation of the road grade and mass. These control systems can be categorized as follows:

- Vehicle longitudinal control (traction and braking) [40], [41]
- Cruise control [42]–[44]
- Space control for automated vehicles [45], [46]
- Transmission shift scheduling
- Energy control strategy of hybrid vehicles

2.2.5 Auxiliary Power Estimation

A limited number of studies have been done for the estimation of vehicle's auxiliary power. Matsubara et al. proposed an estimator device for torque estimation of a variable displacement compressor [47]. They calculated the torque required for driving the compressor based on the compressor signal. This device requires many sensors such as temperature sensor, pressure sensor, and rotational speed sensor for the estimation. Most other similar algorithms such as those reported in [48] and [49] need same sensors, which may not be cost-effective.

2.3 Power Management System of PHEVs

In the literature, there is no study focused on the power management system of BPS; however, reviewing control strategies of PHEVs, with similar configuration to BPS, will provide a good insight

into designing an optimal power management system. The power management system of PHEVs can be categorized into two main groups: Rule based and Optimization based.

2.3.1 Rule-Based Control Strategies

In the rule-based control strategy, predefined rules are set to operate the HEV at its highest efficiency point without any prior information about the trip [50]. Most popular rule-based control strategies are Max-SOC, and Engine ON-OFF (Thermostat) [51]. The rules in the Max-SOC use the engine as a main source of power, and the electric motor is utilized only when demand power is greater than the power engine can produce. Furthermore, when the power demand is less than the power that the engine can generate while operating on its optimum line, the motor works as a generator and use the remaining power of the engine to charge the battery until it reaches the maximum allowable SOC. In the thermostat control strategy, the engine goes OFF when the SOC of the battery reaches a maximum value, and the vehicle operates in the electric mode only. The engine is turned ON again when the SOC reaches the low setting. The performance of rule-based control strategies can be improved by utilizing fuzzy logic control methods. The main advantages of fuzzy rule-based strategies is their robustness against measurements error and their adaptation since the fuzzy rules can be easily tuned [52]. Li *et al.* have proposed a fuzzy control strategy that determines torque ratio of the engine and the electric motor [53]. This method ensures the engine operates in the neighborhood of optimal region while prevents the battery from over-discharging.

2.3.2 Optimization-Based Control Strategies

Although rule-based control strategies are easy to be implemented, their performance can be far from optimal solutions as they do not use prior information to do the optimization for the whole cycle. Optimization-based control strategies find an optimal split ratio between sources of power in order to minimize a cost function, which is usually the cost function of fuel consumption. These control strategies can be categorized into two groups; Global Optimization, and Real-Time Optimization.

Global optimization is a non-causal method since it needs full knowledge of future driving cycles to find minimum fuel consumption. This method is also highly computationally demanding, and it is not possible to be processed by standard vehicle on-board processors. Therefore, it cannot be implemented as a real-time controller, but it can be used to design rules for rule-based control strategies, and it is a good benchmark to evaluate the performance of other controllers. The most popular technique

to obtain the global optimal solution for the power management controller of hybrid vehicles is Dynamic Programming (DP) [54]. To address the problems associated with real-time implementation of DP, many research has been conducted recently. Since trip prediction has been greatly improved by rapid development of intelligent transportation systems (ITS), geographical information systems (GIS), and global positioning systems (GPS) [55]–[57], a rout preview with a good level of accuracy is available for the DP. Gong et al. proposed a driving cycle modeling using traffic information in order to implement a DP-based power management scheme for PHEVs [58]. Furthermore, the authors in another study proposed a two-scale DP to reduce computational effort of this technique [59]. In this method, the driving cycle was first obtained with averaging of the historical data, and SOC profile was found by solving the macro-scale DP problem. Then, the whole trip was divided into a number of segments, and for each segment a smaller DP was solved using online traffic information. The SOC obtained in the macro-scale DP solution at terminal location was reinforced to be the final value.

On the other hand, real-time control optimization is a casual method as they only use past and current information to minimize the cost function. Model Predictive Control (MPC) and Equivalent Fuel Consumption Minimization Strategy (ECMS) are two widely used real-time control schemes for the power management of PHEVs. MPC is a model-based method with the advantage of solving nonlinear constrained optimization problem that is performed over a moving finite horizon. Taghavipour et al. showed the effectiveness of this method on minimizing fuel consumption of PHEVs [60]. ECMS is a method that seeks to find real-time suboptimal solution for the power management system of hybrid vehicles [61]. In this method, instantaneous sum of actual fuel consumption and equivalent fuel consumption of the power used by the battery is minimized. An equivalent weight factor is required to find the equivalent fuel consumption of the electrical energy, which is stored in or drawn from the battery. If a big value is selected for the equivalent weight factor, discharging battery is penalized and more fuel is consumed. However, a small equivalent weight factor leads to more usage of electrical energy, thereby decreasing battery SOC [62], [63]. As a result, this parameter should be tuned so that the SOC reaches the minimum allowable value at the end of a trip. To achieve this goal, a-priori knowledge of the driving cycle is required, and the equivalent weight factor can be determined offline by an iterative search or optimization method. To address this problem and implement this strategy online, Adaptive Equivalent Fuel Consumption Strategy (A-ECMS) that updates equivalent weight factor online was proposed [64]. Many different methods for adaptation of the equivalent weight factor has been proposed. These method can be categorized into three groups [65]:

- Adaptation based on driving cycle prediction [66], [67]
- Adaptation based on driving pattern recognition [68]
- Adaptation based on affine function of SOC error

The third option is the most popular method for the adaptation of the equivalent weight factor. In this method, the equivalent weight factor is changed dynamically in order to maintain SOC around a reference value. The affine function of SOC error can be based on a P controller [69], a PI controller [70], [71], or a PI controller along with a tangent function of SOC [72].

2.4 Chapter Summary

This chapter reviewed idle reduction technologies for service vehicles. Among all these technologies, battery-powered systems (BPS) was the best option to be implemented on service vehicles. However, this technology can be greatly improved by a new system that is introduced in this study. This chapter also reviewed the literature on the estimation of the parameters involved in drive and service loads. In the literature, there was no study focused on power management system of BPS; however, control strategies of PHEVs, with similar configuration to BPS, were briefly reviewed.

Chapter 3
Identification of Drive and Service Loads

Drive and service loads identification is a primary step for determining the size of RAPS components. In order to identify these loads, all the parameters in the vehicle power balance equation should be measured; otherwise, an estimation of each is necessary. In the vehicle power balance equation, power of engine-driven auxiliary devices, vehicle mass, and road grade are the parameters with unknown variations. The auxiliary power can be time varying during a driving cycle. For example, in a refrigerator truck, power consumption of the refrigerator changes with respect to the evaporator and condenser temperatures. In addition, vehicle mass can be different from one driving cycle to another depending on the freight load. This can change up to 500% from loaded to unloaded [73], [74]. Moreover, a small change in the road grade can affect the torque response of a heavy-duty vehicle considerably [27]. Although road grade information is not available in the vehicle CAN bus, it can be provided by employing a GPS unit in the vehicle. Therefore, auxiliary power and vehicle mass are two parameters that require estimation.

3.1 Vehicle Power Balance Model

The system model can be obtained by balancing the vehicle power. That is, the generated power by the engine is equal to the power required for moving the vehicle, i.e. drive load, plus the power consumed by the engine-driven auxiliary devices, i.e. service load:

$$P_{eng} = P_{dl} + P_{sl} \tag{3-1}$$

The generated power by the engine (P_{engine}) is equal to:

$$P_{eng} = T_e \omega_e \tag{3-2}$$

where T_e is the engine torque, and ω_e is the engine rotational speed.

The drive load (P_{dl}) is the portion of engine power required to accelerate/decelerate the vehicle and its driveline, to overcome the gravity force due to road grade, and to overcome resistance forces due to rolling resistance, aerodynamic forces, and driveline friction (see Figure 3-1) [75]:

$$P_{dl} = \left(M\dot{u} + F_A + F_g + F_{RR}\right)\frac{u}{\eta_{dl}} + \left(I_e + I_t + \frac{I_d}{N_t^2} + \frac{I_w}{N_{tf}^2}\right)\dot{\omega}_e\omega_e \tag{3-3}$$

where *M* is the total vehicle mass (i.e. curb mass plus cargo mass), u is the vehicle longitudinal speed, $\dot{u}$ is the vehicle longitudinal acceleration, F_A is aerodynamics resistance, F_g is grade resistance, F_{RR} is tire rolling resistance, η_{dl} is the efficiency of driveline, I_e is rotational inertia of the engine, I_t is rotational inertia of the transmission, I_d is rotational inertia of the driveshaft, I_w is rotational inertia of the wheels and axles shafts, N_t is the transmission ratio, N_{tf} is the combined ratio of the transmission and final drive, ω_e is the engine rotational speed, and $\dot{\omega}_e$ is the engine rotational acceleration.

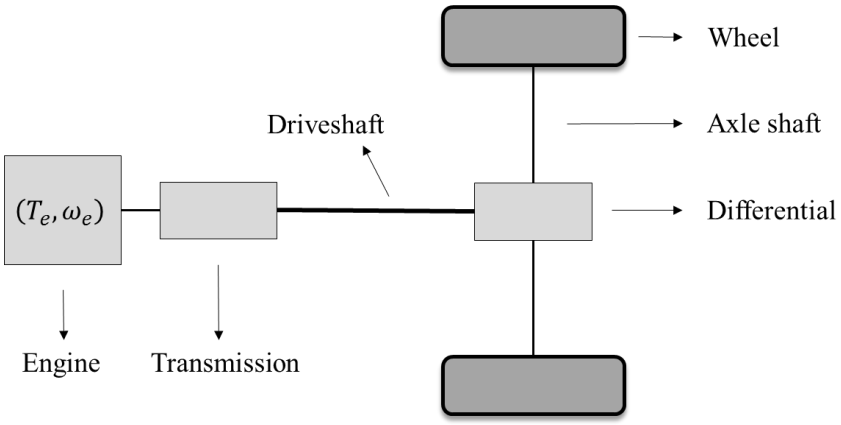

Figure 3-1 Driveline components of the vehicle

To simplify the second term on the right-hand side of the Equation (3-3), the inertia of all the components can be replaced by I_{tot}. Therefore, this equation can be rewritten as:

$$P_{dl} = \left(M\dot{u} + F_A + F_g + F_{RR}\right)\frac{u}{\eta_{dl}} + I_{tot}\dot{\omega}_e\omega_e \tag{3-4}$$

Finally, by substituting the following equations for F_A, F_g, and F_{RR}, P_{dl} can be defined as:

$$F_A = \frac{1}{2}\rho C_D A_f u^2 \tag{3-5}$$

$$F_g = Mg\ \sin\alpha \tag{3-6}$$

$$F_{RR} = C_{rr}Mg\ \cos\alpha \tag{3-7}$$

$$P_{dl} = \left(M\dot{u} + \frac{1}{2}\rho C_D A_f u^2 + Mg\ \sin\alpha + C_{rr}Mg\ \cos\alpha\right)\frac{u}{\eta_{dl}} + I_{tot}\dot{\omega}_e\omega_e \tag{3-8}$$

where ρ is the mass density of the air, C_D is the coefficient of aerodynamic resistance, A_f is the frontal area of the vehicle, g is the acceleration due to gravity, α is the angle of slope, and C_{rr} is the coefficient of rolling resistance.

The service load (P_{sl}) is the amount of power consumed by auxiliary devices that are connected to the engine:

$$P_{sl} = T_{aux}\omega_e \tag{3-9}$$

where T_{aux} is the torque of auxiliary devices. In the above equation, it is assumed the auxiliary devices are driven at the same speed as the engine. A transmission factor is required when the assumption is not valid.

By substituting Equations (3-2), (3-8), and (3-9) into Equation (3-1), the power balance of the vehicle can be rewritten as follows:

$$T_e\omega_e = \left(M\dot{u} + \frac{1}{2}\rho C_D A_f u^2 + Mg\ \sin\alpha + C_{rr}Mg\ \cos\alpha\right)\frac{u}{\eta_{dl}} + I_{tot}\dot{\omega}_e\omega_e + T_{aux}\omega_e \tag{3-10}$$

The vehicle speed can be related to engine speed by:

$$u = \frac{R\omega_e}{N_{tf}} \tag{3-11}$$

where *R* is the tire radius. Finally, Equation (3-10) and (3-11) can be combined to obtain system model as:

$$T_e = \left(M\dot{u} + \frac{1}{2}\rho C_D A_f u^2 + Mg\ sin\alpha + C_{rr}Mg\ cos\alpha\right)\frac{R}{N_{tf}\ \eta_{dl}} + I_{tot}\dot{\omega}_e + T_{aux} \tag{3-12}$$

To implement a parameter estimation algorithm, which will be described in the next section, the system model should be discretized. Therefore, Equation (3-12) can be approximated by the Euler's method [76]:

$$\begin{aligned} T_e(k) = \Bigg(M\frac{u(k)-u(k-1)}{\Delta t} + \frac{1}{2}\rho C_D A_f u(k)^2 + Mg\ sin\alpha(k) \\ + C_{rr}Mg\ cos\alpha(k)\Bigg)\frac{R}{N_{tf}\ \eta_{dl}} + I_{tot}\frac{\omega_e(k)-\omega_e(k-1)}{\Delta t} + T_{aux}(k) \end{aligned} \tag{3-13}$$

where Δt is step size, and k denotes the discrete time instant.

In Equation (3-13), engine torque (T_e), vehicle speed (u), and engine speed (ω_e) are the signals available through the vehicle control area network (CAN). The acceleration signal is provided by the vehicle accelerometer, and in a case that this signal is not available, it can be obtained from the vehicle speed. By comparing the engine speed and vehicle speed, combined ratio of the transmission and final drive (N_{tf}) can be calculated. Moreover, road grade (α) is assumed to be provided by a GPS receiver. Inertia of driveline components (I_{tot}), efficiency of driveline (η_{dl}), rolling resistance coefficient (C_{rr}), mass density of the air (ρ), coefficient of aerodynamic resistance (C_D), and frontal area of the vehicle (A_f) are vehicle's parameters and are known. Therefore, the only unknown parameters will be the vehicle mass (M) and the torque of auxiliary devices (T_{aux}) that need to be estimated.

3.2 Estimation Method

For the online estimation of the vehicle mass and auxiliary torque, a Kalman filter method is used. The Kalman filter is a recursive solution to the discrete–data linear filtering problem, which was first developed by Rudolf E. Kalman in 1960 [77]. The Kalman filter is a method that provides an efficient computational means to estimate the state of a process, in a way that minimizes the mean of the squared errors. This method supports estimations of past, present, and even future states when the precise model of the system is unknown [78].

Usually the Kalman filter is applied as an observer for the estimation of states. However, it can be also applied for the parameter estimation. To treat parameters as states, the following equation can be generated for the parameter estimation problem [79]:

$$\begin{aligned} \theta(k) &= \theta(k-1) + w(k) \\ z(k) &= \theta^T(k)\phi(k) + v(k) \end{aligned} \tag{3-14}$$

where $\theta(k)$ represents the n-dimensional unknown system parameter vector, $z(k)$ is process output, $\phi(k)$ is the regression vector, $w(k)$ is a vector denote parameters variation at time instant k, and $v(k)$ is measurement noise. It is assumed that $w(k)$ and $v(k)$ are Gaussian process with zero mean value.

The goal of this method is to find the model output ($\hat{z}$) that best approximates the process output (z) with the minimal sum of squared error (see Figure 3-2).

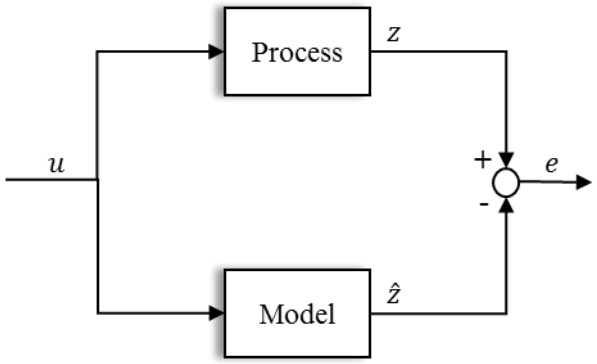

Figure 3-2 Process and model outputs

The model output can be calculated as follows:

$$\hat{z}(k) = \hat{\theta}_1(k)\phi_1(k) + \hat{\theta}_2(k)\,\phi_2(k) + \cdots + \hat{\theta}_n(k)\phi_n(k) \tag{3-15}$$

To find the best model output ($\hat{z}$), the Kalman filter finds the best linear combination of regressors (ϕ_i) by optimizing the unknown parameters ($\hat{\theta}_i$). The first step for the parameter estimation is to form a parametric model of the system [80]. To achieve this goal, one must gather the unknown parameters i.e. M and T_{aux} in a vector and express them in the form of a parametric model:

$$z(k) = \theta^T(k)\phi(k) \tag{3-16}$$

where z is the actual output, θ represents the actual values of the parameters, and ϕ is the regression vector. Since Equation (3-13) is in a nonlinear form, the unknown parameters are selected as $\frac{1}{M}$ and $\frac{1}{M}T_{aux}$ to be able to form a parametric model as follows:

$$\begin{cases} z(k) = \left(\dfrac{u(k)-u(k-1)}{\Delta t} + g\,\sin\alpha(k) + C_{rr}g\,\cos\alpha(k)\right)\dfrac{R}{N_{tf}\eta_{dl}} \\ \theta(k) = \left[\dfrac{1}{M} \quad \dfrac{1}{M}T_{aux}(k)\right]^T \\ \phi\,(k) = \left[T_e(k) - I_{tot}\dfrac{\omega_e(k)-\omega_e(k-1)}{\Delta t} - \dfrac{R}{2N_{tf}\eta_{dl}}\rho C_D A_f u(k)^2 \quad -1\right]^T \end{cases} \tag{3-17}$$

The next step is to form an estimation model that is the same as a parametric model with estimated values of the unknown parameters:

$$\begin{cases} \hat{z}(k) = \hat{\theta}^T(k)\phi(k) \\ \hat{\theta}(k) = [\hat{\theta}_1(k) \quad \hat{\theta}_2(k)]^T \end{cases} \tag{3-18}$$

where $\hat{z}$ is the model output and $\hat{\theta}$ represents the estimated values of the parameters.

The estimation error is the difference between the output of the parametric and the estimation models. This reflects the distance between θ and $\hat{\theta}$ and is defined by:

$$e(k) = z(k) - \hat{z}(k) \tag{3-19}$$

Now, the estimation error is used to drive the adaptive law that generates $\hat{\theta}(k)$ online. The Kalman filter calculates the new parameter estimate $\hat{\theta}(k+1)$ at a time instant $(k+1)$ by adding a correction vector to the previous parameter estimate $\hat{\theta}(k)$ at time instant (k):

$$\hat{\theta}(k+1) = \hat{\theta}(k) + K(k)e(k) \tag{3-20}$$

where K is the Kalman gain that is calculated by:

$$\begin{cases} K(k) = \dfrac{P(k)\phi(k)}{R_2 + \phi^T(k)P(k)\phi(k)} \\ P(k+1) = P(k) + R_1 - K(k)\phi^T(k)P(k) \end{cases} \tag{3-21}$$

where $P(k)$ is the estimation error covariance, R_1 and R_2 are covariance matrices of process and measurement noise. Note that if we select $R_1 = 0$ and $R_2 = 1$, then this equation becomes standard least-squares algorithm, which is usually used where the parameters are constant.

The Kalman filter can track time-varying parameters reasonably well as long as its gain vector $K(k)$ keeps away from zero. A nonzero gain vector is guaranteed if the covariance matrix satisfies the matrix inequality [81]:

$$P(k) \geq \alpha I, \tag{3-22}$$

where α is a positive scalar. Therefore, a good Kalman filter in terms of tracking performance can be designed by choosing a suitable matrix sequence $R_1 \geq 0$ to guarantee above-mentioned matrix inequality for some appropriate positive number α. The diagonal entries of R_1 should be chosen based on how fast the corresponding parameter changes with respect to time. As a result, if a parameter is known to change quickly, the corresponding entry in R_1 should be large and vice versa [79]. Considering the vehicle mass is constant and the auxiliary torque is time varying during a driving cycle, this procedure helps to control the forgetting individually for each parameter. Furthermore, measurement noise covariance is usually measured prior to the filter operation by taking some off-line

sample measurements. In order to obtain the best performance of the filter, these covariance matrices should be frequently tuned off-line [78].

The stability of the Kalman filter is generally guaranteed if the covariance matrix satisfies the matrix inequality [81]:

$$P(k) \leq \beta I \tag{3-23}$$

for some scalar $\beta > 0$.

Equations (3-22) and (3-23) not only guarantee the tracking ability and stability of the Kalman filter, but also ensure some basic convergence properties. For the more details about the Kalman filter based estimation algorithm and its proof of stability and convergence, interested readers are referred to [82]–[84].

In many practical problems, prior knowledge about parameters that shows where they are located in R^n may be available. This knowledge usually comes in terms of upper or lower bounds. This procedure that constrains estimation of parameters in the set where the parameters are located is called parameter projection [85]. In the problem in hand, a condition is required to avoid $\widehat{M} = 0$. To achieve this condition, the projection algorithm must be utilized. This algorithm keeps $\widehat{M} > M_{min}$ while maintaining stability and convergence of the Kalman filter. Additionally, it is obvious that the auxiliary torque is a positive value. Therefore, $T_{aux} \geq 0$ can be added as another condition.

3.3 Simulation Results

To simulate performance of the estimation algorithm, a refrigerator truck with the specifications listed in Table 3-1 is selected. The refrigeration system of this vehicle has an engine-driven compressor with performance curve presented in Figure 3-3. This curve shows that the power consumption of the compressor has a linear relationship with its speed. Therefore, the compressor has a constant torque of $45\ Nm$ at all engine speeds. It should be noted that the refrigeration system has an ON/OFF control scheme.

Table 3-1 Specification of a service vehicle

Symbol	Parameter	Value
M	Total mass of vehicle and freight	6000 kg
R	Tire radius	0.387 m
C_{rr}	Coefficient of rolling resistance	0.015
C_D	Drag coefficient	0.4
A_f	Frontal area	3.23 m^2
ρ	Air density ($T = 20$ ℃)	1.204 $kg.m^{-3}$

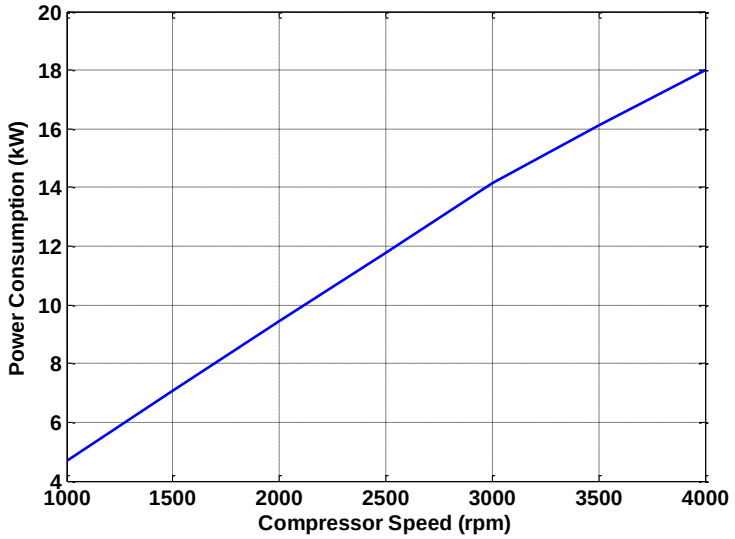

Figure 3-3 Performance curve of the refrigeration system's compressor

Two case scenarios are considered for the simulations: (I) the compressor is OFF at the beginning of the drive cycle, (II) the compressor is ON when the vehicle starts moving. Also, to show the performance of the estimation algorithm in both highway and city cycles, the simulations have been done for FTP-75 and HWFET driving cycles.

Simulation results for a scenario are shown in Figure 3-4. As it can be seen, there is an error in the estimated parameters when the auxiliary device turns ON or OFF until both parameters converge to their actual values again. If this change occurs when the system has low excitation (i.e. small variation in vehicle speed), the convergence time is increased. To address this issue, a two-stage estimation algorithm is considered, which will be described below.

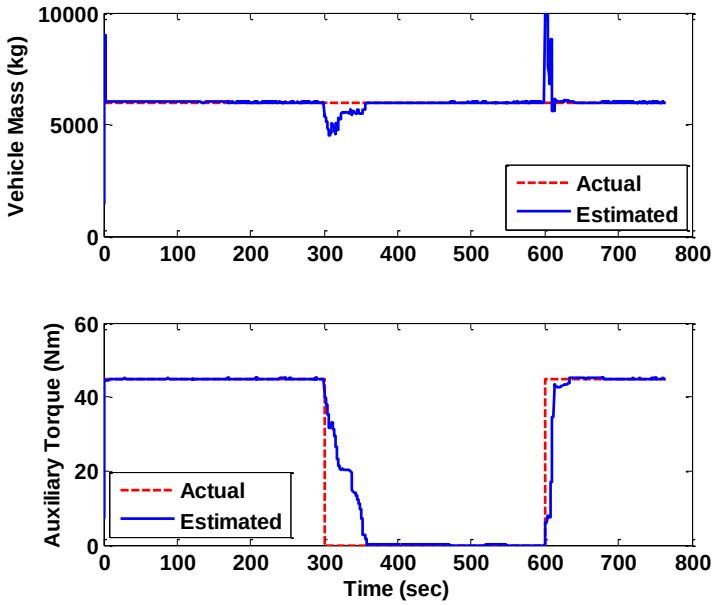

Figure 3-4 Error in estimation when the auxiliary device turns ON or OFF

3.3.1 Algorithm Improvement (Two-Stage Estimation)

During a driving cycle, vehicle mass is almost constant and the torque of auxiliary device is time-varying. However, when the torque of auxiliary device changes, estimated vehicle mass oscillates until the convergence of both parameters. It is obvious that vehicle mass does not change during a driving cycle. Therefore, a condition is added to the estimation algorithm to improve the results. According to this condition, there are two stages for the estimation. In the first stage, the algorithm works until it estimates an acceptable value for the vehicle mass. In the next stage, the vehicle mass is kept on the estimated value, and thus the torque of auxiliary device can be estimated. The parametric model of the second stage can be defined as:

$$\begin{cases} z_{s2}(k) = \left(\dfrac{u(k)-u(k-1)}{\Delta t} + g\,\sin\alpha(k) + C_{rr} g\,\cos\alpha(k)\right)\dfrac{R}{N_{tf}\eta_{dl}} - \\ \qquad \dfrac{1}{M_{est}}\left(T_e - I_{tot}\dfrac{\omega_e(k)-\omega_e(k-1)}{\Delta t} - \dfrac{R}{2N_{tf}\eta_{dl}}\rho C_D A_f u(k)^2\right) \\ \theta_{s2}(k) = T_{aux} \\ \phi_{s2}(k) = -\dfrac{1}{M_{est}} \end{cases} \tag{3-24}$$

where M_{est} is the estimated vehicle mass, which has been obtained from stage one. Other parts of the estimation algorithm operate the same as stage one.

As presented in Figure 3-5, when the system error (e) is less than a predefined value in a long enough period of time, the estimation algorithm goes from stage one to stage two. The required parameters for defining this condition should be tuned for each specific vehicle by a trial and error method.

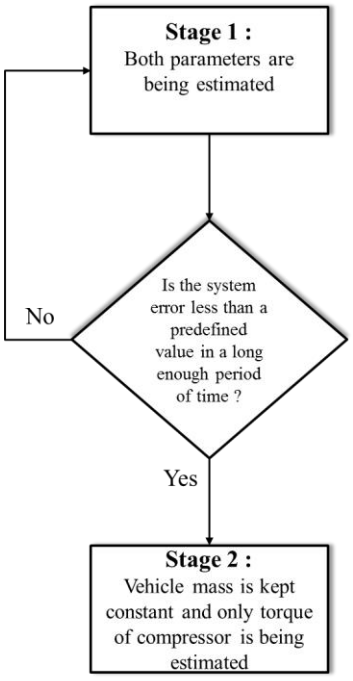

Figure 3-5 Two-stage estimation of mass and torque of auxiliary device

After applying this condition to the estimation algorithm, the previously defined scenarios are simulated and presented in the subsequent sections.

3.3.2 FTP-75 Driving Cycle

FTP-75 is a city driving cycle based on Urban Dynamometer Driving Schedule (UDDS), which simulates an urban rout with frequent stops. Figure 3-6 and Figure 3-7 illustrate the estimation of the parameters in FTP-75 driving cycle. The results show that actual and estimated values are in a good agreement in most of the time. By adding the condition described in Section 3.3.1 to the algorithm, vehicle mass is kept constant until the end of the driving cycle. Therefore, when the auxiliary device turns ON or OFF, no error is added to the estimated parameters. In addition, Table 3-2 shows percent mass error and root-mean-square (RMS) error in the auxiliary torque. This table also summarizes RMS error in identified drive and service loads that can be obtained by substituting the estimated values into Equation (3-8) and (3-9). Furthermore, a comparison of the estimation errors between two-stage and one-stage estimation algorithms is available in this table. This comparison states that the final value of the vehicle mass obtained by the one-stage estimation algorithm may have smaller error, but the errors in identified drive and service loads are considerably decreased by employing the proposed two-stage algorithm.

3.3.3 HWFET Driving Cycle

HWFET is a highway driving cycle, which simulates a high-speed cycle with no stops. Figure 3-8 and Figure 3-9 depict the estimation of the parameters in HWFET driving cycle. In this driving cycle, actual and estimated values are in a good agreement too. Despite the fact that a vehicle in a highway cycle has small speed variations, which results in poor excitation of the regressor matrix, the Kalman filter is able to estimate the parameters at the beginning of the cycle with more excitation (the vehicle has high acceleration when it starts moving). As a result, the estimation algorithm switches to the second stage quickly, and consequently the auxiliary torque in the middle of the cycle with low excitation is estimated very well. Table 3-3 summarizes estimation errors for this driving cycle. The errors in the identified drive and service loads by one-stage algorithm in this driving cycle is even worse because when the auxiliary device turns ON or OFF, the convergence rate is slower on account of poor excitation in the highway cycle.

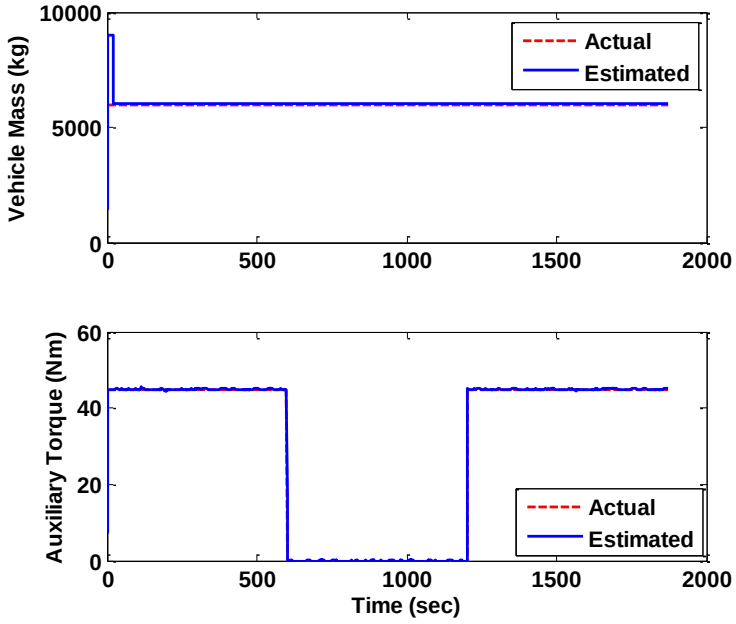

Figure 3-6 Estimation of vehicle mass and auxiliary torque in case scenario (I) during FTP-75 driving cycle

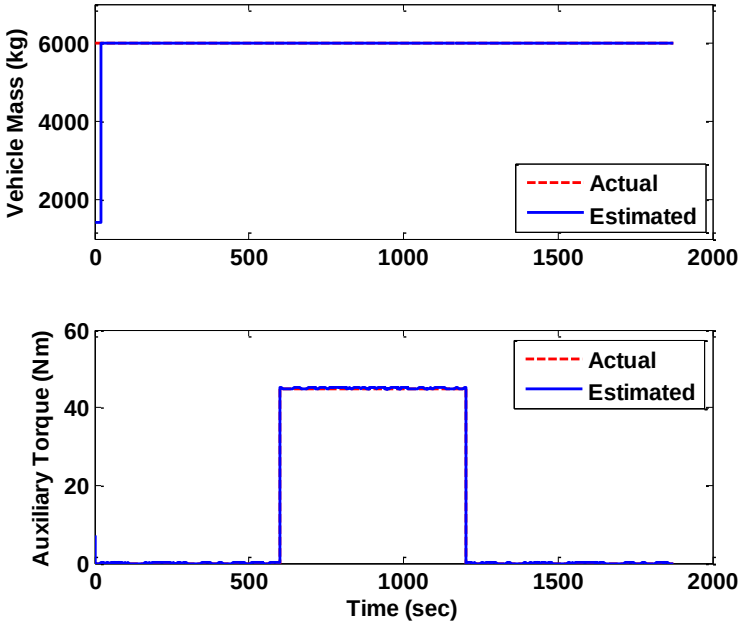

Figure 3-7 Estimation of vehicle mass and auxiliary torque in case scenario (II) during FTP-75 driving cycle

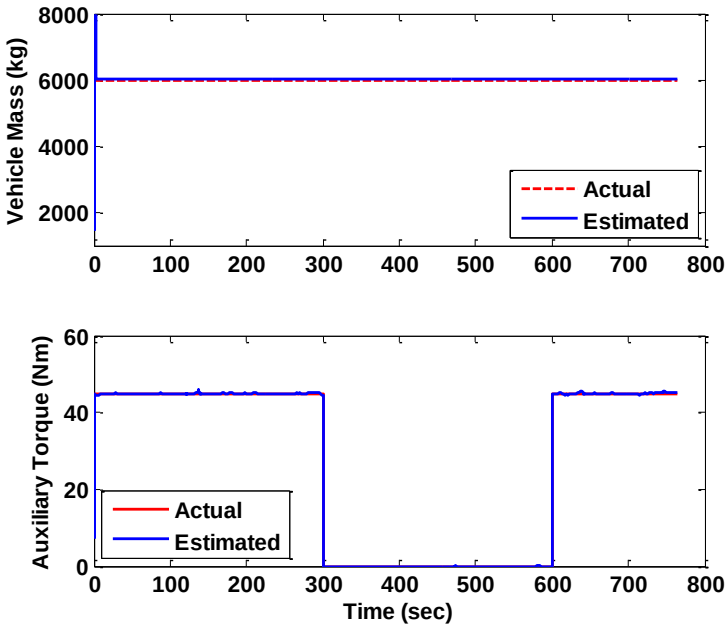

Figure 3-8 Estimation of vehicle mass and auxiliary torque in case scenario (I) during HWFET driving cycle

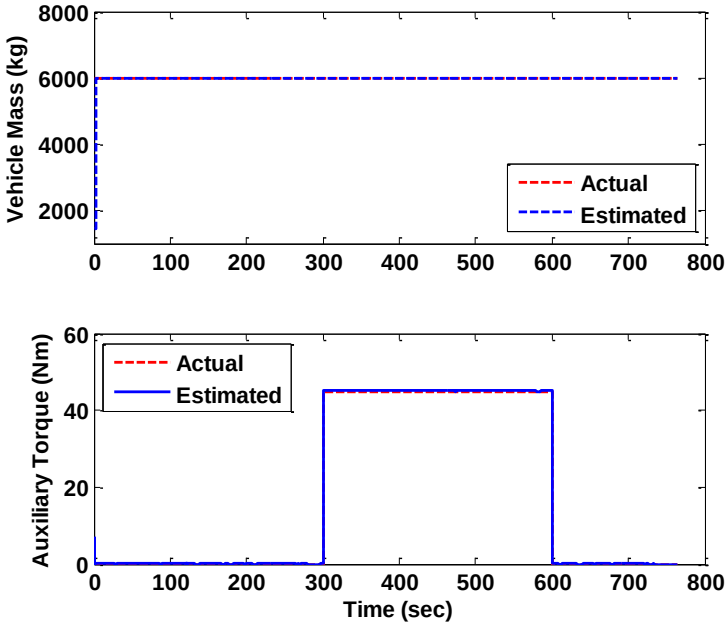

Figure 3-9 Estimation of vehicle mass and auxiliary torque in case scenario (II) during HWFET driving cycle

Table 3-2 Percent mass error and RMS error in auxiliary torque, drive load, and service load during FTP-75 driving cycle

	Scenario (I)		Scenario (II)	
	Two-Stage Estimation	**One-Stage Estimation**	**Two-Stage Estimation**	**One-Stage Estimation**
Percent Mass Error	0.1%	0	0	0
RMSE in Auxiliary Torque	0.36 Nm	1.99 Nm	0.20 Nm	3.12 Nm
RMSE in Drive Load	33.37 W	310.11 W	0	856.08 W
RMSE in Service Load	58.80 W	312.86 W	40.82 W	852.70 W

Table 3-3 Percent mass error and RMS error in auxiliary torque, drive load, and service load during HWFET driving cycle

	Scenario (I)		Scenario (II)	
	Two-Stage Estimation	**One-Stage Estimation**	**Two-Stage Estimation**	**One-Stage Estimation**
Percent Mass Error	0.12%	0	0	0
RMSE in Auxiliary Torque	0.54 Nm	7.6 Nm	0.31 Nm	8.98 Nm
RMSE in Drive Load	42.91 W	2.06e+03 W	0	2.11e+03 W
RMSE in Service Load	88.03 W	1.78+03 W	68.24 W	2.10e+03 W

3.4 Chapter Summary

The drive load is the amount of power that is required for moving the vehicle, while the service load is the power consumption of the auxiliary devices. To identify drive and service loads, all the parameters in the vehicle power balance equation should be either measured or estimated. Two parameters with unknown variations in this equation are vehicle mass and torque of auxiliary devices that are required to be estimated. This chapter proposed a model-based algorithm that utilizes available signals in the CAN bus of the vehicle as well as road grade information provided by a GPS receiver for simultaneous estimation of these two parameters. This algorithm operates in two stages: in the first stage, the Kalman filter works until it estimates an acceptable value for the vehicle mass; in the next stage, the vehicle mass is kept constant, and only auxiliary torque is estimated. The algorithm switches from stage one to two when the system error is less than a predefined value in a long enough period of time. The simulation results showed a good agreement between estimated and actual values at different levels of excitation (city and highway cycles).

Chapter 4
Identification Validation Using HIL Simulations

Hardware-in-the-loop (HIL) simulation provides an effective platform for test and evaluation of a system components as well as validation of control systems. Recently, this technique has been widely used in industry for following reasons [86]:

- Pressure to reduce development cycles
- Safety requirements that mandate comprehensive testing of a control system before it can be implemented on a real system
- The need to prevent costly failures
- Reduced cost and more availability of the components required for HIL simulations

In automotive industry, HIL has been utilized for many applications such as component and subsystem evaluation [87], [88], controller validation [89]–[92], measuring efficiency of subsystems [93], etc.

The proposed identification algorithm was tested by numerical simulations in Chapter 3. Although this is the most cost-effective approach, the results are strongly relied on the accuracy of the model used for the actual system. As a result, the algorithm needs to be tested in more realistic situations. The best approach is to test the algorithm on a real vehicle (pure hardware), however due to associated costs and required time, the proposed identification method is evaluated on a HIL platform. This test setup and results are discussed in this chapter.

4.1 HIL Test Setup

As illustrated in Figure 4-1, the HIL test setup includes one input AC dynamometer motor for simulating vehicle's engine and two identical output AC dynamometers for simulating drive and service loads. The input and output dynamometers, which are from Mustang Dynamometers, include $\pm 0.1\%$ accuracy torque meters, magnetic speed sensors, and CompactLogix controller. Specifications of input and output dynamometers are summarized in Table 4-1.

Table 4-1 Specifications of dynamometers

Symbol	Parameter	Input Dynamometer	Output Dynamometers
T_{max}	Maximum torque	$250\ Nm$	$630\ Nm$
ω_{max}	Maximum rotational speed	$1800\ rpm$	$1400\ rpm$
P_{max}	Maximum power	$60\ hp$	$60\ hp$

The input dynamometer (A) is connected to the output dynamometer (B) by a 6-speed manual transmission (Eaton Fuller FS-5306A). The output dynamometer (C) is also connected to a power take-off (Muncie CS6). The power take-off (PTO) is a gearbox attached to the transmission and is utilized to transfer power from the engine to the auxiliary devices. The PTO may be engaged by means of a cable, pneumatic or hydraulic pressure. In the selected PTO, a pneumatic system is deployed for this purpose. A portion of power generated by the input dynamometer is transferred through transmission to one of the output dynamometers that simulates drive load. The remaining goes to the second dynamometer, which simulates the auxiliary load, through the PTO. A schematic of power flow in the HIL setup is shown in Figure 4-2.

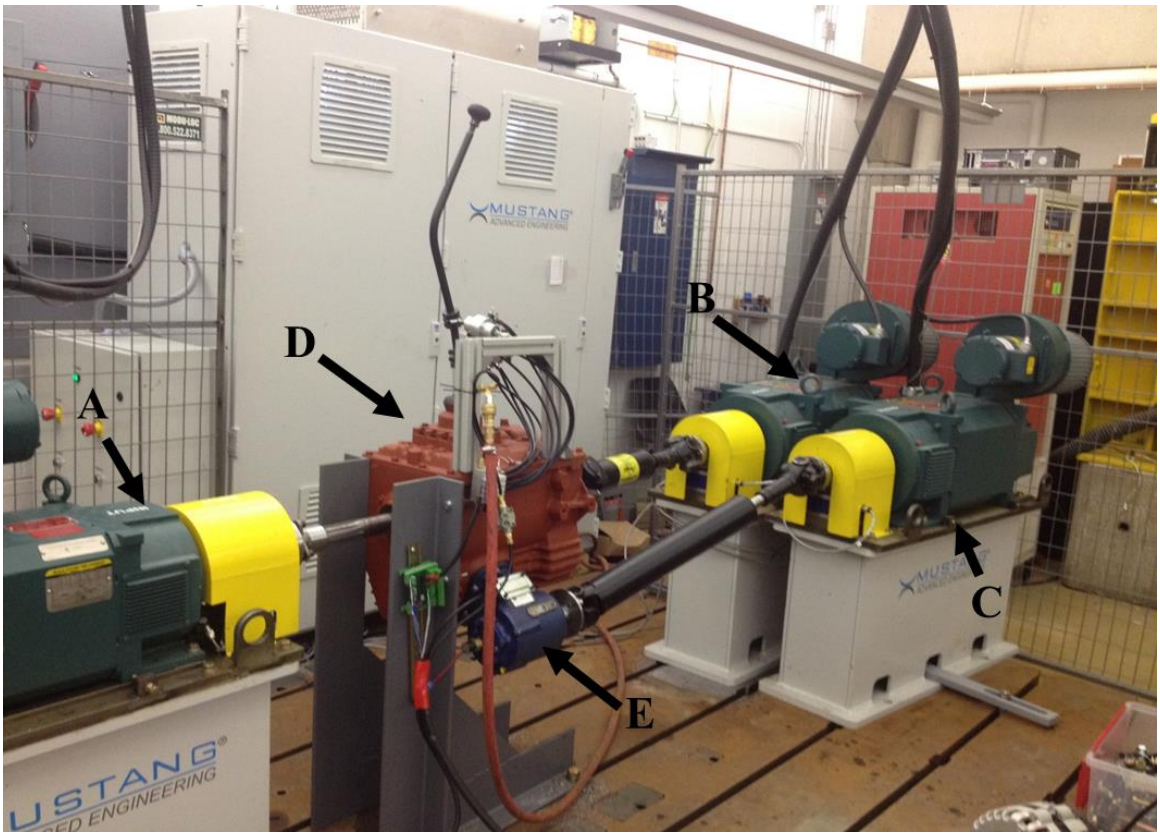

Figure 4-1 HIL setup: (A) Input dynamometer for simulating engine performance, (B) Output dynamometer for simulating drive load, (C) Output dynamometer for simulating service load, (D) Transmission, (E) Power take-off (PTO)

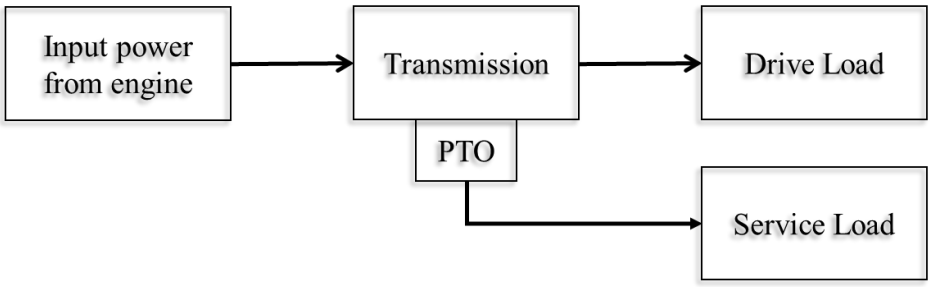

Figure 4-2 Schematic of power flow in HIL setup

A pneumatic system has been designed to shift the transmission gears based on a drive cycle. Two pneumatic actuators, as illustrated in Figure 4-3, are attached to the gear stick and operate together for gear shifting. A microcontroller is used to control the pneumatic system.

Figure 4-3 Pneumatic system for gear shifting

In this HIL system, the driving cycle, auxiliary device ON/OFF signal, road grade information, and vehicle specifications are used in a Matlab/Simulink code to find the drive load (for dynamometer B), service load (for dynamometer C), speed of input dynamometer (A), and gear number. A software designed by Mustang Dynamometer (MD), as shown in Figure 4-4, is used to control the speed of the input dynamometer and torque of output dynamometers by a PID controller. MD software is also used as data acquisition system for collecting torque and speed signals of the dynamometers. Speed and torque signals of the input dynamometer (A), as well as speed of the output dynamometer (B) are required for the identification task. Other signals are measured to verify performance of the PID controller in tracking desired values. Based on the desired gear number obtained by the Matlab/Simulink code, the microcontroller controls the gear shifting. Finally, a manually-operated

pneumatic valve is utilized to engage or disengage the PTO clutch to turn the auxiliary load ON or OFF. The schematic of HIL control system is illustrated in Figure 4-5.

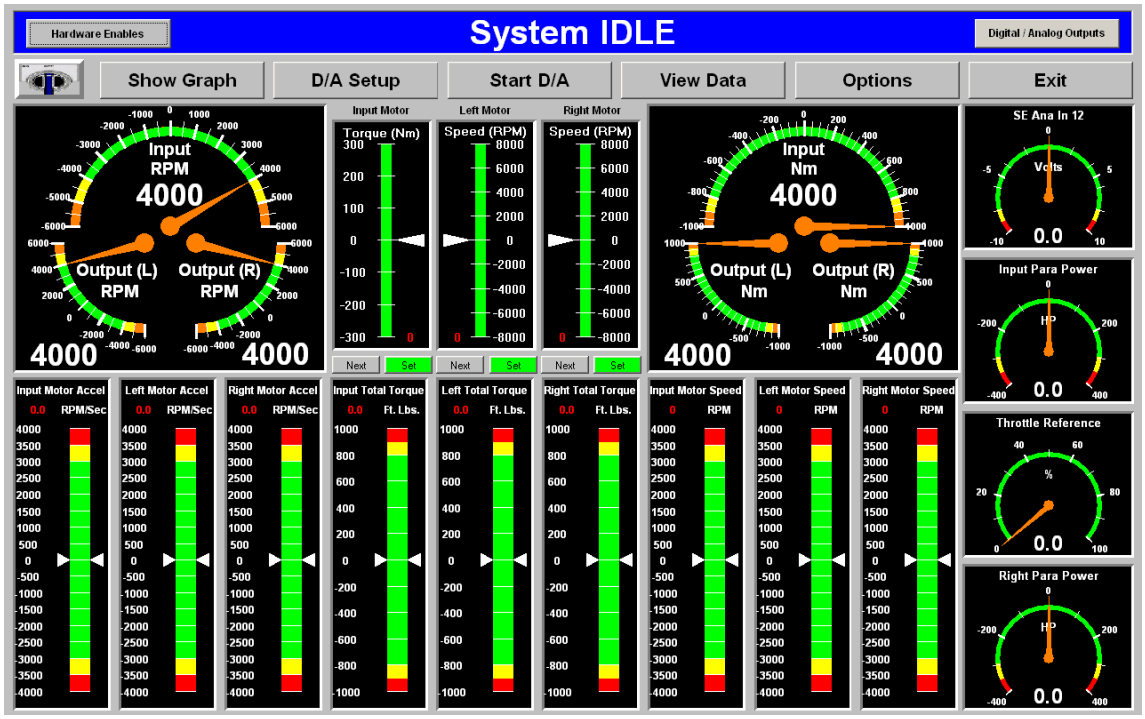

Figure 4-4 User interface of the MD software for controlling speed and torque of the dynamometers

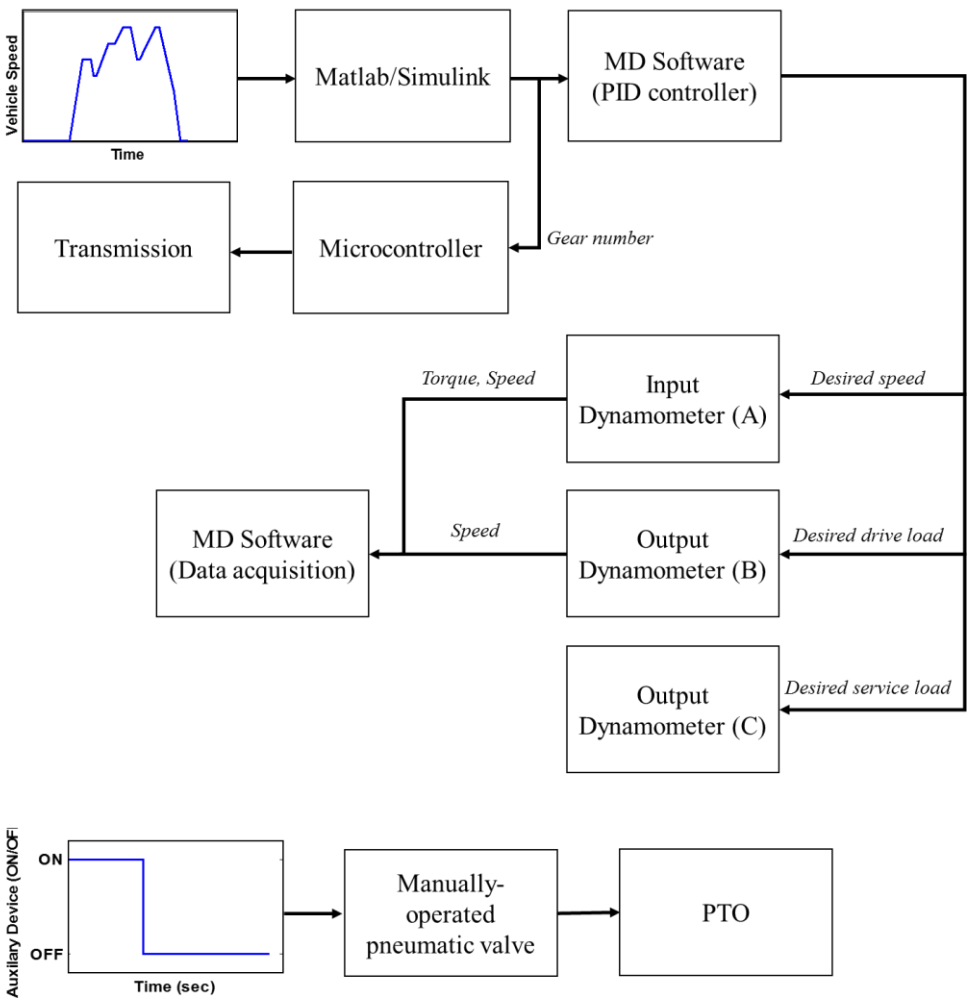

Figure 4-5 Schematic of HIL control system

4.2 Model Scaling

As shown in Table 4-1, the maximum speed of the input dynamometer is 1800 rpm, whereas this speed can reach up to 5000 rpm in gasoline engines and 2500 rpm in diesel engines. This means that for simulating a driving cycle in the HIL setup, the vehicle speed needs to be scaled down. To scale the vehicle, the well-known Buckingham's Pi theorem, which is the basic theorem of dimensional analysis, will be applied. This theorem states that two systems are dynamically similar if the corresponding dimensionless variables (Pi groups) are equal. Interested readers are referred to [94] for more details and the proof of the theorem. Following steps should be taken to apply this theorem [94]:

1- List all the variables associated with the system.

2- Determine the number of Pi groups. The number of Pi groups (n_{pi}) is equal to the number of variables (p) minus the number of dimensions (q).

3- Select repeating variables. The repeating variables should be dimensionally independent and include all the dimensions.

4- Form Pi groups. Each variable should be multiplied by repeating variables to form a Pi group.

In the problem in hand, all the variables associated with the system and their corresponding dimensions are listed in Table 4-2. The number of Pi groups is calculated as follows:

$$n_{pi} = p - q = 12 - 3 = 9 \tag{4-1}$$

M, R, and u are selected as repeating variables in this system, and the first Pi group is calculated as:

$$\pi_1 = TM^a R^b u^c = [M][L]^2[T]^{-2}[M]^a[L]^b[L]^c[T]^{-c} \tag{4-2}$$

The exponents of repeating variables are obtained by making the Pi group dimensionless:

$$\begin{gathered} 1 + a = 0 \\ 2 + \mathrm{b} + \mathrm{c} = 0 \\ -2 - \mathrm{c} = 0 \\ a = -1, \;\; b = 0, \;\; c = -2 \end{gathered} \tag{4-3}$$

By substituting the obtained values into Equation (4-2), π_1 is calculated as:

$$\pi_1 = \frac{T}{M\,u^2} \tag{4-4}$$

Similarly, other Pi groups, as listed in Table 4-2, can be found.

Table 4-2 Variables associated with the system and their corresponding Pi groups

Variables	Symbols	Dimensions	Pi group
Torque of dynamometers	T	$[M][L]^2[T]^{-2}$	$\pi_1 = \frac{T}{Mu^2}$
Rotational speed	ω	$[T]^{-1}$	$\pi_2 = \frac{\omega_e R}{u}$
Vehicle mass	M	$[M]$	Repeating variable
Speed	u	$[L][T]^{-1}$	Repeating variable
Frontal area	A_f	$[L]^2$	$\pi_3 = \frac{A_f}{R^2}$
Drag coefficient	C_d	[]	$\pi_4 = C_d$
Tire radius	R	$[L]$	Repeating variable
Air density	ρ	$[M][L]^{-3}$	$\pi_5 = \frac{\rho R^3}{M}$
Road grade	α	[]	$\pi_6 = \alpha$
Inertia	I	$[M][L]^2$	$\pi_7 = \frac{I}{MR^2}$
Efficiency	η	[]	$\pi_8 = \eta$
Gear ratio	N_{tf}	[]	$\pi_9 = N_{tf}$

Due to the limitation of speed in HIL setup, vehicle speed should be scaled down to 1/3 (considering the vehicle has a gasoline engine). Equality equation for the Pi groups of real vehicle and HIL system can be written as follows:

$$
\begin{aligned}
(\pi_1)_{Veh} &= (\pi_1)_{HIL} \\
\left(\frac{T}{M\,u^2}\right)_{Veh} &= \left(\frac{T}{M\,u^2}\right)_{HIL} \\
\left(\frac{T_{HIL}}{T_{Veh}}\right) &= \left(\frac{M_{HIL}}{M_{Veh}}\right)\left(\frac{u_{HIL}}{u_{Veh}}\right)^2 \\
S_T &= S_M S_u^2 = (1)(1/3)^2 = 1/9
\end{aligned}
\tag{4-5}
$$

where S_T , S_M , S_u are the ratio of engine torque, mass, and speed in HIL system to those of a real vehicle, respectively.

Similarly,

$$
\begin{aligned}
(\pi_2)_{Vehicle} &= (\pi_2)_{HIL} \\
\left(\frac{\omega R}{u}\right)_{Vehicle} &= \left(\frac{\omega R}{u}\right)_{HIL} \\
\left(\frac{\omega_{HIL}}{\omega_{Veh}}\right) &= \left(\frac{u_{HIL}}{u_{Veh}}\right)\left(\frac{M_{Veh}}{M_{HIL}}\right) \\
S_{\omega_e} &= \frac{S_u}{S_R} = \frac{1/3}{1} = 1/3
\end{aligned}
\tag{4-6}
$$

where S_{ω_e} , and S_R are the ratio of engine speed, and tire radius in HIL system to those of a real vehicle, respectively. Other Pi groups do not change when vehicle speed is scaled. As a result, when the vehicle speed is scaled down to 1/3, rotational speed of dynamometers should be scaled to 1/3 and torque of dynamometers need to be scaled to 1/9. It should be mentioned that the collected data from the HIL setup are scaled up by similar procedure before they are used for the estimation purposes.

4.3 Transmission Efficiency

The efficiency of transmission is usually assumed to be a constant value for each gear. However, this assumption is not valid when the input torque of transmission is small. As this situation rarely happens

in vehicles, this assumption can be held. Since the torque of all dynamometers are scaled down to 1/9 in the HIL setup, assumption of constant efficiency for the transmission causes noticeable error in the HIL simulation results. As a result, some tests are required in order to obtain the transmission efficiency in the operating region of the HIL setup. To achieve this goal, the input dynamometer is run at a constant speed while the torque increases step by step. This procedure is performed from the lowest possible speed and torque to the highest desired speed and torque. Then, the efficiency at each speed and torque is obtained by:

$$\eta_t = \frac{P_{t-out}}{P_{t-in}} = \frac{T_{t-out}\,\omega_{t-out}}{T_{t-in}\,\omega_{t-in}} \tag{4-7}$$

where P_{out} , P_{in} are the output and input power of transmission, respectively.

For each gear an efficiency map in terms of input speed and input torque is obtained. Figure 4-6 shows efficiency map of gear 1 to gear 6. As shown, the efficiency of the transmission in HIL system ranges from 31% to 97%. The higher the gear number, the better efficiency. The maximum efficiency of each gear occurs at the minimum speed and maximum torque. Moreover, the efficiency of each gear is improved when the torque is increased at a constant speed, and also the efficiency is decreased when the speed is increased at a constant torque.

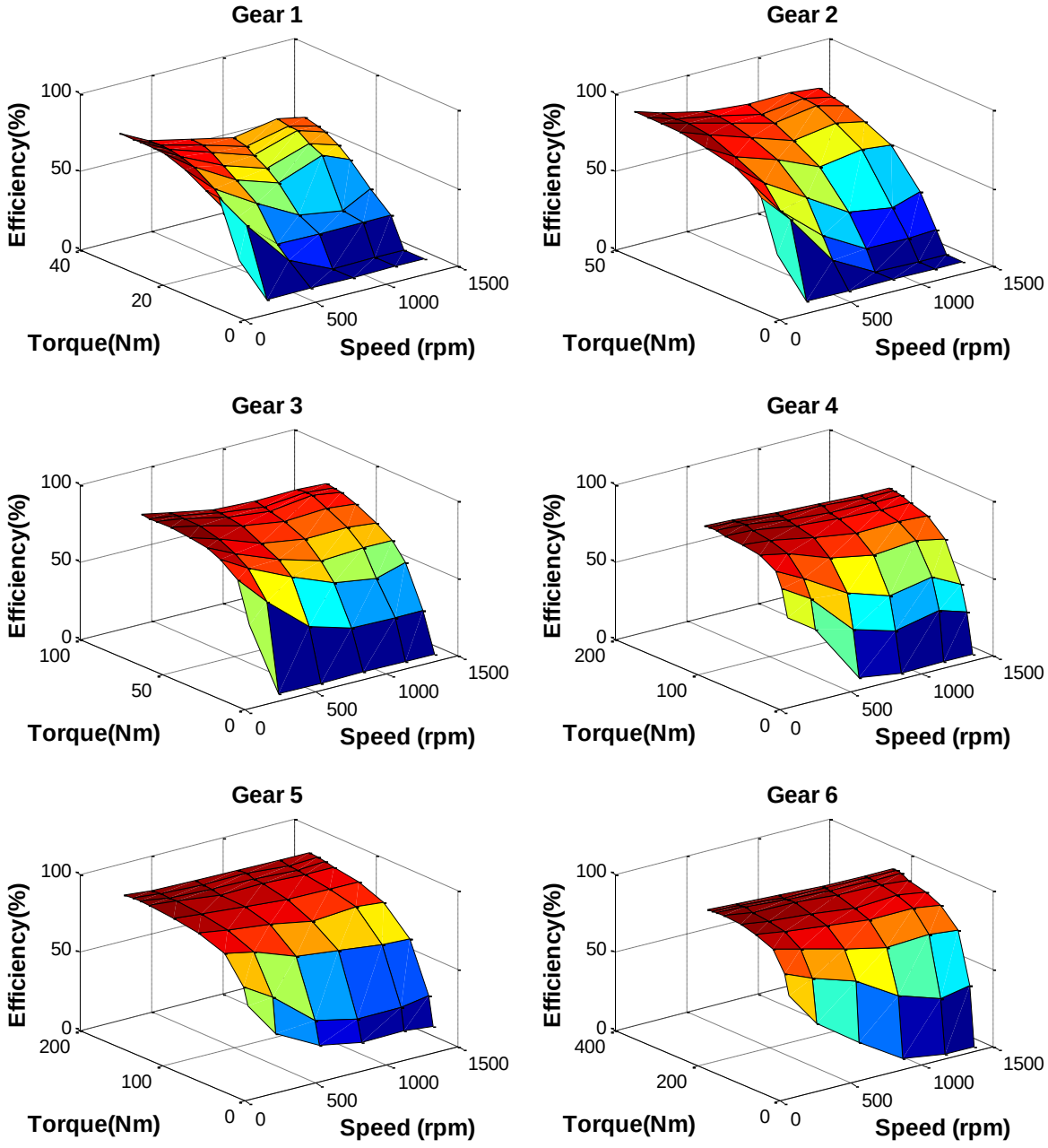

Figure 4-6 Efficiency map of gear 1 to 6

4.4 Test Results

HIL simulations are conducted for the service vehicle described in Section 3.3. To determine the validity of the system model, the engine torque that is obtained by the model is compared to the measured engine torque. To achieve this goal, the vehicle specifications as well as the measured engine speed and vehicle speed are substituted in the Equation (3-13) to find the engine torque. Then, this value is compared with the measured torque of the input dynamometer, which simulates the engine torque. Figure 4-7 shows a comparison of these values for a driving cycle when the auxiliary device is ON for the whole cycle. The results confirm that the system is properly modeled for HIL simulations.

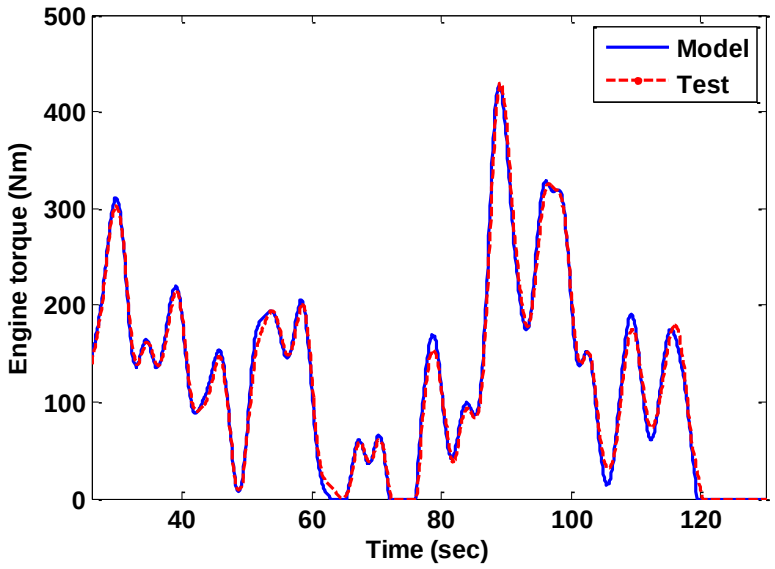

Figure 4-7 Comparison of the engine torque obtained by the model with that of measured from the input dynamometer.

The HIL simulations are done for a driving cycle shown in Figure 4-8. Three case scenarios are considered for the simulations: (I) the PTO is disengaged, which means that auxiliary device is OFF, (II) the PTO is engaged to provide constant torque of 45 Nm for the auxiliary device, (III) the auxiliary device is ON in the beginning of the cycle and then it turns OFF.

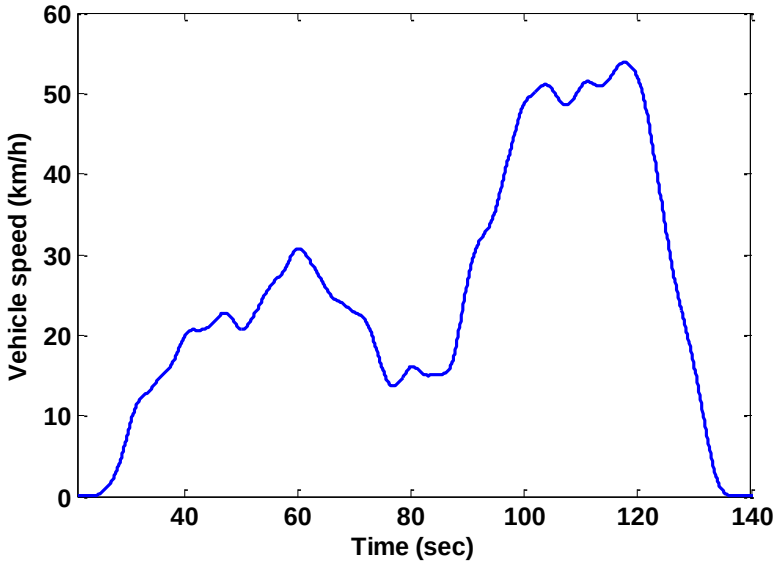

Figure 4-8 A driving cycle used for HIL simulations

Before applying the estimation algorithm, some considerations should be taken into account. Some data points obtained from simulations cannot be utilized by the estimation algorithm. When the following conditions are met, the estimation is put on hold and previous values are used as the estimated parameters. These conditions include: braking, gear shifting, and low-acceleration periods. The brake pressure is available in the CAN bus of heavy-duty vehicles, but determining brake torque from brake pressure requires an accurate model for each specific vehicle. Additionally, during gear shifting, the drive torque signal is not accurate and hence will not be used in the estimation algorithm. In addition, when the vehicle has low acceleration, the excitations of measurement signals are not rich enough for the estimation purposes. Therefore, during braking, gear shifting, and low acceleration periods ($\dot{u} < 0.1\ m/s^2$) the estimation algorithm becomes inactive and previous values are used.

By considering the above-mentioned points, the estimation algorithm is applied to the collected data. Figure 4-9, Figure 4-10, and Figure 4-11 illustrate the estimation of vehicle mass and auxiliary torque for the three case scenarios. Furthermore, Table 4-3 shows percent mass error, RMS error in auxiliary torque, and RMSE in drive and service loads. As seen, there is a good agreement between the actual and estimated values. The estimation switches from stage one to two, as discussed in Section 3.3.1, when the percentage of system error is less than 2% for 4 seconds. This happens after 36

sec, 55 sec and 36 sec in case scenario I, II, and III, respectively. As a result, the estimation of the vehicle mass remains unchanged after an acceptable value is found. The estimated mass in the second stage has a small error (less than 3%) in all cases. The estimation of auxiliary torque converges to the actual value in a reasonable amount of time. If the auxiliary device turns ON or OFF during the estimation (e.g. case scenario III), the convergence rate of estimated auxiliary torque to the actual value is dependent on the situation. For instance, if this happens when the system has low level of excitation, the convergence rate will be slower. The results illustrate that the estimation of the parameters is inactive when previously-described conditions are met. For example, at the end of the cycle when the brake is applied and speed of the vehicle reduces from 55 km/h to zero, the algorithm provides the pre-braking estimation.

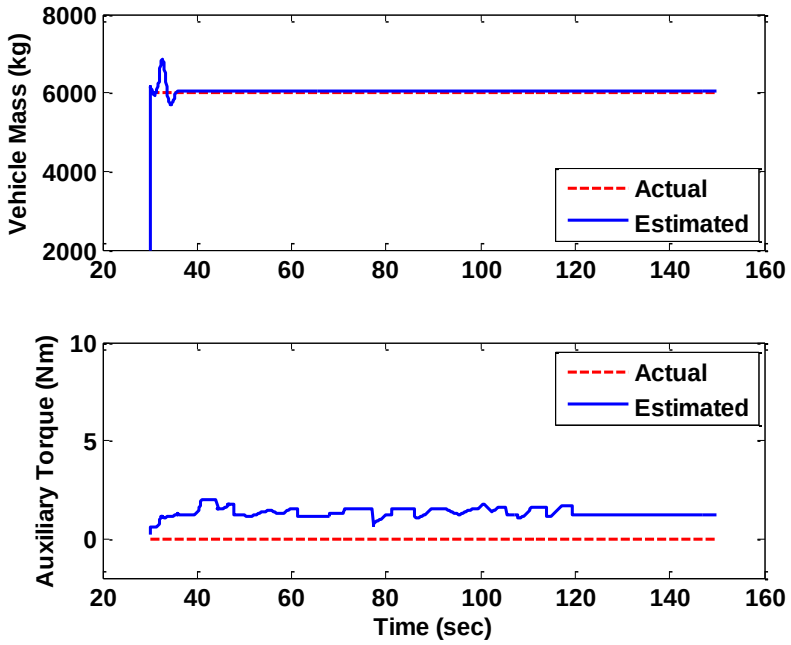

Figure 4-9 Estimation of vehicle mass and auxiliary torque in case scenario (I)

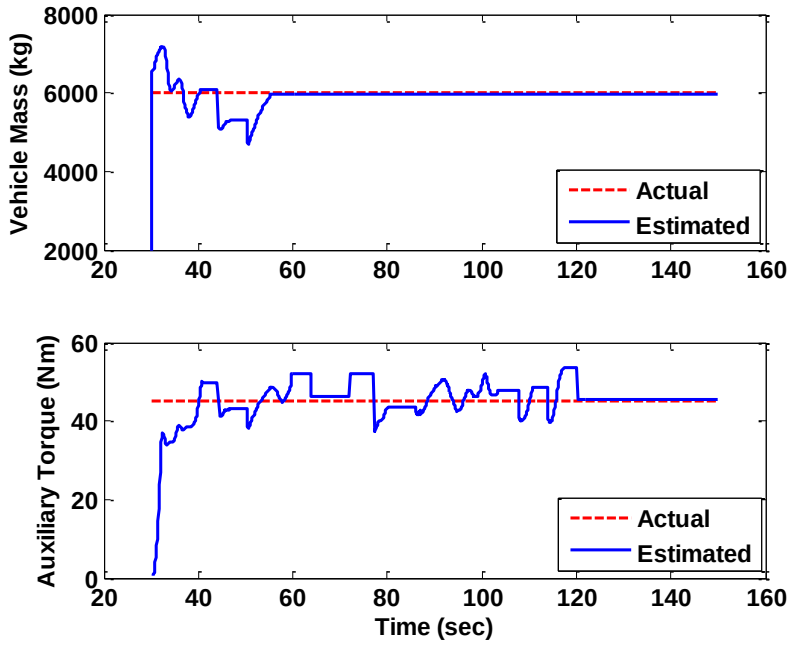

Figure 4-10 Estimation of vehicle mass and auxiliary torque in case scenario (II)

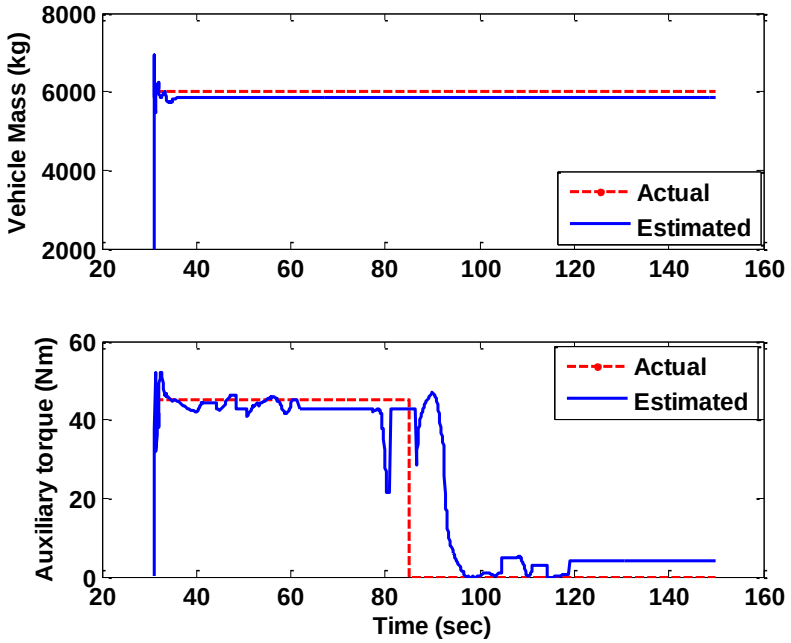

Figure 4-11 Estimation of vehicle mass and auxiliary torque in case scenario (III)

Table 4-3 Percent mass error and RMS error in auxiliary torque, drive load, and service load

	Percent Mass Error	RMSE in Auxiliary Torque	RMSE in Drive Load	RMSE in Service Load
Scenario (I)	0.7 %	1.35 Nm	2.56 kW	0.23 kW
Scenario (II)	-1.09 %	6.24 Nm	2.63 kW	0.67 kW
Scenario (III)	-2.72 %	11.38 Nm	4.31 kW	1.54 kW

4.5 Sensitivity Analysis

In Equation (3-13), some parameters are assumed to be known in advance. In this section, the sensitivity of the estimation algorithm is evaluated with respect to these parameters. Three main parameters that can be different from our assumption are rolling resistance coefficient (C_{rr}), coefficient of aerodynamic resistance (C_D), and tire radius (R). The sensitivity analysis is done on the set of data collected in case of scenario (II). For this study, these three parameters are varied in a reasonable range, and the estimation errors are calculated for each variation.

Change of aerodynamic coefficient has a very small effect on regression vector (see Equation (3-17)). Therefore, as illustrated in Figure 4-12, the estimation algorithm is not very sensitive to the variation of aerodynamic coefficient, and change of error in estimated mass and auxiliary torque is trivial.

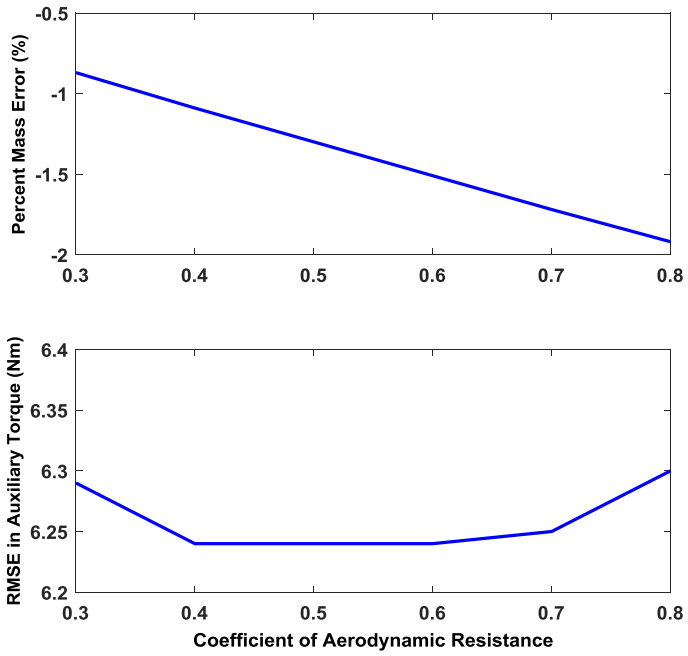

Figure 4-12 Sensitivity of the estimation algorithm with respect to coefficient of aerodynamic resistance

Furthermore, Figure 4-13 shows that variation of the rolling resistance coefficient does not have a profound effect on the estimation of the vehicle mass. On the other hand, the estimation of auxiliary torque is more sensitive to this variation. This is because, rolling resistance coefficient and torque of auxiliary devices affect the system model in the same way. As a result, in order to properly identify service loads, more accurate value of rolling resistance coefficient is required.

Finally, Figure 4-14 presents the sensitivity of the estimation algorithm with respect to the tire radius. Considering the tire radius has direct effect on traction torque, mass estimation is affected considerably when this value is not accurate. Therefore, the tire radius should be determined precisely for better identification of the drive load.

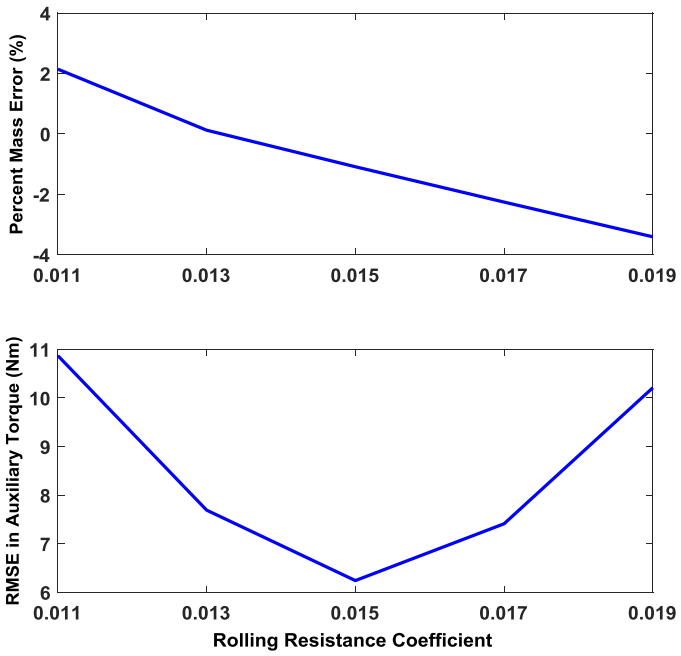

Figure 4-13 Sensitivity of the estimation algorithm with respect to rolling resistance coefficient

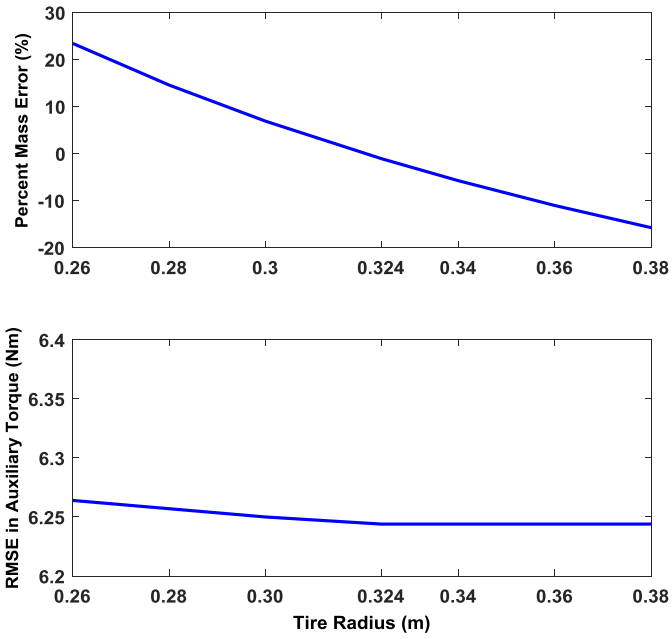

Figure 4-14 Sensitivity of the estimation algorithm with respect to tire radius

4.6 Chapter Summary

To evaluate the estimation algorithm in more realistic situations, HIL simulations were carried out. In this chapter, a test setup required for these HIL simulations was introduced. This test setup has three dynamometers for simulating generated power by the engine, drive loads, and service loads. The dynamometers are connected to each other by a manual transmission and a PTO, and their speed and torque are controlled by a PID controller provided in the MD software. The gear shifting is also done by two pneumatic actuators attached to the gear stick. Considering the speed limit of the dynamometers is smaller than the actual speed of an engine, the vehicle was scaled down using Buckingham's Pi theorem. To make measurable signals in the tests comparable to actual available signals in the CAN bus, some data points did not use for the estimation. When the following conditions were met, the estimation was put on hold and previous values were used as estimated parameters. These conditions include: braking, gear shifting, and low acceleration periods. By HIL simulations, more realistic results were obtained that confirmed a good performance of the estimation algorithm.

Chapter 5
RAPS Power Management System

A regenerative auxiliary power system (RAPS) can supply auxiliary power using the battery, generator (or alternator), or combination of these two sources. In the battery only mode, all auxiliary power demand is provided by the battery, and no auxiliary load is added to the engine by the generator. The system can operate in this mode until the state of charge (SOC) of the battery reaches a predefined minimum allowable value. In the generator only mode, the auxiliary power is supplied by the engine-driven generator. Moreover, extra power can be generated by the generator to charge the battery as required. Finally, in the combined mode, both battery and generator provides the auxiliary power demand. The ideal scenario is to use the battery for the whole trip where it can be charged by an external electrical source, but the problem would be the size and cost of the battery. As a result, the power management system of the RAPS should determine the split of auxiliary power demand between the generator and battery in the whole trip in order to minimize fuel consumption. The other objective of the power management system is to guarantee that the battery has enough energy for powering auxiliary devices for all the stops where the engine is OFF.

5.1 System Model

A simplified backward model is employed for the powertrain of a service vehicle since utilizing complex model is neither required nor necessary for developing the power management system. The drive cycle and auxiliary load demand are the inputs to the model, and the engine fuel consumption and the battery SOC are the outputs. The model of each powertrain's component is described in this section. All these models are extracted from Autonomie, which is a commercially-available software for modeling and simulation of powertrain systems.

A service vehicle that is selected for this study is a refrigerator delivery truck with specifications listed in Table 5-1. In addition, the specifications of the RAPS' components, i.e. the battery and generator, are available in this Table.

Table 5-1 Vehicle Specifications

Symbol	Parameter	Value
M	Vehicle mass	6000 kg
R	Tire radius	0.387 m
C_{rr}	Coefficient of rolling resistance	0.015
C_D	Drag coefficient	0.44
A_f	Frontal area	3.23 m^2
$P_{eng-max}$	Engine maximum power	205 kW
$P_{gen-max}$	Generator maximum power	5.5 kW
E_{batt}	Battery energy	9 kWh

5.1.1 Engine

The model that is used for the engine takes the engine speed and engine torque as inputs and generates fuel consumption of the engine as an output using the engine's fuel rate map:

$$\dot{m}_f = f_1(\omega_e, T_e) \tag{5-1}$$

where the engine torque (T_e) is sum of the drive torque and generator torque, and the engine speed (ω_e) is calculated using vehicle speed and combined ratio of the transmission and final drive in the backward model.

5.1.2 Generator

The generator model takes generator speed and generator torque as inputs and provides the generator power as an output using a generator efficiency map:

$$P_{gen} = f_2(\omega_{gen}, T_{gen}) \tag{5-2}$$

where the generator torque is determined by the RAPS controller, and the generator speed is either equal to the engine speed or can be obtained by considering the engine-generator transmission ratio.

5.1.3 Battery

A simplified model is used for the lithium-ion battery of the RAPS. In this model, the dynamics of the battery SOC is defined as:

$$\dot{SOC} = -\frac{V_{OC} - \sqrt{{V_{OC}}^2 - 4P_{batt}R_{int}}}{2R_{int}C} \tag{5-3}$$

where V_{OC} is the open-circuit voltage of the battery, P_{batt} is the battery power, R_{int} is the internal resistance of the battery, and C is the battery capacity. The power that is drawn from or charged into the battery is determined by the RAPS controller, and its sign is positive when the battery is discharged and negative when it is charged.

5.2 Control Strategy

As stated earlier, the control strategy of a RAPS needs to satisfy two requirements; it needs to minimize fuel consumption in the whole cycle, and it needs to ensure the battery has enough energy to power auxiliary devices when the engine is OFF. This section discusses three possible control schemes for the RAPS: rule-based, dynamic programming (DP), and a new two-level control strategy (DP-AECMS).

5.2.1 Rule-Based Control Strategy

In the rule-based control strategy, it is assumed that no prior information about drive and duty cycles is available. Therefore, to ensure the battery has enough energy at all engine-OFF stops, the controller charges the battery to the maximum allowable SOC when the engine is ON, and it keeps the SOC at the maximum value until the battery is discharged again at the next engine-OFF stop. This strategy can

be far from optimal solution because the battery might be charged when the engine operates inefficiently, and it is very likely that the battery is fully charged at the end of a trip, which is not desirable in terms of fuel consumption.

5.2.2 **Dynamic Programming (DP)**

A service vehicle specifically a refrigerator delivery truck has usually the same route and auxiliary load (duty cycle) every day. This can provide a load preview with an acceptable level of accuracy for a better performance of the control strategy. To take advantage of this feature, a DP technique, which provides a global optimal solution to constrained nonlinear control problems, can be utilized to find an SOC trajectory for the following operating day of the vehicle. The future information that is required by DP is attainable using historical data and sensory data such as the weight of freight, ambient temperature, traffic information, distance to next stop, etc. Prediction of drive and duty cycles based on this data will be discussed in Chapter 6.

In order to implement DP, the system model can be defined as:

$$SOC(k+1) = f\big(SOC(k), u_d(k)\big) \tag{5-4}$$

where $SOC(k)$ is the state of the system representing state of the charge of the battery at each instant, and $u_d(k)$ is the control input that determines the split ratio of the auxiliary power between the generator and battery as follows:

$$\begin{aligned} P_{gen}(k) &= u_d(k) \\ P_{batt}(k) &= P_{aux} - u_d(k) \end{aligned} \tag{5-5}$$

where P_{gen} is the power of the generator, P_{batt} is the power of the battery, and P_{aux} is demanded auxiliary power. This equation states that if the generator power, which is determined by the controller, is greater than the demanded auxiliary power, then the battery will be charged (the power of the battery will be negative).

The optimization problem is to find $u_d(k)$ in order to minimize the following cost function:

$$J = \sum_{k=0}^{N} V(SOC(k), u_d(k)) = \sum_{k=0}^{N} m_f(k) \tag{5-6}$$

where V is the cost of each instant that is equal to the total fuel consumption of the engine. The optimization problem is subjected to the following constraints:

$$\begin{aligned} SOC_{min} \le SOC(t) \le SOC_{max} \\ T_{eng-min} \le T_{eng}(t) \le T_{eng-max} \\ T_{gen-min} \le T_{gen}(t) \le T_{gen-max} \end{aligned} \tag{5-7}$$

where $T_{eng-min}$ and $T_{eng-max}$ are the minimum and maximum engine torques, and $T_{gen-min}$ and $T_{gen-max}$ are the minimum and maximum generator torques.

After defining the optimization problem and system model, DP can be applied to obtain optimal control $u_d^*(k)$, which gives the optimal state $SOC^*(k)$. Based on Bellman's principle of optimality, the optimal solution at any stage (k) can be found by solving following sub-problem backward from the terminal condition [95]:

$$J_k^*\big(SOC(k)\big) = \min_{u_d(k)} \Big(V\big(SOC(k), u_d(k)\big) + J_{k+1}^*\big(SOC^*(k+1)\big)\Big) \tag{5-8}$$

with

$$J_k^*\big(SOC(N)\big) = \min_{u_d(N)} \Big(V\big(SOC(N), u_d(N)\big)\Big) \tag{5-9}$$

For the final stage N.

To solve Equation (5-8) numerically, backward DP algorithm, which is described in [95] is used.

5.2.3 **Two Level Control System (DP-AECMS)**

The main drawback of DP control strategy is high computational cost. Therefore, the processing power it requires cannot be facilitated by standard vehicles' on-board processors, especially when the SOC trajectory is required to be updated online for example when new future information is available. To address this problem, a new two-level controller is proposed. In the high level of this controller, a fast dynamic programing technique is employed to find optimal values of the initial and final SOC for each segment based on available a-priori knowledge. A segment, as illustrated in Figure 5-1, is a duration when the vehicle is driven, or when the vehicle is stopped for delivery or pick up and the engine is OFF. In the low level, a real-time control scheme determines the split ratio of auxiliary power between the generator and the battery with the initial and final SOC obtained by the high-level controller.

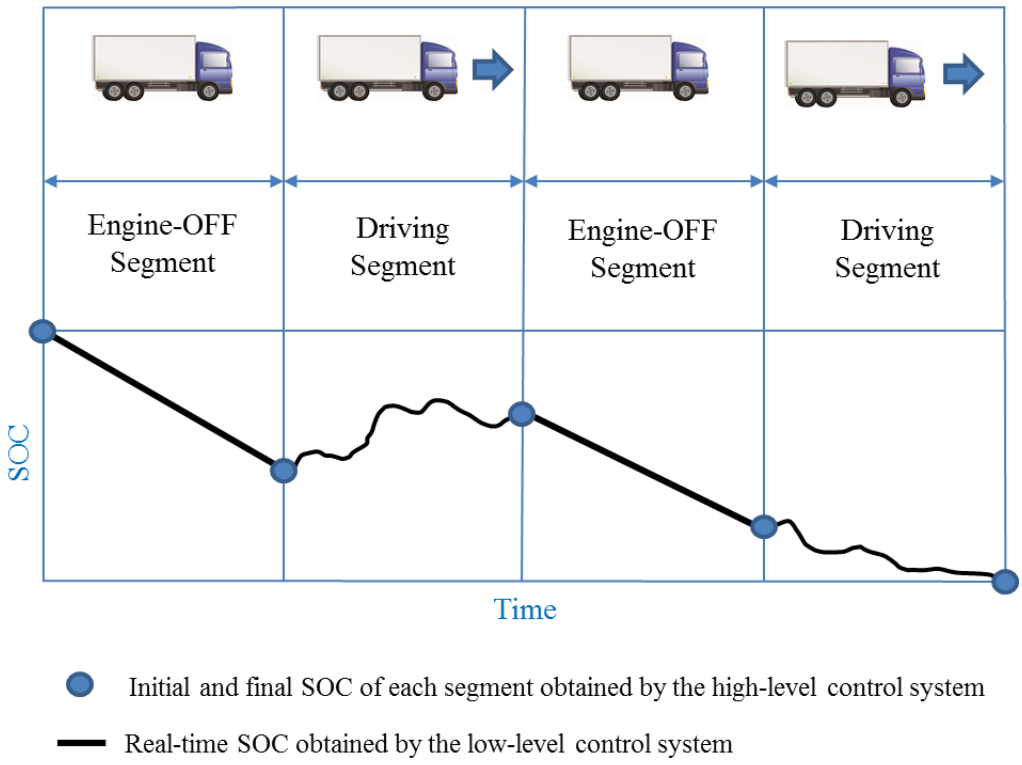

Figure 5-1 Definition of segments and SOC trajectory

5.2.3.1 High-Level Control System

In the high-level control system a fast DP technique determines the optimal amount of energy, which can be discharged from or charged into the battery in each segment. This level also ensures the battery has enough energy at all possible stops when the engine is OFF. Due to the fact that DP should be run for only a few points (number of segments), the computational time is significantly reduced, and an optimal solution can be obtained online quickly.

In this level of the control system, instead of finding the optimal solution at each instant, it is determined for each segment. The system model can be defined as:

$$SOC(n+1) = f\big(SOC(n), u_h(n)\big) \tag{5-10}$$

where $SOC(n)$ is the initial SOC of the battery at each segment. The model that is used to find the battery SOC in this level is different from the one described in Section 5.1.3 and it is defined as:

$$SOC(n) = \frac{E_{batt-rem}(n)}{E_{batt}} \tag{5-11}$$

where E_{batt} is the total energy of the battery, and $E_{batt-rem}(n)$ is the remaining energy in the battery. Furthermore, $u_h(n)$ is the control input that determines the split ratio of the auxiliary energy between the generator and battery as follows:

$$\begin{aligned} E_{gen-seg}(n) &= u_h(n) \\ E_{batt-seg}(n) &= E_{aux-seg}(n) - E_{regen-seg}(n) - u_h(n) \end{aligned} \tag{5-12}$$

where $E_{gen-seg}$ is the total produced electrical energy by the generator in a segment that is used for powering the auxiliary device as well as charging the battery, $E_{batt-seg}$ is the energy that is charged into or discharge from the battery in the segment, $E_{aux-seg}$ is the total auxiliary energy demanded in

the segment, and $E_{regen-seg}$ is the total electrical energy generated by regenerative braking in the segment. The goal is to obtain $u_h(n)$ so that the following cost function is minimized:

$$J = \sum_{n=0}^{N_s} m_f(n) \tag{5-13}$$

where (N_s) is the number of segments plus one, and m_f is total fuel consumption of the engine in a segment. To find the fuel consumption of each segment, the engine power at each instant that is used for driving the vehicle plus the generator power is required. While the DP technique finds the generator energy in the segment, the distribution of this energy, which is needed to acquire the generator power, is not known. To address this problem, it is assumed that this energy is distributed equally at each instant in the segment. While this assumption is not valid in calculating real fuel consumption, it provides accurate enough information to find a suboptimal solution in the high-level control system.

The fuel consumption of each segment should be calculated numerous times for all possible solutions when DP is in process. In order to reduce the computation burden of this calculation, a new method is proposed. In this method, which is based on the features extracted from the prediction of the drive cycle [96], a histogram of the engine speed and engine torque for each segment is constructed. This histogram bins engine speed and torque into a 10-by-10 grid of equally spaced containers (see Figure 5-2).

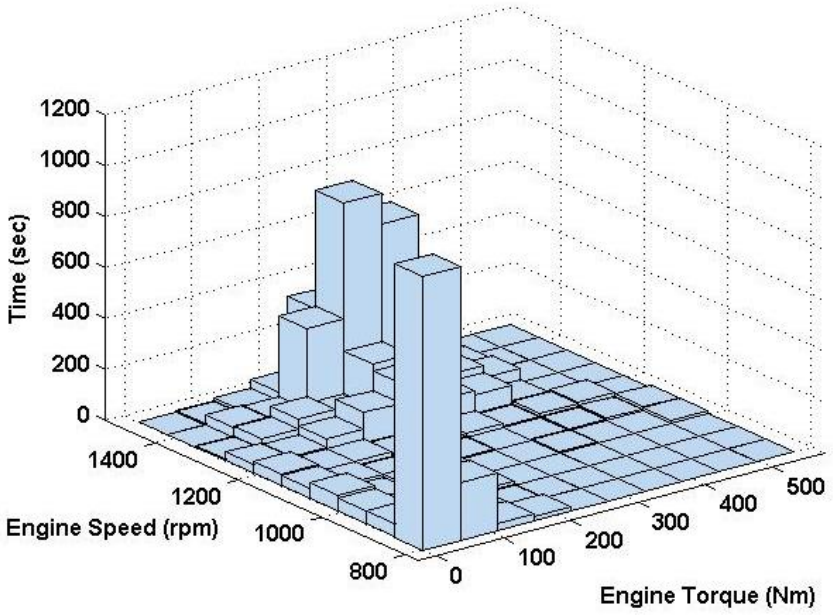

Figure 5-2 Histogram plot of engine torque and engine speed for a segment

Then, the energy of the generator found by DP is divided by the total time of the segment to find the generator power. The generator power is divided by the speed index of the histogram to obtain generator torque. Subsequently, the generator torque is added to the torque index of the histogram to calculate a new engine torque. Now, the histogram represents the engine speed and engine torque, which is sum of the drive torque and generator torque. Afterward, the corresponding speed and torque of each bin are utilized by the model described in Equation (5-1) to obtain the fuel rate. To find the fuel consumption of each bin, the fuel rate is multiplied by the height of each bin, which represents the duration that the engine operates at a correlated speed and torque. Finally, the fuel consumption of the segment is calculated by adding the fuel consumption of all the bins. In employing this method, processing time is decreased dramatically because instead of using all points in the segment, only 100 points are used to obtain the fuel consumption. This process is illustrated in Figure 5-3 for more clarification.

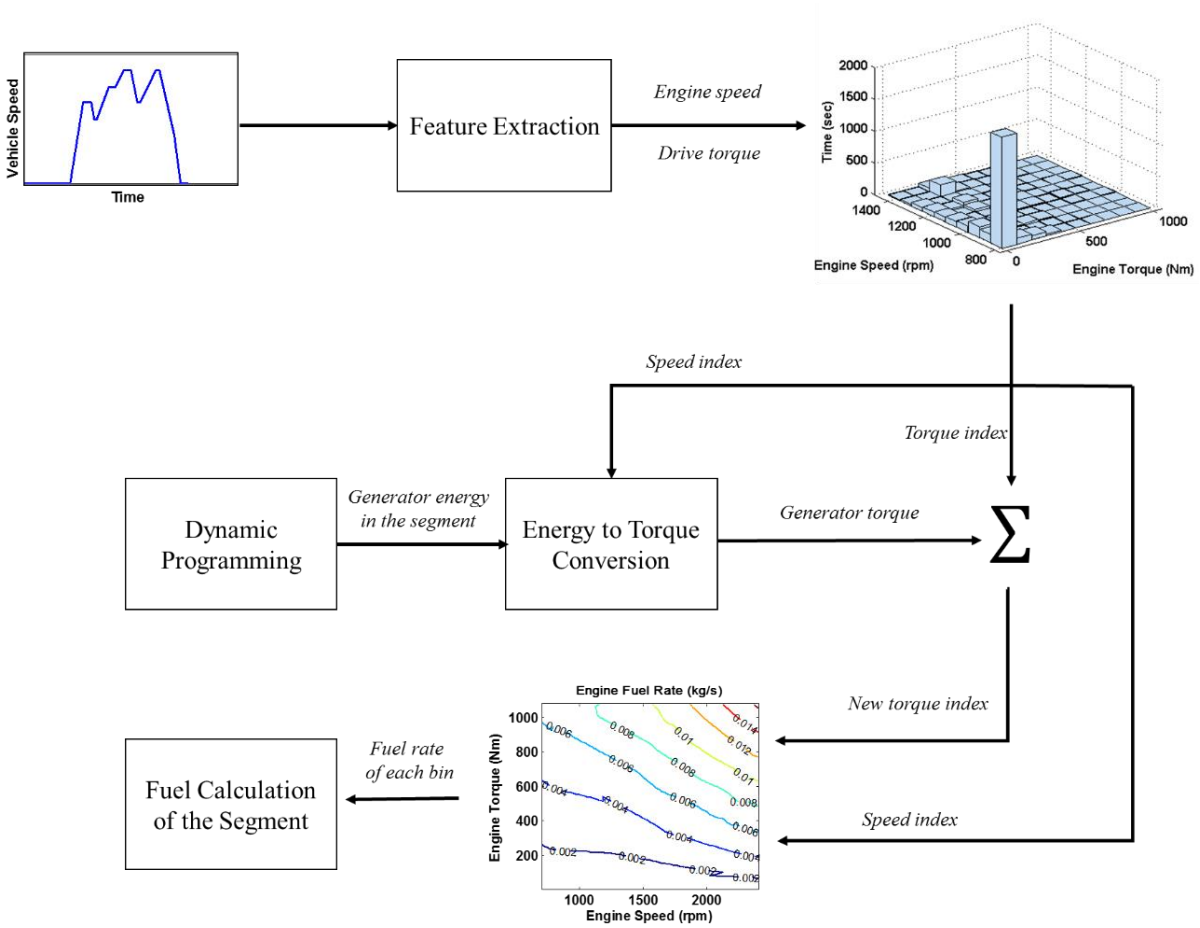

Figure 5-3 Fuel consumption calculation for each segment in DP

Since in this level of the control system, the optimization is done for the segments (not each instant) the constraints on the engine torque and generator torque cannot be applied, and they will be considered in the low level. The only constraint that should be satisfied in this level is on the battery as follows:

$$SOC_{min} \leq SOC(k) \leq SOC_{max} \tag{5-14}$$

where SOC_{min} and SOC_{max} are the minimum and maximum allowable states of the charge of battery, respectively.

Finally, to obtain optimal control $u_h^*(k)$, which gives the optimal state $SOC^*(n)$, the same method that was described in the previous section should be applied.

5.2.3.2 Low-Level Control System

In the high-level control system, the optimal initial and final SOC of each segment was determined. This ensures that the battery has enough energy for the engine-OFF stops and also it is fully depleted at the end of a trip. Now, in the low-level control system, a real-time control strategy is required to determine the optimal ratio of the auxiliary power between the battery and generator by considering the desired initial and final SOC. To meet this objective, an adaptive equivalent fuel consumption minimization strategy (A-ECMS), which has shown good performance on HEVs and PHEVs, will be employed. The algorithm will be refined to improve results and reduce computational load.

The objective of equivalent fuel consumption minimization strategy (ECMS) is to minimize instantaneous equivalent fuel rate ($\dot{m}_{f,equ}$), which is defined as [97]:

$$\dot{m}_{f,equ}\big(t, u_l(t)\big) = \dot{m}_f(t, u_l) + s\frac{P_{batt}(t, u_l)}{LHV} \tag{5-15}$$

where u_l is the split ratio of auxiliary power between the battery and generator, $\dot{m}_f$ is the fuel consumption rate of the engine, P_{batt} is the battery power charged into or discharged from the battery, LHV is the lower heating value of the fuel, and s is the equivalent weight factor that converts the electrical energy of the battery to equivalent fuel. If a big value is selected for the equivalent weight factor, discharging battery is penalized and more fuel is consumed, but a small equivalent weight factor leads to more usage of electrical energy, thereby decreasing battery SOC.

At each instant, all the possible $u_l(t)$ are substituted in Equation (5-15) to calculate $\dot{m}_{f,equ}$ using the powertrain model defined in Section 5.1. Then, $u_l^*(t)$, which gives the minimum $\dot{m}_{f,equ}$, is selected as the optimal solution by considering following constraints:

$$\begin{aligned} SOC_{min} \le SOC(t) \le SOC_{max} \\ T_{eng-min} \le T_{eng}(t) \le T_{eng-max} \\ T_{gen-min} \le T_{gen}(t) \le T_{gen-min} \end{aligned} \tag{5-16}$$

Using Pontryagin's minimum principle, it can be shown that the true value for the equivalent weight factor can be found if future information is available [98]. This optimal value (s_{opt}) ensures the final SOC is equal to the desired SOC. Since the future information is assumed to be known in the RAPS, an iterative optimization algorithm can be utilized to find the equivalent weight factor. However, this is not a computationally-efficient method mainly if the initial guess is not close to correct solution. Therefore, this method is still not the best option for real-time implementation because it takes a long time to find new solution when future information, e.g. traffic information, is updated. Adaptive equivalent fuel consumption minimization strategy (A-ECMS) is a method that updates equivalent weight factor (s) online. Many different methods for adaptation of the equivalent weight factor has been used, but the most popular one utilizes the affine function of SOC error based on a PI controller [70]:

$$s\,(SOC,t) = s_0 + k_p\left(SOC_{ref} - SOC(t)\right) + k_i\int_0^t \left(SOC_{ref} - SOC(t)\right) \tag{5-17}$$

where s_0 is the initial guess for the equivalent weight factor, k_p is a proportional gain, k_i is an integral gain, and SOC_{ref} is reference SOC, which can be defined as:

$$SOC_{ref} = SOC_0 - \left(SOC_0 - SOC_f\right)\frac{D(t)}{D_{tot}} \tag{5-18}$$

where SOC_0 and SOC_f are the initial and final SOC of the segment, respectively, $D(t)$ is the distance travelled by the vehicle, and D_{tot} is the total distance that the vehicle will travel in a segment. This equation states that the SOC is changed linearly with respect to the distance that the vehicle travels in a segment. Therefore, it is assured that the battery is charged or discharged at the end of the segment as determined by the high-level control system.

In Equation (5-17), s_0, k_p, and k_i are three tuning parameters that should be determined so that the SOC is close to the one with s_{opt} (s that is obtained offline based on full a-priori knowledge). To tune

the k_p value, first we compare SOC_{ref} with SOC_{opt} (SOC of the battery when s_{opt} is selected) in a segment. As shown in Figure 5-4, the SOC of the battery with s_{opt} deviates around the SOC_{ref}. Therefore, k_p should be selected so that SOC can deviate rather than strictly follow SOC_{ref}.

Figure 5-5, Figure 5-6, and Table 4-1 illustrate the SOC, equivalent weight factor and the fuel economy of the vehicle in the same segment with high and low values for k_p. The issue with a high k_p is that the SOC cannot deviate, and consequently, the result is not optimal as more fuel is consumed. On the other hand, with a low k_p, the final desired SOC is not guaranteed to be reached. As a result, in order to let the SOC deviate and to reach final desired SOC at the same time, it is proposed to switch k_p from a low value to high one when 70 percent of the distance of a segment has been travelled. As presented in Table 5-2, with switching gain, the fuel consumption and final SOC are very close to the optimal result.

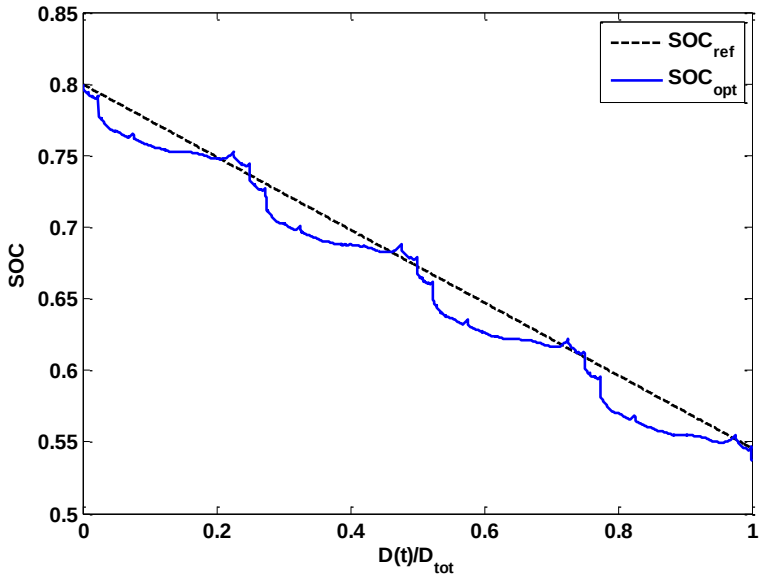

Figure 5-4 A comparison between optimal and reference SOC in a segment

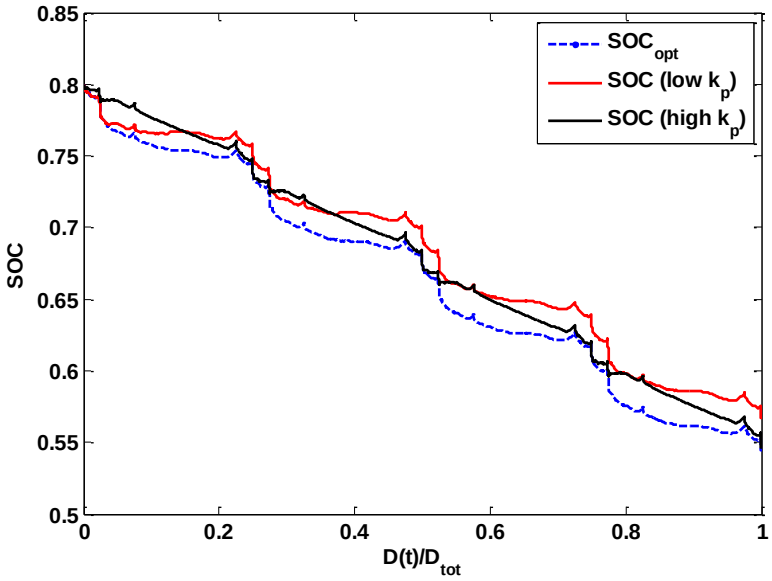

Figure 5-5 A comparison of optimal SOC and SOCs that are obtained by high and low proportional gain

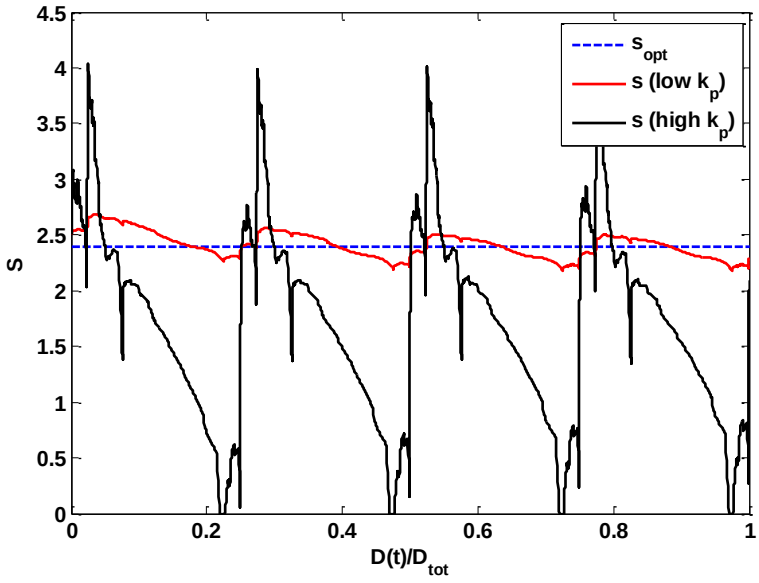

Figure 5-6 A comparison of optimal equivalent weight factor and the ones that are obtained by the high and low proportional gains

Table 5-2 Fuel economy and final SOC of the vehicle in a segment with different methods for the adaptation of the equivalent weight factor

Method	Fuel Economy	Final SOC
s with low k_p	24.06 L/100km	0.567
s with high k_p	24.18 L/100km	0.546
s with switching k_p	23.97 L/100km	0.546
s_{opt}	23.74 L/100km	0.544

The other parameter that can affect the performance of the controller is the initial value of the equivalent weight factor (s_0). This parameter can be determined offline using historical data; however, the sensitivity analysis is carried out to discover how the results change if the guess for (s_0) is not close to optimal. Figure 5-7 shows the percent increase of the fuel consumption in a segment with different (s_0). The result states that if (s_0) is selected in the neighborhood of the optimal value, the fuel consumption is very close to the optimal result. As mentioned earlier, since most delivery vehicles have the same drive and duty cycles every day, an acceptable value for (s_0) can be guessed based on historical data, which ultimately results in the controller's good performance.

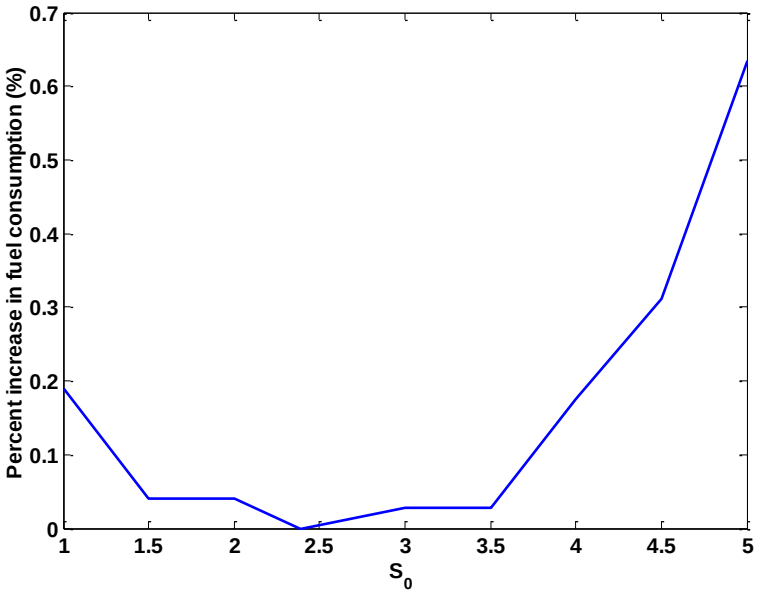

Figure 5-7 Percent increase of fuel consumption with different initial equivalent weight factors

5.3 Simulation Results

To evaluate performance of the controllers described in the previous Section, two case scenarios are considered for the refrigerator truck specified in Table 5-1. The vehicle in the first case is driven mostly in city cycles. The vehicle is loaded at the beginning of the cycle, and a portion of the freight is unloaded at each stop. At the last stop where the vehicle is fully unloaded, the refrigerator is turned OFF. Therefore, this stop is not included in the duty cycle of the vehicle. In the second case scenario, the vehicle is driven in highway cycles. The duty cycle is similar to the first case with less stops for deliveries. For both case scenarios, the initial and final SOC of the battery are 80% and 30%, respectively. More details of these scenarios are summarized in Table 5-3, and their auxiliary load profiles (duty cycles) are shown in Figure 5-8.

Table 5-3 Simulation details of the case scenario 1 and 2

	Case Scenario 1		Case Scenario 2	
	Driving/ Engine OFF	**Freight Weight**	**Driving/ Engine OFF**	**Freight Weight**
Segment 1	Loading- Engine OFF (30 minutes)	1500 kg	Loading- Engine OFF (30 minutes)	1500 kg
Segment 2	Driving (4 × HD-UDDS)	1500 kg	Driving (3 × HHDDT-cruise)	1500 kg
Segment 3	Delivery- Engine OFF (30 minutes)	1000 kg	Delivery- Engine OFF (60 minutes)	500 kg
Segment 4	Driving (4 × HD-UDDS)	1000 kg	Driving (3 × HHDDT-cruise)	500 kg
Segment 5	Delivery- Engine OFF (30 minutes)	500 kg	-	-
Segment 6	Driving (4 × HD-UDDS)	500 kg	-	-

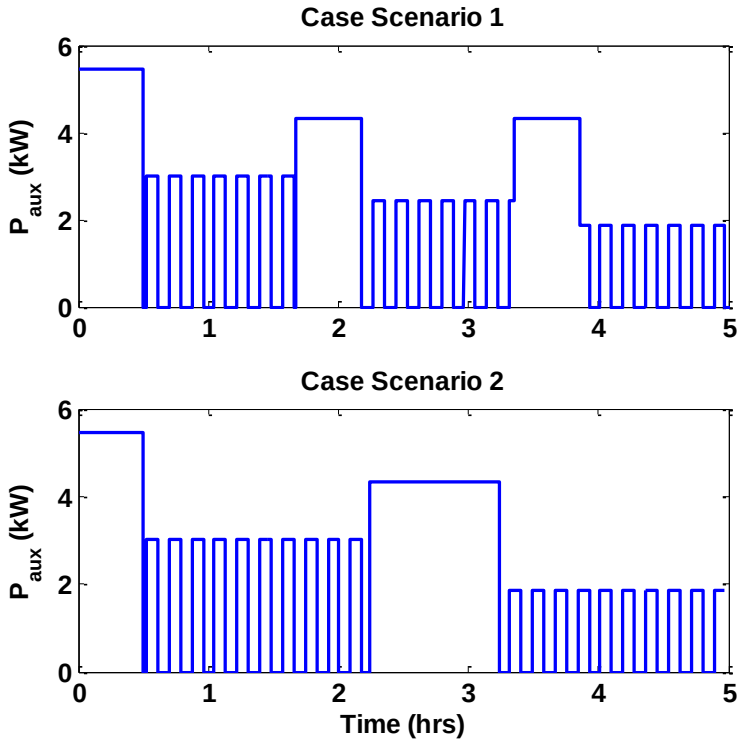

Figure 5-8 Auxiliary load profile of case scenario 1 (top) and case scenario 2 (bottom)

All the simulations are conducted on a computer with an Intel Core i7-3770 CPU and an 8-GB memory. The numbers of discretized state and control input for DP and high-level of DP-AECMS are selected reasonably to provide fast and accurate solutions. Moreover, in the low level of DP-AECMS, as discussed earlier, a better guess for s_0 will result in lower fuel consumption. However, a constant value for s_0 is selected in these simulations to simplify the algorithm. The tuning parameters of the controller are listed in Table 5-4.

Table 5-4 Controller's tuning parameters for the simulations

Symbol	Parameter	Value
DP		
Δt	Step time	1 sec
n_{soc}	Number of discritized state	100
n_u	Number of discretized control input	100
High-level of DP-AECMS		
n_{soc}	Number of discritized state	100
n_u	Number of discretized control input	100
Low-level of DP-AECMS		
s_0	Initial guess of equivalent weight factor	2.4
k_{p-high}	High proporsional gain	300
k_{p-low}	Low proporsional gain	10
k_i	Integral gain	0.5

As discussed earlier, the main issue associated with the implementation of DP on the RAPS is the high computational time. It takes about $5600\,sec$ to run DP for these case scenarios while the processing time for the high-level of DP-AECMS is only 4 sec. Consequently, DP-AECMS decreases the processing time dramatically, and the SOC trajectory, which is obtained by the high-level control system, can be updated quickly when it is required.

Table 5-5 and Table 5-6 list SOC of the segments obtained by the controllers in the case scenario 1 and 2, respectively. The results show that the SOC trajectory that is found by the high-level of DP-AECMS is very close to the one obtained by DP. Moreover, the real-time final SOC of each segment (which are attained by the low-level of DP-AECMS) agrees with the ones found by the high-level of DP-AECMS. This means that the PI controller of the low-level control system can track the SOC trajectory very well. On the other hand, the rule-based control strategy charges the battery to the maximum allowable SOC after the battery is discharged at engine-OFF stops.

Table 5-5 Initial and final SOC of the segments obtained by different controllers in case scenario 1

	DP	**High-Level of DP-ECMS**	**Low-Level of DP-ECMS**	**Rule-Based**
Initial SOC	0.800	0.800	0.800	0.800
Final SOC of Segment 1	0.499	0.499	0.499	0.499
Final SOC of Segment 2	0.633	0.687	0.686	0.800
Final SOC of Segment 3	0.389	0.444	0.444	0.564
Final SOC of Segment 4	0.553	0.543	0.543	0.800
Final SOC of Segment 5	0.306	0.300	0.300	0.564
Final SOC	0.300	0.300	0.307	0.800

Table 5-6 Initial and final SOC of the segments obtained by different controllers in case scenario 2

	DP	High-Level of DP-ECMS	Low-Level of DP-ECMS	Rule-Based
Initial SOC	0.800	0.800	0.800	0.800
Final SOC of Segment 1	0.499	0.499	0.499	0.499
Final SOC of Segment 2	0.791	0.786	0.788	0.8
Final SOC of Segment 3	0.306	0.300	0.302	0.312
Final SOC	0.300	0.300	0.300	0.800

Figure 5-9 and Figure 5-10 show simulation results for case scenarios 1 and 2 obtained by DP-AECMS. According to the results, the battery is the only source of power for the refrigerator when the vehicle is stopped for loading or unloading, thereby eliminating vehicle idling. In addition, the high-level control system properly finds the initial and final battery SOC of the segments so that the battery has enough energy when the engine is OFF. Moreover, the negative power of the battery shows that the battery is charged by the generator because either the battery needs more energy in the future or extra energy from regenerative braking, which should be stored in the battery, is available.

As presented in Figure 5-11 and Figure 5-12, by utilizing the rule-based control strategy, the engine idling is completely eliminated too. However, the battery is fully charged at the end of the trip while it was supposed to be completely depleted.

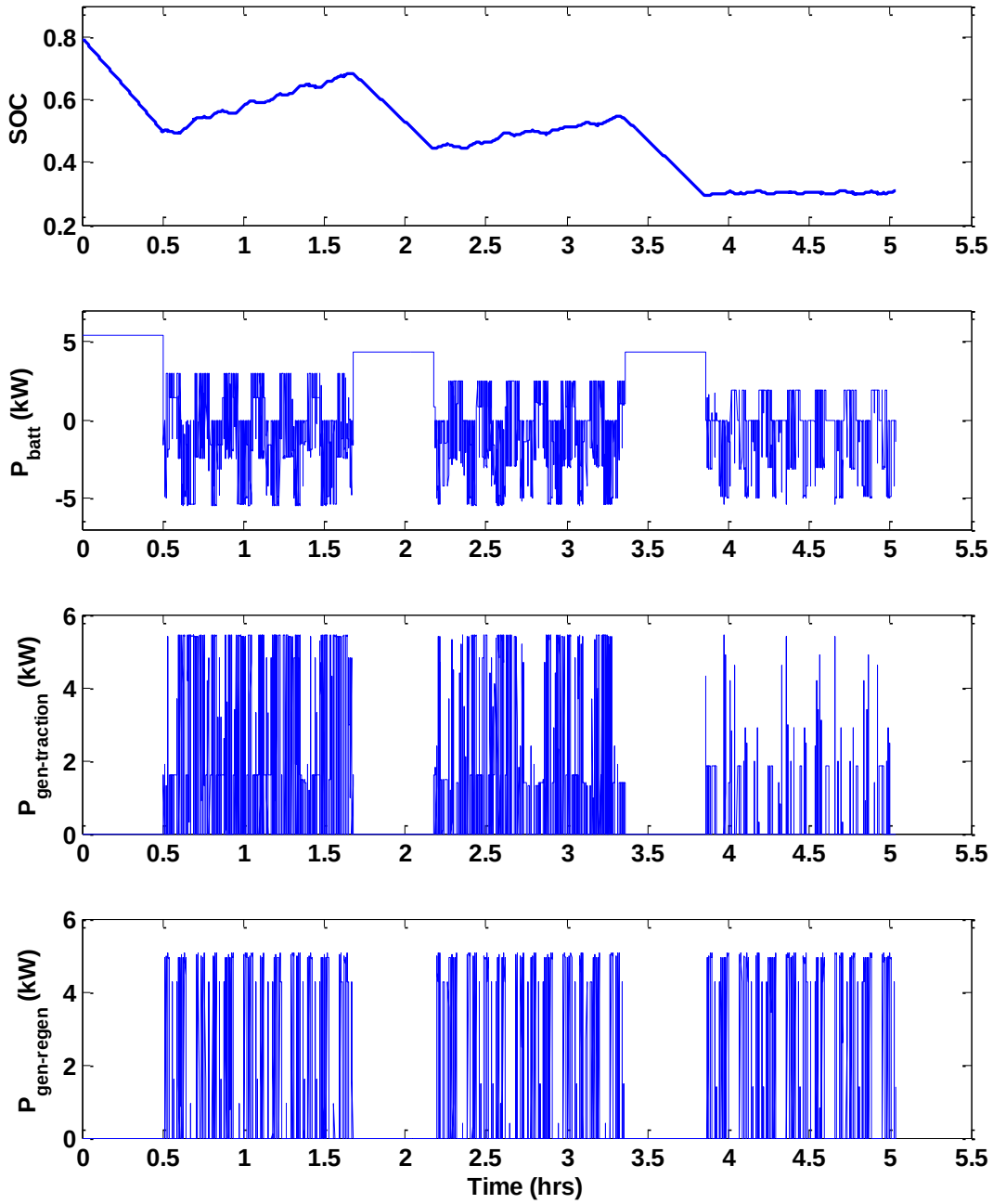

Figure 5-9 Battery SOC, battery power, generator power during traction, and generator power during braking (regenerative braking) for the case scenario 1 using DP-AECMS control strategy

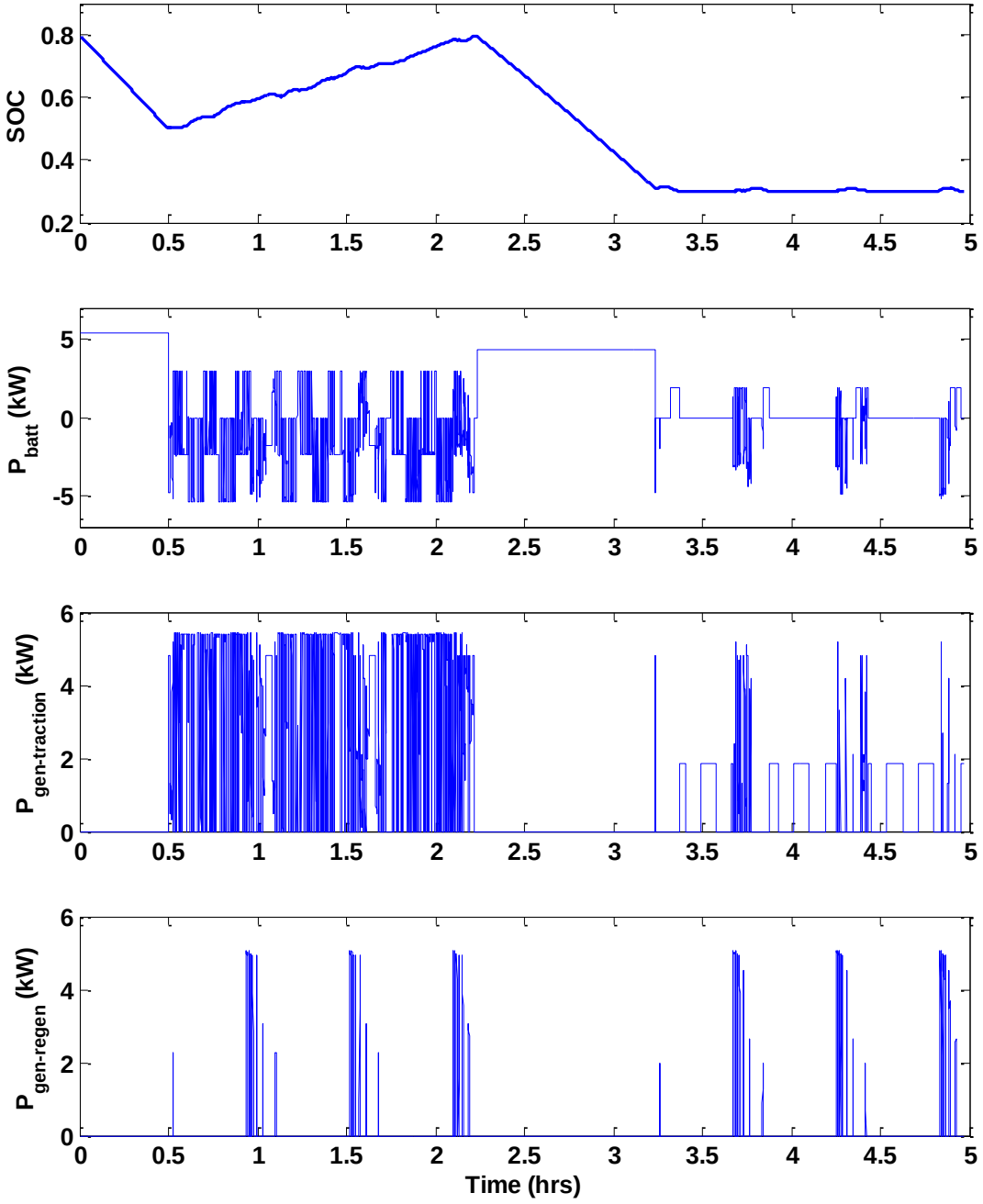

Figure 5-10 Battery SOC, battery power, generator power during traction, and generator power during braking (regenerative braking) for the case scenario 2 using DP-AECMS control strategy

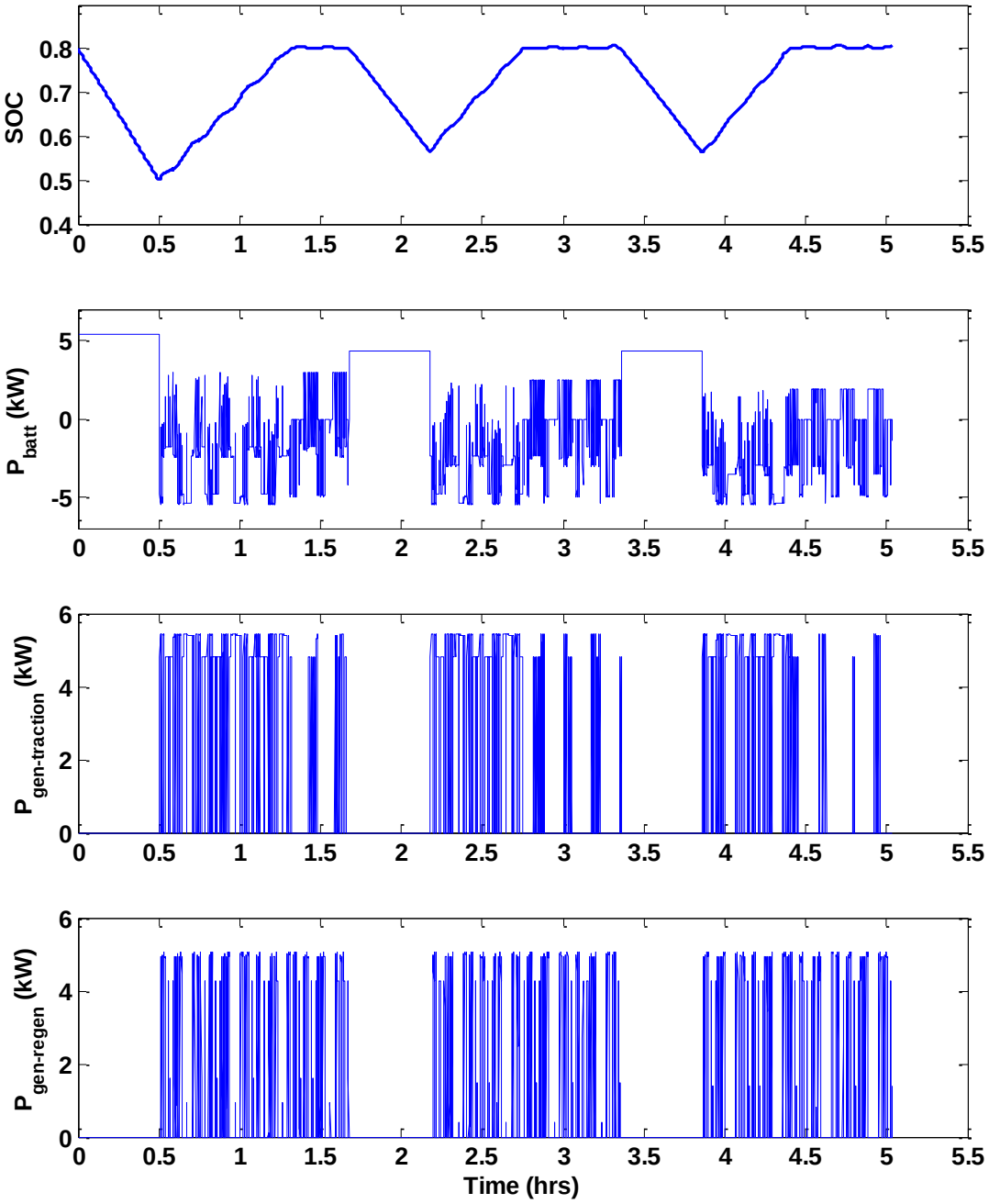

Figure 5-11 Battery SOC, battery power, generator power during traction, and generator power during braking (regenerative braking) for the case scenario 1 using rule-based control strategy

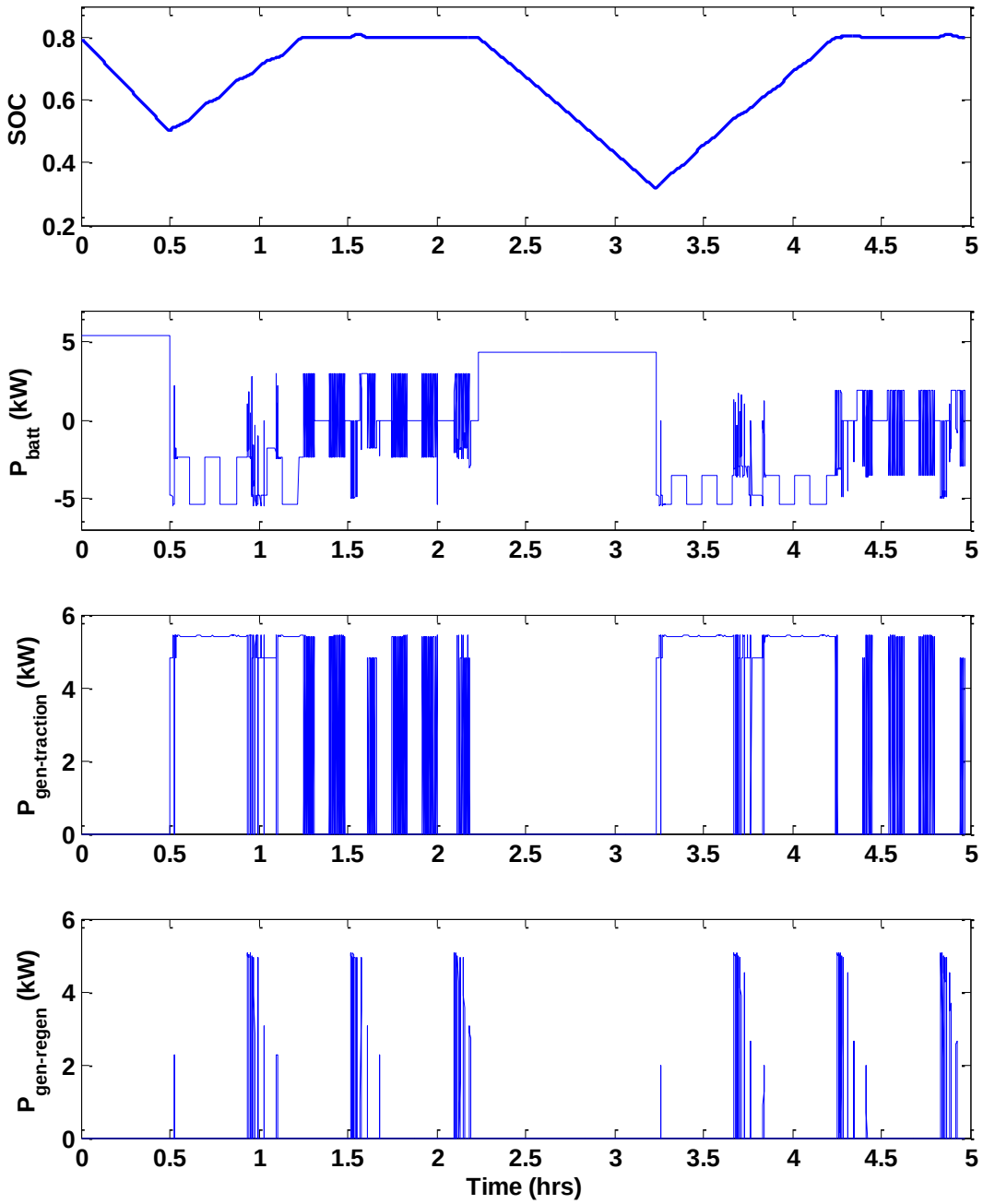

Figure 5-12 Battery SOC, battery power, generator power during traction, and generator power during braking (regenerative braking) for the case scenario 2 using rule-based control strategy

The performance of the proposed control system (DP-AECMS) in terms of fuel economy is compared with that of DP and the rule-based control strategy, and the results are summarized in Table 5-7 and Table 5-8. These tables also include the fuel economy of a conventional refrigerator delivery truck with an engine-driven compressor. Considering the conventional vehicle does not have any anti-idling system, the engine should be kept ON during all loading/unloading stops. Due to the fact that the engine operates very inefficiently when it idles, the fuel consumption during these stops is 3L, which is a significant ratio of the total fuel consumption. The results confirm that in addition to idle elimination, the RAPS improves the fuel economy of the vehicle significantly. This improvement for the city cycle, with more available regenerative power, is 11.9% and for the highway cycle is 6.6%.

The proposed real-time controller shows that it can be used effectively instead of a global optimization method (DP), which is impossible for real-time implementation on the RAPS due to high processing time. Furthermore, since the rule-based control strategy does not deplete the battery at the end of the trips, the improvement in fuel economy is significantly less than the DP-AECMS control scheme.

Table 5-7 A comparison of fuel economy between RAPS (with DP-AECMS, rule-based, and DP control strategies) and conventional configuration for the case scenario 1

	Fuel Consumption	**Fuel Economy**	**Improvement**
DP-AECMS	20.52 L	19.31 L/100 km	11.9 %
Rule-based	22.55 L	21.22 L/100 km	3.17 %
DP	20.21 L	19.02 L/100 km	13.2 %
Conventional	23.29 L	21.92 L/100 km	-

Table 5-8 A comparison of fuel economy between RAPS (with DP-AECMS, rule-based, and DP control strategies) and conventional configuration for the case scenario 2

	Fuel Consumption	Fuel Economy	Improvement
DP-AECMS	31.52 L	14.15 L/100 km	6.6 %
Rule-based	32.85 L	14.74 L/100 km	2.69 %
DP	31.36 L	14.06 L/100 km	7.2 %
Conventional	33.76 L	15.15 L/100 km	-

In these simulations, the size of the battery and the generator have been selected reasonably based on cost of components and the given duty cycle of the vehicle. However, the bigger the battery and the generator in the RAPS, the more fuel can be saved. To study the effect of the size of these components, the first case scenario is simulated with different size of batteries and generators. Table 5-9 shows that the increase in the size of the battery and improvement in the fuel consumption has almost a linear relationship. This table also presents the amount of energy supplied by the battery and regenerative braking for the total demanded auxiliary energy of 11.3 kWh. The remaining energy is provided by the generator. It can be concluded that the maximum battery size that can be used for the given duty cycle is 18 kWh; otherwise, the battery is not fully depleted at the end of the trip. Moreover, the smallest battery for this case scenario is 6 kWh; otherwise, the engine idling cannot be completely eliminated.

According to the results listed in Table 5-10, when a bigger generator is selected, more braking power can be recovered by the regenerative braking, thereby lowering fuel consumption. The reason that the battery is less discharged with bigger generator is that the available regenerative energy is greater than demanded power in the last segment. As a result, the battery is charged in this segment even if the initial SOC is set on the minimum value. Based on this study, the size of the battery and generator can be selected by considering their cost as well as cost of fuel and electrical power.

Table 5-9 Fuel consumption improvement, battery energy consumption, and regenerative braking energy in case scenario 1 with 5.5-kW generator and different size of batteries

	6-kWh Battery	9-kWh Battery	12-kWh Battery	18-kWh Battery
Fuel Consumption Improvement	9.1 %	11.9 %	13.8 %	15.9 %
Battery Energy Consumption	2.75 kWh	4.32 kWh	5.85 kWh	8.26 kWh
Regenerative Braking Energy	2.51 kWh	2.51 kWh	2.51 kWh	2.51 kWh

Table 5-10 Fuel consumption improvement, battery energy consumption, and regenerative braking energy in case scenario 1 with 9-kWh battery and different size of generators

	5.5-kW Generator	8-kW Generator	12-kW Generator
Fuel Consumption Improvement	11.9 %	13.3%	14.8%
Battery Energy Consumption	4.32 kWh	4.21 kWh	3.72 kWh
Regenerative Braking Energy	2.51 kWh	3.43 kWh	4.97 kWh

5.4 Chapter Summary

The power management system of the RAPS should determine the split ratio of auxiliary power demand between the generator and battery in order to minimize fuel consumption. It should also guarantee that the battery has enough energy for powering auxiliary devices for all the engine-OFF stops. To meet these objectives, a two-level control system was proposed in this chapter. In the high-level control system, a fast dynamic programming technique that utilized extracted features of the predicted drive and service loads obtained an SOC trajectory (initial and final SOC of the segments). In order to reduce computational effort of the DP, a method for calculating fuel consumption of each segment that utilized a histogram of the engine speed and engine torque was proposed. In the low-level control system, an adaptive equivalent fuel consumption minimization (A-ECMS) technique employed to find optimal split ratio of the auxiliary power between the sources by considering initial and final SOC found by the high-level control scheme. For adaptation of the equivalent weight factor, affine function of the SOC error based on a PI controller was utilized. Additionally, to improve performance of the PI controller, the proportional gain was switched from a low value to a high value when 70% of the distance in a segment was travelled. The simulation results showed, in addition to complete idle elimination, significant amount of fuel can be saved by employing the RAPS in a service vehicle.

Chapter 6
Drive and Service Loads Prediction

As discussed in Chapter 5, the proposed power management system of the RAPS takes advantage of a-priori knowledge of drive and service loads for a better performance. Since service vehicles, specifically delivery trucks, have a similar route and duty cycle every day, obtaining this information is less challenging compared to other vehicles. In the high-level of the proposed control system, full knowledge of drive and service loads is required, but distances of the segments are the only necessary future information in the low-level control system. Therefore, a prediction of all the parameters that affect drive and service loads based on historical data is required. This chapter will start with analyzing the sensitivity of the control system to the accuracy of drive and service loads' prediction. This analysis is necessary to find out how accurately these loads should be predicted in order to have an acceptable performance by the controller. This chapter will also introduces a method for the prediction of the parameters involved in these loads (i.e. drive cycle, vehicle mass, auxiliary power, location and duration of engine-OFF stops).

6.1 Sensitivity Analysis

The sensitivity of the controller with respect to the prediction of drive and service loads will be studied in this section. To meet this objective, the performance of the controller will be evaluated when the a-priori knowledge of the drive load (drive cycle and vehicle mass) and service load (auxiliary power) is not accurate. For all these sensitivity analyses, the first case study discussed in Chapter 5 will be considered.

6.1.1 Drive Cycle

A drive cycle can be characterized by three parameters: total time, total distance, and type of driving cycle, i.e. city or highway. The prediction of distance can affect the performance of the high-level and low-level control systems. However, the prediction of two other parameters only affects the high-level control system.

Total time of a driving cycle is influenced by traffic conditions. A change in the time of a driving cycle will result in the change of total auxiliary power consumed in the corresponding segment. The performance of the high-level control system is evaluated when traffic is heavier or lighter than the

predicted value (20% increase and decrease in the time). As shown in Figure 6-1, the controller is not very sensitive to the prediction of the time of the driving cycle due to the fact that the high-level control system attempts to provide enough electrical energy for the engine-OFF segments, and as a result when the driving time is increased or decreased, the difference in demanded auxiliary energy is compensated by increasing or reducing the amount of energy supplied by the generator. Therefore, SOC trajectory will not change significantly when traffic information does not conform to the prediction, and increase in fuel consumption will be less than 1%.

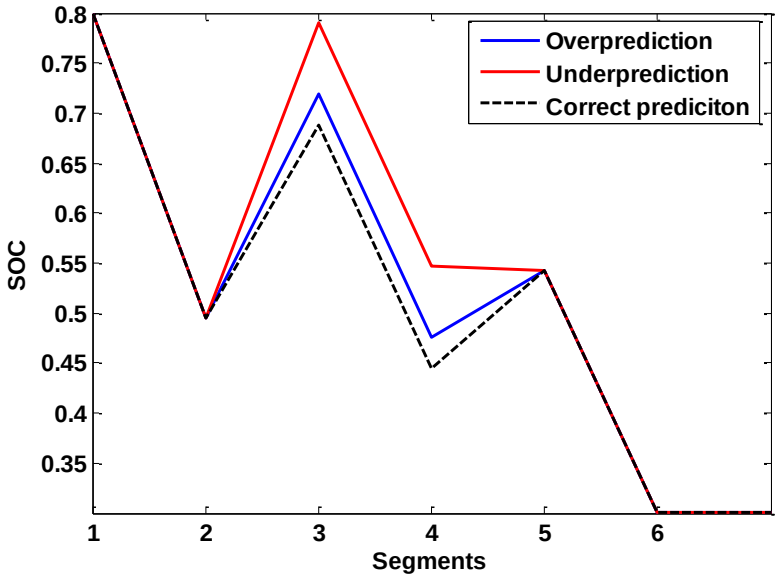

Figure 6-1 SOC trajectory obtained by high-level control system with different prediction of drive cycle's time

When a vehicle is driven in a city cycle rather than highway, more fuel can be saved by the RAPS because more regenerative auxiliary power is available. Therefore, the type of driving cycle impacts the performance of the controller. As a result, the sensitivity of the controller to the prediction of the type of the driving cycle needs to be studied. The worst case scenario for this study would be to predict that a driving cycle is a highway cycle while the actual cycle is a city cycle or vice versa. Figure 6-2 illustrates that the SOC trajectory obtained by the high-level control system changes when the type of drive cycle is mistakenly predicted to be a highway cycle instead of a city cycle. The change in the fuel consumption, however, is very small (less than 0.5%). Therefore, the performance of the controller is not very sensitive to the prediction of the type of the driving cycle either.

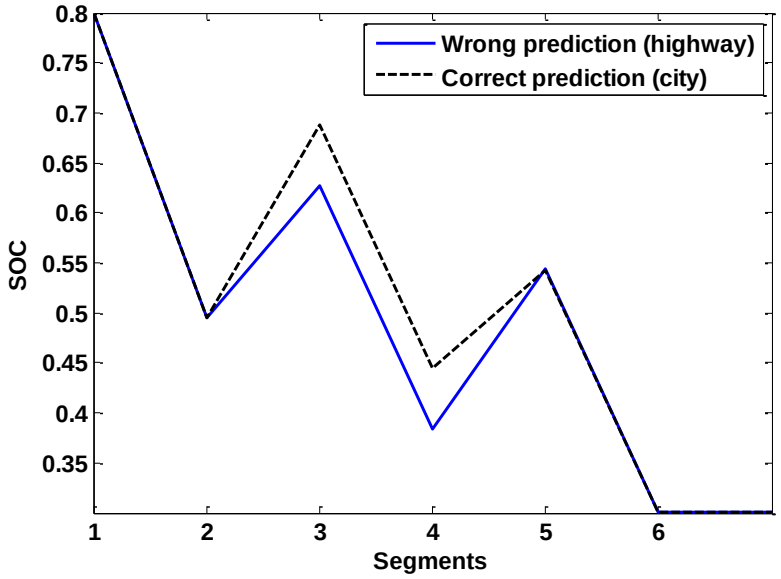

Figure 6-2 SOC trajectory obtained by high-level control system with wrong and correct prediction of drive cycle's type

Unlike the two previous parameters, the distance of the driving cycle affects both high-level and low-level control systems. When the prediction of the distance is greater than the actual value, the battery cannot be charged or discharged completely as determined by the high-level controller. Therefore, the battery either will lack energy at the stops or will not be fully depleted at the end of a trip. On the other hand, when the prediction is shorter than the actual distance, the SOC of the battery reaches the desired value in the middle of a segment and then it should be kept constant to the end. Consequently, the performance of the controller is reduced and the fuel consumption is increased. As shown in Figure 6-3, in the case that the distance is over predicted, the SOC goes below the minimum value in the last engine-OFF stop, which means that the engine needs to be turned ON. In the other case that the distance is under predicted, the constraint of the SOC limit is satisfied, but the fuel consumption is increased by about 0.5%.

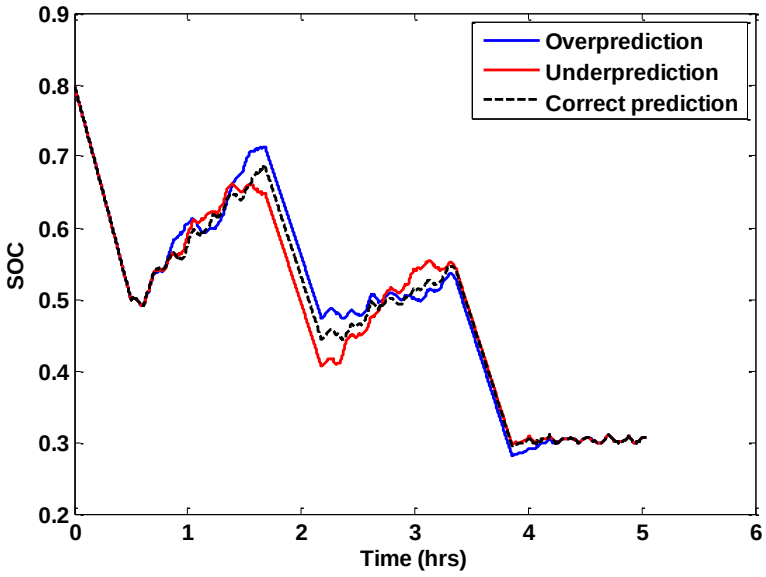

Figure 6-3 Change in battery SOC with different prediction of drive cycle's time

6.1.2 Vehicle Mass

The other parameter that influences the drive load is the vehicle mass. Therefore, the sensitivity of the control system with respect to the accuracy of mass prediction should be studied. For this study, two cases are considered: first, it is predicted that the vehicle is fully loaded during the whole cycle ($M = 7500\ kg$) and second, the weight of freight is not included in the prediction of the vehicle mass ($M = 6000\ kg$). Although the prediction of the mass is different in these cases, it is assumed that the demanded auxiliary power is the same. As shown in Figure 6-4, the accuracy of the mass prediction can change the SOC trajectory a little bit; however, this change has a small effect on total fuel economy (less than 0.6%) in comparison with the case that the vehicle mass is correctly predicted. As a result, the control system is insensitive to the mass prediction when the auxiliary load is independent from the mass.

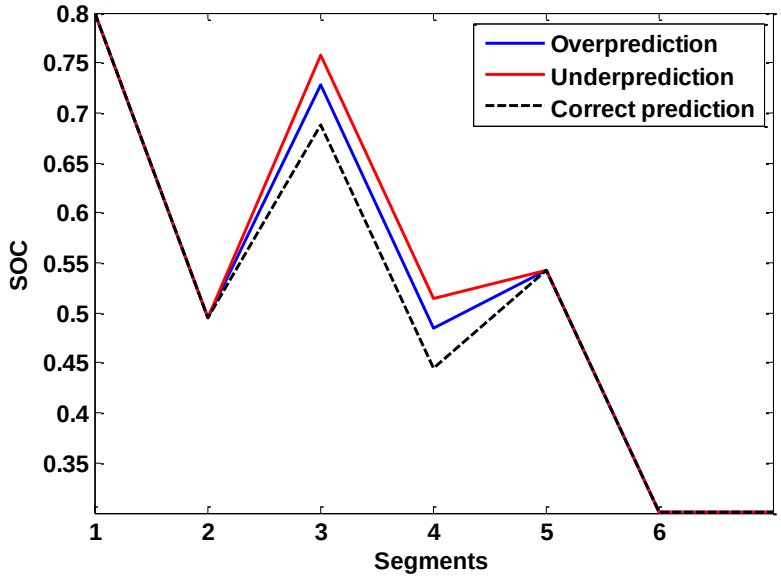

Figure 6-4 SOC trajectory obtained by high-level control system with different prediction of vehicle mass

6.1.3 Auxiliary Power

This section studies the effect of auxiliary power prediction on the control system's performance. For this purpose, the SOC trajectory obtained by the high-level control system with the correct auxiliary power prediction is compared with the cases in which the auxiliary power is over predicted or under predicted by 20%. As illustrated in Figure 6-5, the accuracy of the auxiliary power prediction can noticeably change the SOC trajectory. Subsequently, to find out the effect of these inaccurate predictions on the real-time controller, the low-level control system is run for each case. Figure 6-6 shows that when the auxiliary load is over predicted, the battery is not fully discharged at the end of the cycle, which results in more fuel consumption and more emissions. On the other hand, when the auxiliary load is under predicted, the minimum limit of the battery SOC is violated at a stop where the engine is supposed to be OFF. Therefore, the engine should be turned ON, which causes engine idling. As a result, it is essential to predict demanded auxiliary power accurately in order to have an optimal solution. As discussed in section 6.1.1, a change in the time of a driving cycle, which results in the change of total auxiliary power of the corresponding segment, does not have a profound impact on the controller. Therefore, it can be concluded that controller is only sensitive to the total amount of auxiliary power in engine-OFF stops.

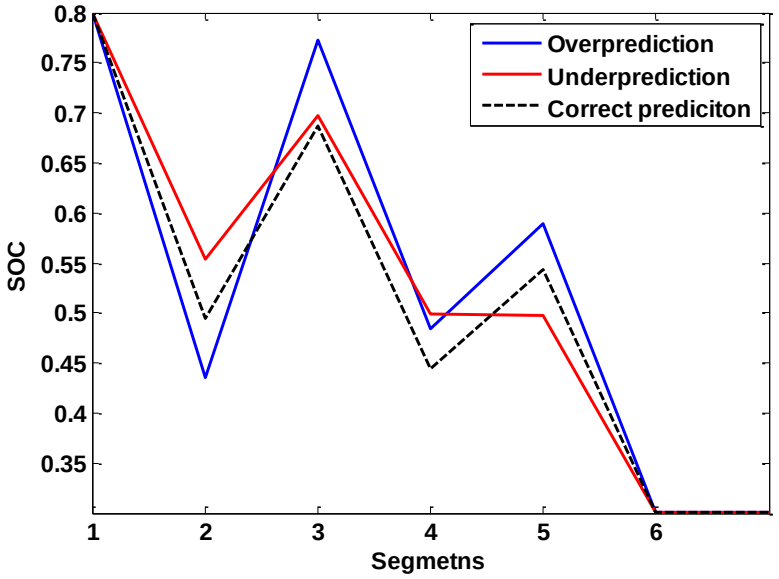

Figure 6-5 SOC trajectory obtained by high-level control system with different prediction of total auxiliary power

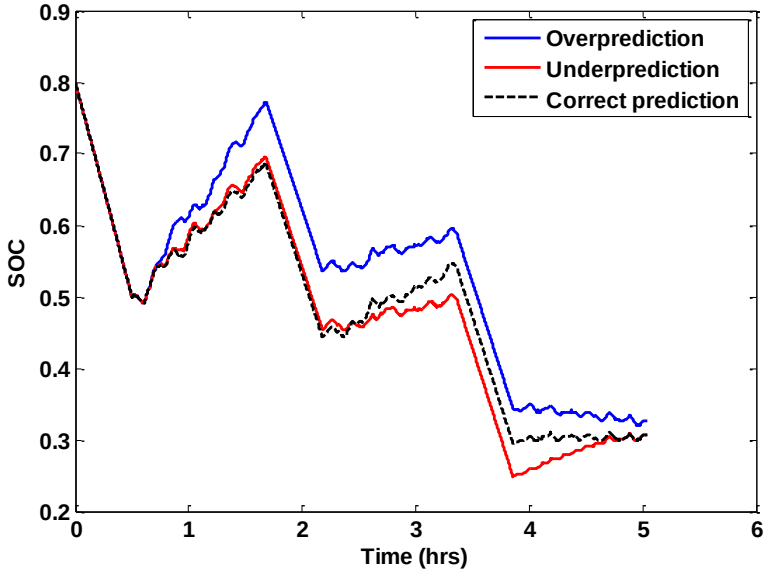

Figure 6-6 Change in battery SOC with different prediction of total auxiliary power

It should be noted that in the above case study the predictions of the auxiliary power for all the segments were incorrect, and consequently the controller could not be adjusted at all. Therefore, the battery was not fully depleted in the over prediction case, and it was over discharged in the under prediction one. However, if the auxiliary power of some segments do not conform to the prediction, the controller compensates for the wrong previous battery charging/discharging in segments that follow. For example, when the prediction of auxiliary power for the first two segments is incorrect, the battery SOC eventually reaches the desired final SOC at the end of the trip, but the fuel consumption is increased about 1.5%.

6.2 Prediction Method

The sensitivity analysis, which was carried out in the previous section, showed that the controller of power management system of the RAPS is not very sensitive to the prediction of time and type of drive cycles as well as the prediction of the vehicle mass. On the other hand, the performance of the controller is reduced when the prediction of the distance of the drive cycle and the total amount of auxiliary power in each segment (specifically the engine-OFF segments) are not very accurate. This section proposes a prediction method for all these parameters based on historical data.

One method to use historical data for the prediction of these parameters is to utilize their values in the last operating day. However, to have more sensible prediction, it is proposed to consider a bigger window of data (a course of 30 operating days) and put a greater weighting factors on the data of immediate past days:

$$\delta_{pred} = \frac{\alpha_1 \delta_1 + \alpha_2 \sum_{i=2}^{8} \delta_i + \alpha_3 \sum_{i=9}^{30} \delta_i}{\alpha_1 + 7\alpha_2 + 22\alpha_3} \tag{6-1}$$

where δ_{pred} is the predicted value of a parameter for the following operating day, δ_i is the value of the parameter for i_th day ($i = 1$ and $i = 30$ represent last day and thirty days ago, respectively), and $\alpha_1 > \alpha_2 > \alpha_3$ are their corresponding weighting factor.

6.2.1 Drive Cycle

As shown in the Section 6.1.1, the control system is insensitive to the type of drive cycles. As a result, one standard driving cycle that is most similar to the real drive cycle of the vehicle can be selected for

the prediction purpose. Then, duration of this drive cycle can be adjusted through the prediction of time of the drive cycle obtained by Equation (6-1). This prediction is accurate enough for a good performance of the high-level control system. However, the low-level control system requires a better method for the prediction of distance, which will be discussed in Section 6.2.4.

6.2.2 Vehicle Mass

The control system is not sensitive to the mass prediction when the auxiliary load is known. Therefore, in some service vehicles such as tour buses that the auxiliary load (e.g. power consumption of AC) is independent from the vehicle mass, reported curb weight by the manufacturer can be utilized as the predicted mass. On the other hand, in some other service vehicles such as refrigerator trucks, the freight mass affects auxiliary load (power consumption of the refrigerator) noticeably, thus its prediction is essential. In this case the vehicle mass can be predicted by Equation (6-1), and then it can be updated online by the estimation algorithm discussed in Chapter 3.

6.2.3 Auxiliary power

The total auxiliary power of each segment is another parameter that should be known in advance. As previously discussed, the controller is more sensitive to auxiliary power of engine-OFF segments. To predict total auxiliary power of each segment, the average auxiliary power is obtained by Equation (6-1), then the average is multiplied by the segment's duration to find total auxiliary power (auxiliary energy). The durations of the segments that the engine is ON have been already obtained by the prediction of the time of the drive cycle, and the durations of engine-OFF segments can be found by the method that will be discussed in the Section 6.2.4.

6.2.4 Location and Duration of Engine-OFF Stops

The prediction of auxiliary energy at the stops where the engine is OFF as well as prediction of the distances of the segments (locations of the stops) impact the performance of the controller. Therefore, it is important to properly predict the location and duration of engine-OFF stops using historical data. One approach to predict these two parameters is an averaging method presented in Equation (6-1). However, if the vehicle stops in some new locations or it does not stop in some old ones, the averaging method cannot figure out if these changes are one-time only or permanent (see Figure 6-7). Therefore, a smart method is required to add and remove the location of stops. To meet this objective, a clustering algorithm that puts the data points of each stop in one cluster can be utilized. Thus, the algorithm creates

a new cluster (as a new stopping location) when enough data points are available, and it removes an old stopping location when the number of data points are reduced in its cluster.

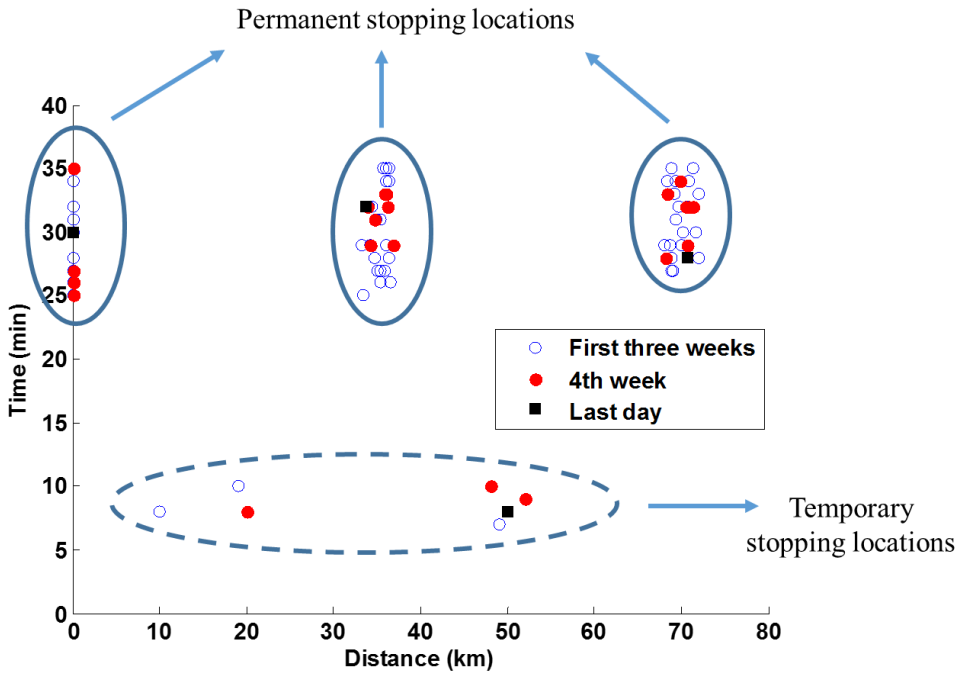

Figure 6-7 Permanent and temporary stopping locations where the engine is OFF

Two most widely used clustering techniques are k-mean [99] and Density-Based Spatial Clustering of Application with Noise (DBSCAN) [100]. The k-mean clustering is a centroid model that seeks to partition n data points into k clusters so that each data point belongs to the cluster with the nearest center (mean). The k-mean algorithm operates by taking following steps:

1- Select k cluster centers randomly.
2- Calculate the Euclidean distance between each data point and cluster centers.
3- Assign the data point to the cluster center whose distance from the cluster center is minimum.
4- Calculate new cluster centers by finding the mean value of all the data points in each cluster.
5- Calculate the Euclidean distance between each data point and new cluster centers.
6- If any data point is assigned to a new cluster center, repeat from step 3; otherwise, stop.

The main drawback of k-mean technique in the problem in hand is that it needs predefined number of clusters. This means that the number of engine-OFF stops should be known in advance, whereas the goal is to add or remove stopping locations spontaneously. The other disadvantage of this technique is inability to handle noisy data or outliers. Consequently, if the vehicle stops in a location only one time, this data point affects the clustering process.

To overcome the problems associated with the k-mean technique, the DBSCAN method, which is a density-based model, can be utilized. This technique does not need predefined number of clusters, and it can handle noisy data efficiently. In this method, each data point is categorized into three groups: core points, border points, and outliers (noise points). A core point, as shown in Figure 6-8, is a point that more than a minimum number of data points ($MinPts$) is available in its Eps-neighborhood. A border point has fewer points than $MinPts$ in its Eps-neighborhood, but it is in the neighborhood of a core point. A noise point is a point that is neither a core point nor a border point.

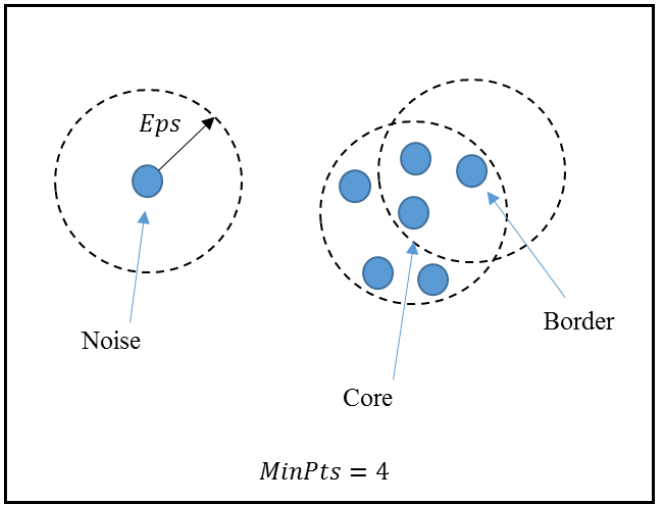

Figure 6-8 Definition of core, border, and noise points in DBSCAN clustering method

Definition. A point p is directly density-reachable from a point q if p is in the neighborhood of q and q is a core point. Also, a point p is density-reachable from a point q if there is a chain of points $p_1, p_2, \dots, p_n$ ($p_1 = p,\ p_n = q$) so that p_{i+1} is directly density-reachable from p_i (see Figure 6-9)

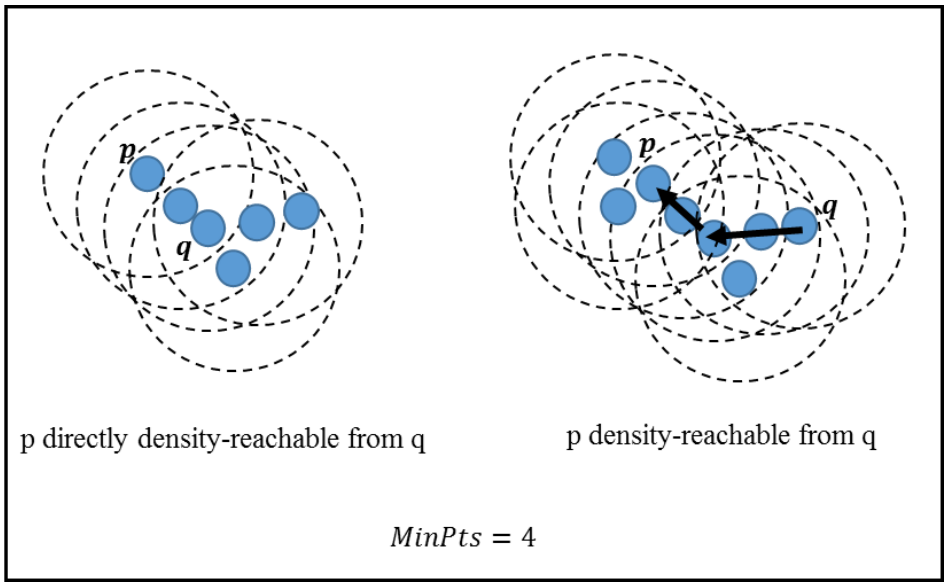

Figure 6-9 Definition of directly density-reachable (left) and density-reachable (right)

The algorithm of DBSCAN is presented in the below box. Furthermore, a simple example of this clustering method is shown in Figure 6-10.

for each data point p
  if p is not yet in a cluster **then**
    if p is a core point **then**
    all data point that are density-reachable from p are assigned to a new cluster
    else
    assign p to Noise point
    end
  end
end

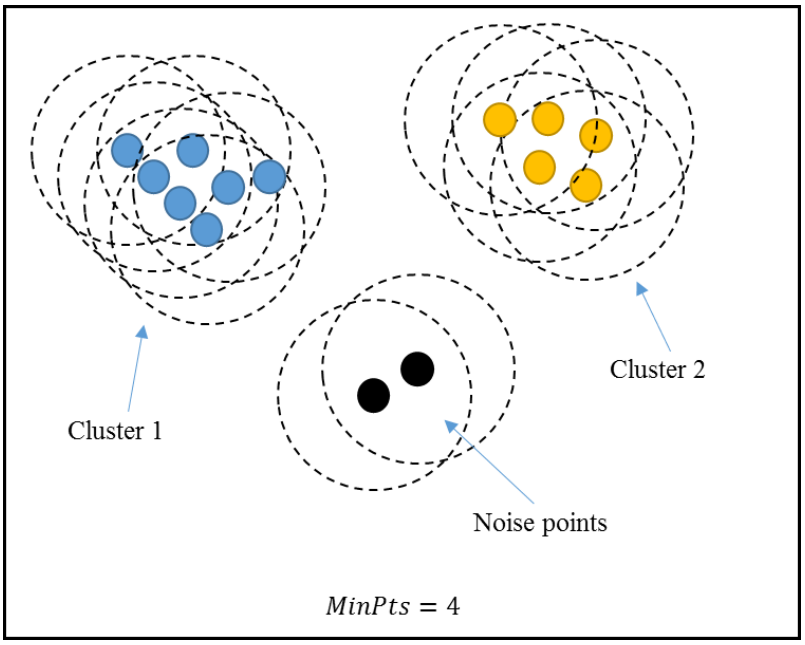

Figure 6-10 An example of DBSCAN clustering

By applying DBSCAN method on the historical data, duration and location of the engine-OFF stops can be predicted by finding the center of the clusters. Each data point is weighted by the factors explained in Equation (6-1). For this case study, the weighting factors, $MinPts$, and Eps are defined as:

Table 6-1 Simulation specifications

Symbol	Parameter	Value
α_1	Weighting factor for the data collected in the last day	5
α_2	Weighting factor for the data collected in 4th week	3
α_3	Weighting factor for the data collected first three weeks	1
$MinPts$	Minimum number of data points in a cluster	8
Eps	Neighborhood radius	5

As presented in Figure 6-11, the data points are assigned to four clusters by DBSCAN method. The center of each cluster, which is the average of all the data points in the cluster, determines the location and duration of one engine-OFF stop. The result shows that, in addition to three permanent stopping locations, it is very likely the vehicle stops in an extra location (cluster 3) in the following operating day. On the other hand, some data points are considered as noise points, so they do not impact on other clusters.

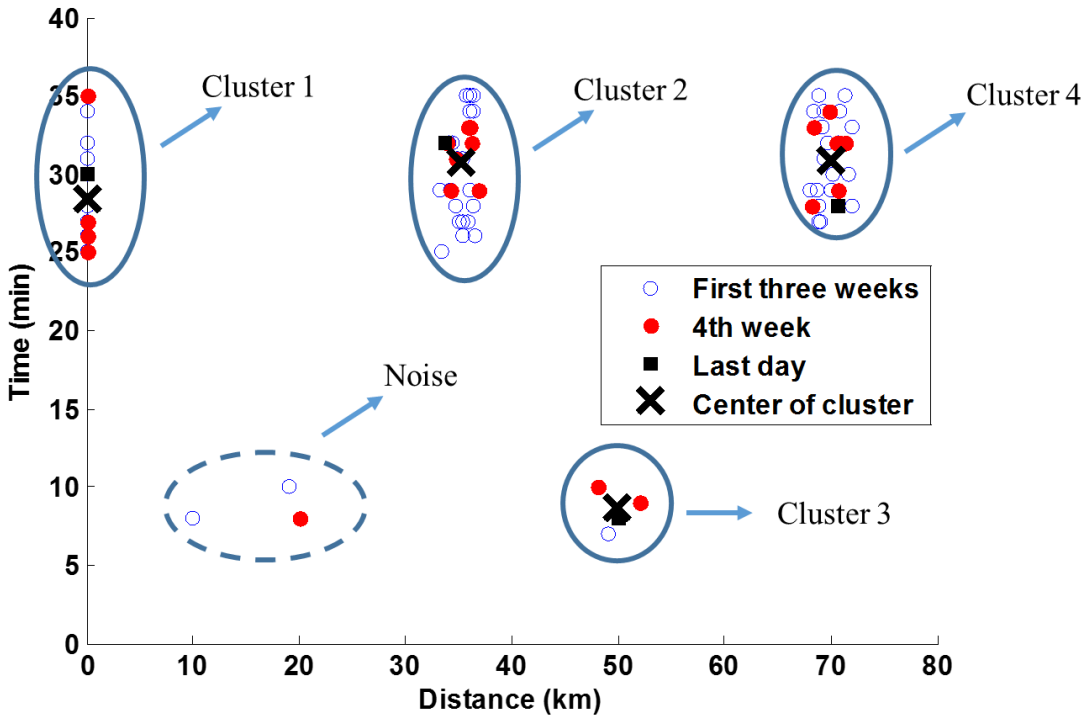

Figure 6-11 Prediction of engine-OFF locations and durations obtained by the DBSCAN method

To summarize, a prediction method (using historical data) for each required parameter, which are listed in Table 6-2, was proposed.

Table 6-2 A summary of methods for the prediction of drive and service loads

Parameters	Prediction Method
Type of drive cycle	One standard drive cycle similar to the actual one
Time of drive cycle	Averaging (Equation 6-1)
Mass	Averaging (Equation 6-1)
Distance of drive cycle	Clustering
Average auxiliary power	Averaging (Equation 6-1)
Duration of engine-OFF stops	Clustering

6.3 Updating Prediction by Real-Time Information

In the previous section, a method for prediction of drive and service loads using historical data was proposed. Due to the fact that a service vehicle has a similar drive and duty cycles every day, this prediction is very reliable. However, to improve the performance of the controller, the prediction can be updated by any available real-time information.

As discussed earlier, the amount of auxiliary power in some service vehicles can be a function of many factors. For example, in refrigerator trucks the variation of freight mass, ambient temperature, solar radiation, etc. can change this value significantly. Therefore, the prediction of auxiliary power can be updated online with a comprehensive model that uses all of this data to obtain future auxiliary power. Some research have been done to develop such a model [101], but further study is much on demand for interested researchers. Additionally, the prediction of vehicle mass can be updated by real-time estimation algorithm proposed in Chapter 3. Furthermore, the prediction of time and distance of a drive cycle can be improved by a navigation system.

If the prediction is updated by the real-time information or the actual SOC does not agree with the predicted SOC trajectory, the high-level control system should be run again to obtain a new SOC

trajectory. Since the high-level control system utilizes a fast dynamic programming method described in Chapter 5, the updating process takes place online with minimum computational effort.

6.4 Chapter Summary

Considering the control scheme of the power management system operates based on a prediction of drive and service loads, this chapter studied the sensitivity of the control system to the accuracy of the prediction of all the parameters involved in these loads. It was shown that the controller is only sensitive to the total power consumption of the auxiliary devices at engine-OFF stops as well as distance of the driving cycles. Based on this study, a prediction method for each parameter using historical data was proposed. Most of the parameters were predicted by an averaging method that considered a big window of data (a course of 30 operating days) and put a greater weighting factor on the collected data in immediate past days. For predicting location and duration of the engine-OFF stops, a DBSCAN clustering method was proposed. This technique provided a better prediction than the averaging method for these parameters because it can handle outliers very well, i.e. the temporary engine-OFF stops, which were unlikely to be repeated in the future, did not affect the prediction.

Chapter 7
Conclusions

In this thesis a new anti-idling system for service vehicles, called Regenerative Auxiliary Power System (RAPS), was proposed and studied. To design an optimum RAPS for given service vehicles, some tools and methods were developed. The contributions of this research are summarized in the next section.

7.1 List of Contributions

Developed a fuel-efficient anti-idling system for service vehicles

This system uses electrical power generated by an engine-driven generator and a battery pack to run electrical auxiliary devices. The battery can be charged by the generator or an external electrical source. With this configuration, the battery is the only source of power for the auxiliary devices when the vehicle stops for a long time. Therefore, the engine idling can be eliminated by turning the engine OFF. During traction, the generator and battery either individually or together supply electric power to the auxiliary devices. Furthermore, during braking, kinetic energy of the vehicle is transmitted from wheels to the output shaft of the engine, and then it is converted to electrical energy by the generator, thereby decelerating the vehicle. This electrical energy is used to run the auxiliary devices and/or to charge the battery. This system has many advantages over current anti-idling systems: the performance and efficiency of the auxiliary devices are improved since they are independent from the engine, and fuel consumption is significantly reduced by enabling regenerative braking and utilizing an optimal power management system.

Developed a model-based algorithm for simultaneous estimation of vehicle mass and torque of auxiliary devices.

To identify drive and service loads, which is an important requirement for determining size of RAPS' components, the torque of auxiliary devices and vehicle mass, as two parameters with unknown variations, need to be estimated. A model-based estimation algorithm, which utilizes signals available through the vehicle control area network (CAN), was proposed to estimate these two parameters simultaneously [102], [103]. This algorithm made use of the Kalman filter for estimating the parameters in two stages. In the first stage, both parameters were estimated until an accepted value for the vehicle

mass was obtained. Then, the vehicle mass was kept constant and only the auxiliary torque was estimated in the second stage. The algorithm worked very well at different level of excitations.

Developed a test setup for hardware-in-the loop simulations of the powertrain of service vehicles.
To verify performance of the identification algorithm, a test setup for hardware-in-the-loop simulations was developed. This test setup can also be used to evaluate performance of an individual powertrain's components of vehicles including transmission, differential, drive shafts, alternator, battery, and power take-off (PTO). Moreover, to test many other control systems in vehicles, this test setup can be utilized. The HIL simulations showed the good performance of the estimation algorithm in more realistic situations.

Developed a real-time control strategy for the power management system of the RAPS.
A new two-level control scheme for the power management system of the RAPS was proposed [104]. In the high-level control system, a new fast dynamic programming (DP) method that utilized extracted features of predicted drive and service loads was proposed. This level of the controller obtained the SOC trajectory of the battery for the whole operating day. In the low-level control system, the SOC trajectory, obtained by the DP algorithm, was tracked by a refined adaptive equivalent fuel consumption minimization method (A-ECMS). The simulation results showed that engine idling can be completely eliminated by implementing the RAPS on a service vehicle. Additionally, fuel consumption of the vehicle was reduced by 12% in city cycles and 7% in highway cycles. Fuel saving can be increased by utilizing a larger battery and generator.

Developed a method for prediction of drive and service loads.
This study proposed a method for predicting all the parameters involved in drive and service loads using historical data collected in the last thirty operating days of the vehicle. This method that was based on averaging technique and data clustering put a greater weighting factor on the most recent operating days for more sensible prediction. The simulation results showed that the prediction method was able to handle outliers very well, i.e. the temporary engine-OFF stops, which were unlikely to be repeated in the future, did not affect the prediction.

7.2 Recommendations for Future Research

Although the performance of the identification algorithm as well as the controller of the power management system were shown to be very promising, there is still room for more research in design and validation of the algorithms as summarized below:

Validation of the controller of the power management system using HIL simulations

With some modifications to the test bench described in Chapter 4, the control scheme of the power management system can be validated by HIL simulations. To meet this objective, the dynamometer that is connected to PTO for simulating the auxiliary device should be replaced by an electrical load simulation module that is powered by a battery pack and a generator connected to the input dynamometer by a belt and pulley mechanism. A microcontroller is required to run the proposed real-time controller for this system.

Using a high-fidelity model for the simultaneous estimation of the vehicle mass and auxiliary power

In this study, a simplified model was used to develop the estimation algorithm. A high-fidelity model can be utilized for this purpose to take some other factors, such as road condition, into account.

Developing a robust estimation algorithm

The performance of the proposed estimation algorithm can be reduced by some disturbances, such as wind. In some applications including determining the size of the RAPS' components, these disturbances do not have a profound impact on the estimation results. However, if this estimation method is employed in some other real-time controllers, the robustness of the algorithm against such disturbance should be studied and some modifications may be required.

Developing a method to predict auxiliary power using available sensory data

The method presented in Chapter 6 used historical data to predict the auxiliary power. As mentioned earlier, this prediction can be updated by some sensory data such as ambient temperature, pressure,

solar radiation, etc. A comprehensive model that uses all of this information can be developed to update the prediction of the auxiliary power.

Field tests to validate performance of the algorithms on a real vehicle

After validating the proposed estimation algorithm and control system by numerical and HIL simulations, they need to be tested on a real vehicle. In the first step, a vehicle with an engine-driven auxiliary device is required for testing the estimation algorithm. In order to do this, an OBD data logger and a GPS receiver should be installed on the vehicle to collect data in different driving cycles. The collected data can be used to determine the size of the battery and the generator for the RAPS. In the next step, the engine-driven auxiliary device should be replaced by an electrical one, and a generator and battery should be added to the vehicle as main components of the RAPS. Then the performance of the RAPS' controller can be tested on the vehicle, and fuel consumption of the vehicle equipped with the RAPS can be compared with the conventional configuration.

Bibliography

[1] Y. Wang, J. Byrne, and W. Rickerson, "Investigating the Cost, Liability, and Reliability of Anti-idling Equipment for Trucks: Final Report to Delaware Department of Transportation," *Univ. Delaware, Cent. Energy Environ. Policy, Newark,* 2007.

[2] F. Stodolsky, L. Gaines, and A. Vyas, "Analysis of technology options to reduce the fuel consumption of idling trucks," Argonne National Lab., IL (US), 2000.

[3] C. Brodrick, D. Sperling, and H. A. Dwyer, "Will Diesel Engines make a Comeback?," *Consum. Res. Mag.*, p. 18, 2002.

[4] N. Lutsey, C.-J. Brodrick, D. Sperling, and C. Oglesby, "Heavy-duty truck idling characteristics: Results from a nationwide truck survey," *Transp. Res. Rec. J. Transp. Res. Board*, no. 1880, pp. 29–38, 2004.

[5] T. L. Perrot, J. D. Tario, J. C. Kim, and C. Hagan, "Installation and economics of a Shorepower facility for long-haul trucks." Albany, NY: New York State Energy Research and Development Authority, 2004.

[6] "Idling Vehicle Emissions for Passenger Cars, Light-Duty Trucks, and HeavyDuty Trucks," 2008. [Online]. Available: http://www3.epa.gov/otaq/consumer/420f08025.pdf.

[7] E. E. Lust, W. T. Horton, and R. Radermacher, "A Review and Cost Comparison of Current Idle-Reduction Technology," in *ASME 2008 Power Conference*, 2008.

[8] "Truck Stop Electrification and Anti-Idling As a Diesel Emissions Reduction Strategy At U.S.-Mexico Ports Of Entry," 2009. [Online]. Available: http://www3.epa.gov/region09/climatechange/pdfs/TSE_Otay_report.pdf.

[9] C. MacDonald, R. Douglas, a. Tamayol, and M. Bahrami, "A Feasibility Study of Auxiliary HVAC Systems for Reducing Idling Time of Long Haul Trucks," *Vol. 1 Heat Transf. Energy Syst. Theory Fundam. Res. Aerosp. Heat Transf. Gas Turbine Heat Transf. Transp. Phenom. Mater. Process. Manuf. Heat*, pp. 323–330, Jul. 2012.

[10] A. Lindermeir, S. Kah, S. Kavurucu, and M. Mühlner, "On-board diesel fuel processing for an SOFC–APU—Technical challenges for catalysis and reactor design," *Appl. Catal. B Environ.*, vol. 70, no. 1, pp. 488–497, 2007.

[11] C.-J. Brodrick, T. E. Lipman, M. Farshchi, N. P. Lutsey, H. A. Dwyer, D. Sperling, S. W. Gouse Iii, D. B. Harris, and F. G. King, "Evaluation of fuel cell auxiliary power units for heavy-duty diesel trucks," *Transp. Res. Part D Transp. Environ.*, vol. 7, no. 4, pp. 303–315, 2002.

[12] Y. Liu, W. Lehnert, H. Janßen, R. C. Samsun, and D. Stolten, "A review of high-temperature polymer electrolyte membrane fuel-cell (HT-PEMFC)-based auxiliary power units for diesel-powered road vehicles," *J. Power Sources*, vol. 311, pp. 91–102, 2016.

[13] H. K. Fathy, D. Kang, and J. L. Stein, "Online vehicle mass estimation using recursive least squares and supervisory data extraction," in *American Control Conference*, 2008, pp. 1842–1848.

[14] R. Rajamani and J. K. Hedrick, "Adaptive observers for active automotive suspensions: theory and experiment," *Control Syst. Technol. IEEE Trans.*, vol. 3, no. 1, pp. 86–93, 1995.

[15] R. Zarringhalam, A. Rezaeian, W. Melek, A. Khajepour, S. Chen, and N. Moshchuk, "A comparative study on identification of vehicle inertial parameters," in *2012 American Control Conference (ACC)*, 2012, pp. 3599–3604.

[16] R. Fremd, "Apparatus for measuring the mass of a motor vehicle," U.S. Patent No. 4656876,14-Apr-1987.

[17] M. C. Best and T. J. Gordon, "Combined state and parameter estimation of vehicle handling dynamics," in *Proceedings of of the 5th International Symposium on Advanced Vehicle Control (AVEC)*, 2000.

[18] T. A. Wenzel, K. J. Burnham, M. V Blundell, and R. A. Williams, "Dual extended Kalman filter for vehicle state and parameter estimation," *Veh. Syst. Dyn.*, vol. 44, no. 2, pp. 153–171, 2006.

[19] S. Rhode and F. Gauterin, "Online estimation of vehicle driving resistance parameters with recursive least squares and recursive total least squares," *Intelligent Vehicles Symposium (IV), IEEE*. pp. 269–276, 2013.

[20] M. T. Breen, "System and method for determining relative vehicle mass," U.S. Patent No. 5482359,09-Jan-1996.

[21] A. Klatt, "Method and apparatus to automatically determine the weight or mass of a moving vehicle," U.S. Patent No. 4548079,22-Oct-1985.

[22] K. Reiner, H. Rieker, and J. Stoll, "Device for determining the mass of a motor vehicle," U.S. Patent No. 4941365,17-Jul-1990.

[23] T. A. Genise, "Control method/system including determination of an updated value indicative of gross combination weight of vehicles," U.S. Patent No. 5490063,06-Feb-1996.

[24] G. G. Zhu, D. O. Taylor, and T. L. Bailey, "Recursive vehicle mass estimation," U.S. Patent No. 6167357,26-Dec-2000.

[25] G. G. Zhu, D. O. Taylor, and T. L. Bailey, "Recursive vehicle mass estimation system," U.S. Patent No. 6438510,20-Aug-2002.

[26] E. G. Gaeke, "Road grade sensor," U.S. Patent No. 3752251,14-Aug-1973.

[27] H. S. Bae, J. Ryu, and J. C. Gerdes, "Road grade and vehicle parameter estimation for longitudinal control using GPS," in *IEEE Conference on Intelligent Transportation Systems, Proceedings, ITSC*, 2001, pp. 166–171.

[28] S. Han and C. Rizos, "Road slope information from GPS-derived trajectory data," *J. Surv. Eng.*, vol. 125, no. 2, pp. 59–68, 1999.

[29] P. Sahlholm and K. Henrik Johansson, "Road grade estimation for look-ahead vehicle control using multiple measurement runs," *Control Eng. Pract.*, vol. 18, no. 11, pp. 1328–1341, 2010.

[30] P. Sahlholm, H. Jansson, E. Kozica, and K. H. Johansson, "A sensor and data fusion algorithm for road grade estimation," 2007.

[31] H. Ohnishi, J. Ishii, M. Kayano, and H. Katayama, "A study on road slope estimation for automatic transmission control," *JSAE Rev.*, vol. 21, no. 2, pp. 235–240, 2000.

[32] D. D. Hrovat, H. E. Tseng, and T. A. Brown, "Method for road grade/vehicle pitch estimation," U.S. Patent No. 6714851,30-Mar-2004.

[33] B. Schmidtbauer and P. Lingman, "Road slope and vehicle mass estimation using Kalman

filtering," in *The Dynamics of Vehicles on Roads and on Tracks: Proceedings of the 17th IAVSD Symposium Held in Lyngby, Denmark, August 20-24, 2001*, 2003, vol. 37, pp. 12–23.

[34] A. Vahidi, M. Druzhinina, A. Stefanopoulou, and H. Peng, "Simultaneous mass and time-varying grade estimation for heavy-duty vehicles," in *American Control Conference*, 2003, vol. 6, pp. 4951–4956.

[35] A. Vahidi, A. Stefanopoulou, and H. Peng, "Experiments for Online Estimation of Heavy Vehicle's Mass and Time-Varying Road Grade," *Dyn. Syst. Control. Vol. 1 2*, vol. 2003, pp. 451–458, 2003.

[36] A. Vahidi, A. Stefanopoulou, and H. Peng, "Recursive least squares with forgetting for online estimation of vehicle mass and road grade: theory and experiments," *Veh. Syst. Dyn.*, vol. 43, no. 1, pp. 31–55, 2005.

[37] M. L. Mcintyre, T. J. Ghotikar, A. Vahidi, X. Song, D. M. Dawson, and S. Member, "A Two-Stage Lyapunov-Based Estimator for Estimation of Vehicle Mass and Road Grade," vol. 58, no. 7, pp. 3177–3185, 2009.

[38] V. Winstead and I. V Kolmanovsky, "Estimation of road grade and vehicle mass via model predictive control," *Proc. 2005 IEEE Conf. Control Appl.*, pp. 1588–1593, 2005.

[39] M. N. Mahyuddin, J. Na, G. Herrmann, X. Ren, and P. Barber, "An adaptive observer-based parameter estimation algorithm with application to road gradient and vehicle's mass estimation," in *Control (CONTROL), UKACC International Conference on*, 2012, pp. 102–107.

[40] A. Vahidi, A. Stefanopoulou, and H. Peng, "Adaptive model predictive control for co-ordination of compression and friction brakes in heavy duty vehicles," *Int. J. Adapt. Control Signal Process.*, vol. 20, no. 10, pp. 581–598, 2006.

[41] H. S. Bae and J. C. Gerdes, "Parameter estimation and command modification for longitudinal control of heavy vehicles," 2003.

[42] M. K. Liubakka, D. S. Rhode, and J. R. Winkelman, "Adaptive automotive speed control," in *Proceedings of Workshop on Advances in Control and its Applications*, 1996, pp. 1–26.

[43] K. Oda, H. Takeuchi, M. Tsujii, and M. Ohba, "Practical estimator for self-tuning automotive cruise control," in *American Control Conference, 1991*, 1991, pp. 2066–2071.

[44] D. Yanakiev and I. Kanellakopoulos, "Speed tracking and vehicle follower control design for heavy-duty vehicles," *Veh. Syst. Dyn.*, vol. 25, no. 4, pp. 251–276, 1996.

[45] P. Ioannou and Z. Xu, "Throttle and Brake Control Systems for Automatic Vehicle Following," *J. Intell. Transp. Syst.*, vol. 1, no. 4, pp. 345–377, 1994.

[46] D. Yanakiev and I. Kanellakopoulos, "Nonlinear spacing policies for automated heavy-duty vehicles," *Veh. Technol. IEEE Trans.*, vol. 47, no. 4, pp. 1365–1377, 1998.

[47] R. Matsubara, S. Umemura, S. Kumazawa, H. Nakaima, and M. Kawaguchi, "Compressor torque estimate device, engine controller and method of estimating compressor torque," U.S. Patent No. 6910344,28-Jun-2005.

[48] Y. Yamanaka, S. Numazawa, Y. Nishi, H. Kishita, and H. Suzuki, "Method and apparatus for calculating torque of variable capacity type compressor," U.S. Patent No. 5385029,31-Jan-1995.

[49] T. Imai and A. Inoue, "Compressor output calculation unit and control unit using the same." EP

Patent 1491375, 29-Dec-2004.

[50] S. G. Wirasingha and A. Emadi, "Classification and review of control strategies for plug-in hybrid electric vehicles," *Veh. Technol. IEEE Trans.*, vol. 60, no. 1, pp. 111–122, 2011.

[51] M. Ehsani, Y. Gao, and A. Emadi, *Modern electric, hybrid electric, and fuel cell vehicles: fundamentals, theory, and design*. CRC press, 2009.

[52] F. R. Salmasi, "Control strategies for hybrid electric vehicles: Evolution, classification, comparison, and future trends," *Veh. Technol. IEEE Trans.*, vol. 56, no. 5, pp. 2393–2404, 2007.

[53] S. G. Li, S. M. Sharkh, F. C. Walsh, and C.-N. Zhang, "Energy and battery management of a plug-in series hybrid electric vehicle using fuzzy logic," *Veh. Technol. IEEE Trans.*, vol. 60, no. 8, pp. 3571–3585, 2011.

[54] A. Brahma, Y. Guezennec, and G. Rizzoni, "Optimal energy management in series hybrid electric vehicles," in *American Control Conference, 2000. Proceedings of the 2000*, 2000, vol. 1, no. 6, pp. 60–64.

[55] B. McQueen and J. McQueen, *Intelligent transportation systems architectures*. 1999.

[56] J. de Dios Ortuzar and L. G. Willumsen, *Modelling transport*. John Wiley & Sons, 2011.

[57] Z.-R. Peng and M.-H. Tsou, *Internet GIS: distributed geographic information services for the internet and wireless networks*. John Wiley & Sons, 2003.

[58] Q. Gong, Y. Li, and Z.-R. Peng, "Trip-based optimal power management of plug-in hybrid electric vehicles," *Veh. Technol. IEEE Trans.*, vol. 57, no. 6, pp. 3393–3401, 2008.

[59] Q. Gong, Y. Li, and Z.-R. Peng, "Trip based power management of plug-in hybrid electric vehicle with two-scale dynamic programming," in *Vehicle Power and Propulsion Conference, 2007. VPPC 2007. IEEE*, 2007, pp. 12–19.

[60] A. Taghavipour, N. L. Azad, and J. McPhee, "An optimal power management strategy for power split plug-in hybrid electric vehicles," *Int. J. Veh. Des.*, vol. 60, no. 3/4, pp. 286–304, 2012.

[61] G. Paganelli, S. Delprat, T.-M. Guerra, J. Rimaux, and J.-J. Santin, "Equivalent consumption minimization strategy for parallel hybrid powertrains," in *Vehicular Technology Conference, 2002. VTC Spring 2002. IEEE 55th*, 2002, vol. 4, pp. 2076–2081.

[62] A. Sciarretta, M. Back, and L. Guzzella, "Optimal control of parallel hybrid electric vehicles," *Control Syst. Technol. IEEE Trans.*, vol. 12, no. 3, pp. 352–363, 2004.

[63] L. Serrao, S. Onori, and G. Rizzoni, *ECMS as a realization of Pontryagin's minimum principle for HEV control*. IEEE, 2009, pp. 3964–3969.

[64] C. Musardo, G. Rizzoni, Y. Guezennec, and B. Staccia, "A-ECMS: An Adaptive Algorithm for Hybrid Electric Vehicle Energy Management," *Eur. J. Control*, vol. 11, no. 4–5, pp. 509–524, Oct. 2005.

[65] S. Onori and L. Serrao, "On Adaptive-ECMS strategies for hybrid electric vehicles," in *Proceedings of the International Scientific Conference on Hybrid and Electric Vehicles, Malmaison, France*, 2011, pp. 6–7.

[66] D. Ambühl and L. Guzzella, "Predictive reference signal generator for hybrid electric vehicles," *Veh. Technol. IEEE Trans.*, vol. 58, no. 9, pp. 4730–4740, 2009.

[67] L. Fu, U. Ozguner, P. Tulpule, and V. Marano, "Real-time energy management and sensitivity

study for hybrid electric vehicles," in *American Control Conference (ACC), 2011*, 2011, pp. 2113–2118.

[68] B. Gu and G. Rizzoni, "An adaptive algorithm for hybrid electric vehicle energy management based on driving pattern recognition," in *ASME 2006 International Mechanical Engineering Congress and Exposition*, 2006, pp. 249–258.

[69] A. Chasse, A. Sciarretta, and J. Chauvin, "Online optimal control of a parallel hybrid with costate adaptation rule," in *Advances in Automotive Control*, 2010, pp. 99–104.

[70] J. T. B. A. Kessels, M. W. T. Koot, P. P. J. Van den Bosch, and D. B. Kok, "Online energy management for hybrid electric vehicles," *Veh. Technol. IEEE Trans.*, vol. 57, no. 6, pp. 3428–3440, 2008.

[71] A. Chasse, G. Corde, A. Del Mastro, and F. Perez, "Online optimal control of a parallel hybrid with after-treatment constraint integration," in *Vehicle Power and Propulsion Conference (VPPC), 2010 IEEE*, 2010, pp. 1–6.

[72] M. Sivertsson and L. Eriksson, "Design and evaluation of energy management using map-based ECMS for the PHEV benchmark," *Oil Gas Sci. Technol. d'IFP Energies Nouv.*, vol. 70, no. 1, pp. 195–211, 2015.

[73] A. Stefanopoulou and L. Moklegaard, "Adaptive continuously variable compression braking control for heavy-duty vehicles," *Ann Arbor*, vol. 1001, p. 48197, 2002.

[74] J. K. Hedrick, D. McMahon, V. Narendran, and D. Swaroop, "Longitudinal vehicle controller design for IVHS systems," in *American Control Conference, 1991*, 1991, pp. 3107–3112.

[75] T. D. Gillespie, *Fundamentals of vehicle dynamics*. SAE, 1992.

[76] K. Atkinson, W. Han, and D. E. Stewart, *Numerical solution of ordinary differential equations*, vol. 108. John Wiley & Sons, 2011.

[77] R. E. Kalman, "A new approach to linear filtering and prediction problems," *J. basic Eng.*, vol. 82, no. 1, pp. 35–45, 1960.

[78] G. Bishop and G. Welch, "An introduction to the kalman filter," *Proc SIGGRAPH, Course*, vol. 8, pp. 23175–27599, 2001.

[79] O. Nelles, *Nonlinear system identification: from classical approaches to neural networks and fuzzy models*. Springer, 2000.

[80] P. Ioannou and B. Fidan, "Adaptive control tutorial, Society for Industrial and Applied Mathematics." 2006.

[81] L. Cao and H. M. Schwartz, "Analysis of the Kalman filter based estimation algorithm: an orthogonal decomposition approach," *Automatica*, vol. 40, no. 1, pp. 5–19, 2004.

[82] L. Guo, "Estimating time-varying parameters by the Kalman filter based algorithm: stability and convergence," *Autom. Control. IEEE Trans.*, vol. 35, no. 2, pp. 141–147, 1990.

[83] L. Guo and L. Ljung, "Exponential stability of general tracking algorithms," *Autom. Control. IEEE Trans.*, vol. 40, no. 8, pp. 1376–1387, 1995.

[84] L. Guo and L. Ljung, "Performance analysis of general tracking algorithms," *Autom. Control. IEEE Trans.*, vol. 40, no. 8, pp. 1388–1402, 1995.

[85] P. A. Ioannou and J. Sun, *Robust adaptive control*. Prentice-Hall, 1996.

[86] D. Maclay, “Simulation gets into the loop,” *IEE Rev.*, vol. 43, no. 3, pp. 109–112, 1997.

[87] Q. Zhang, J. F. Reid, and D. Wu, “Hardware-in-the-loop simulator of an off-road vehicle electrohydraulic steering system,” *Trans. ASAE-American Soc. Agric. Eng.*, vol. 43, no. 6, pp. 1323–1330, 2000.

[88] N. Shidore, H. Lohse-Busch, R. W. Smith, T. Bohn, and P. B. Sharer, “Component and subsystem evaluation in a systems context using Hardware in the Loop,” in *Vehicle Power and Propulsion Conference, 2007. VPPC 2007. IEEE*, 2007, pp. 419–424.

[89] Y.-H. Hung, C.-H. Wu, S.-M. Lo, B.-R. Chen, E.-I. Wu, and P.-Y. Chen, “Development of a hardware in-the-loop platform for plug-in hybrid electric vehicles,” in *Computer Communication Control and Automation (3CA), 2010 International Symposium on*, 2010, vol. 1, pp. 45–48.

[90] D. Ramaswamy, R. McGee, S. Sivashankar, A. Deshpande, J. Allen, K. Rzemien, W. Stuart, W. Lee, M. Yoon, M. Sunwoo, Y.-H. Hung, C.-H. Wu, S.-M. Lo, B.-R. Chen, E.-I. Wu, and P.-Y. Chen, “A cost-and time-effective hardware-in-the-loop simulation platform for automotive engine control systems,” in *Proceedings of the Institution of Mechanical Engineers, Part D: Journal of Automobile Engineering*, 2003, vol. 217, no. 1, pp. 41–52.

[91] W. Lee, M. Yoon, and M. Sunwoo, “A cost-and time-effective hardware-in-the-loop simulation platform for automotive engine control systems,” *Proc. Inst. Mech. Eng. Part D J. Automob. Eng.*, vol. 217, no. 1, pp. 41–52, 2003.

[92] R. S. Razavian, N. L. Azad, and J. McPhee, “A battery hardware–in–the–loop setup for concurrent design and evaluation of real–time optimal HEV power management controllers,” *Int. J. Electr. Hybrid Veh.*, vol. 5, no. 3, pp. 177–194, 2013.

[93] A. Hentunen, J. Suomela, A. Leivo, M. Liukkonen, and P. Sainio, “Hardware-in-the-loop verification environment for heavy-duty hybrid electric vehicles,” in *Vehicle Power and Propulsion Conference (VPPC), 2010 IEEE*, 2010, pp. 1–6.

[94] E. Buckingham, “On physically similar systems; illustrations of the use of dimensional equations,” *Phys. Rev.*, vol. 4, no. 4, pp. 345–376, 1914.

[95] D. S. Naidu, *Optimal control systems*. CRC press, 2002.

[96] S. Fallah, B. Yue, O. Vahid-Araghi, and A. Khajepour, “Energy management of planetary rovers using a fast feature-based path planning and hardware-in-the-loop experiments,” *Veh. Technol. IEEE Trans.*, vol. 62, no. 6, pp. 2389–2401, 2013.

[97] C. Zhang and A. Vahidi, “Route preview in energy management of plug-in hybrid vehicles,” *Control Syst. Technol. IEEE Trans.*, vol. 20, no. 2, pp. 546–553, 2012.

[98] a. Vahidi, “Route Preview in Energy Management of Plug-in Hybrid Vehicles,” *IEEE Trans. Control Syst. Technol.*, vol. 20, no. 2, pp. 546–553, Mar. 2012.

[99] J. MacQueen, “Some methods for classification and analysis of multivariate observations,” in *Proceedings of the fifth Berkeley symposium on mathematical statistics and probability*, 1967, vol. 1, no. 14, pp. 281–297.

[100] M. Ester, H.-P. Kriegel, J. Sander, and X. Xu, “A density-based algorithm for discovering clusters in large spatial databases with noise.,” in *Kdd*, 1996, vol. 96, no. 34, pp. 226–231.

[101] M. A. Fayazbakhsh and M. Bahrami, “Comprehensive modeling of vehicle air conditioning

loads using heat balance method," SAE Technical Paper, 2013.

[102] S. Mohagheghi Fard, A. Khajepour, A. Rezaeian, and C. J. Mendes, "Refrigeration Load Identification of Hybrid Electric Trucks," SAE Technical Paper, 2014.

[103] S. M. Fard and A. Khajepour, "Concurrent Estimation of a Vehicle's Mass and Auxiliary Power," in *ASME 2014 International Mechanical Engineering Congress and Exposition*, 2014, pp. V04BT04A006–V04BT04A006.

[104] S. M. Fard and A. Khajepour, "An optimal power management system for a regenerative auxiliary power system for delivery refrigerator trucks," *Appl. Energy*, vol. 169, pp. 748–756, 2016.